CHARACTERIZATION OF BRACHYPODIUM QUAC1, AN ANION CHANNEL INVOLVED IN STOMATAL MOVEMENT

A Thesis Submitted to the College of

Graduate and Postdoctoral Studies

In Partial Fulfillment of the Requirements

For the Degree of Doctor of Philosophy

In the Department of Veterinary Biomedical Sciences

University of Saskatchewan

Saskatoon

By

Gia-Khanh Luu

Permission to use

In presenting this thesis in partial fulfillment of the requirements for a Postgraduate degree from the University of Saskatchewan, I agree that the Libraries of this University may make it freely available for inspection. I further agree that permission for copying of this thesis in any manner, in whole or in part, for scholarly purposes may be granted by the professor or professors who supervised my thesis work or, in their absence, by the Head of the Department or the Dean of the College in which my thesis work was done. It is understood that any copying or publication or use of this thesis or parts thereof for financial gain shall not be allowed without my written permission. It is also understood that due recognition shall be given to me and to the University of Saskatchewan in any scholarly use which may be made of any material in my thesis.

Requests for permission to copy or to make other uses of materials in this thesis in whole or part should be addressed to:

Head of the Department of Veterinary Biomedical Sciences
University of Saskatchewan
Saskatoon, Saskatchewan S7N 5B4
Canada

OR

College of Graduate and Postdoctoral Studies
University of Saskatchewan
116 Thorvaldson Building, 110 Science Place
Saskatoon, Saskatchewan S7N 5C9
Canada

Abstract

Stomata are pores formed by guard cells in the leaf epidermis of plants. These pores are essential in responding to both abiotic and biotic stress such as drought, heat, pathogen infection, and therefore strictly regulated in plants. Uptake and release of ions from guard cells are the keys to stomatal function. For plants to close their stomata, at least two types of anion channels present in the guard cell membrane are required: the rapid (R-type) and the slow (S-type) activating anion channels. Quick anion channel 1 (QUAC1), initially named ALMT12, a member of the aluminum-activated malate transporter family, has been shown to encode an R-type anion channel in guard cells in *Arabidopsis thaliana*, a dicot model. Sequence alignments between dicot and monocot QUAC1 show as high as 56 % identity at the protein level. The purpose of this study was to investigate whether the monocot QUAC1s maintain the properties and functions as reported for the dicot AtQUAC1, and further characterize the monocot channel.

The monocot model *Brachypodium dystachyon* (commonly called stiff brome) was used for this study. To examine the properties of *Bd*QUAC1, the protein was expressed in HEK293 cells, and activities of the channel were measured using the patch clamp technique. Data collected in this study showed that *Bd*QUAC1 is activated by malate, consistent with what had been reported for AtQUAC1. However, the malate activation occurred only in the presence of Ca^{2+} and was inhibited by a calmodulin (CaM) inhibitor. By computational predictions, the *Bd*QUAC1 sequence was shown to include a CaM -binding domain (CBD). Direct interaction between the CBD and CaM was confirmed by two different methods: isothermal titration calorimetry and CaM agarose affinity pulldown. Electrophysiological analyses showed that site directed mutations at some of the basic residues in the CBD affect the activities of the channel. In addition, the hormone abscisic acid (ABA), which is known to cause an increase in cytosolic Ca^{2+} concentration and plays a

significant role in stomatal closure, did not have any direct electrophysiological effects on *Bd*QUAC1 protein expressed in the HEK293 system.

The role of *Bd*QUAC1 in stomatal closure was also assessed *in planta*. QUAC1-knockdown in *Brachypodium* showed an increase in the width of stomata aperture compared to wildtype. Overexpression of *Bd*QUAC1 also showed a significant reduction of stomatal width and additionally, an effect on stripe rust infection which is known to infect via stomata.

Altogether, this study has explored the regulation of *Bd*QUAC1, suggesting an activation of *Bd*QUAC1, that requires malate, Ca^{2+}, and CaM. Although, in plants, the activation of anion channels is through ABA signalling pathways, ABA does not have any direct *in vitro* effects on *Bd*QUAC1. This highlights the involvement of Ca^{2+} and CaM in the ABA signaling pathway mediating stomatal response. Altering the expression of the *Bd*QUAC1 gene affects stomatal function and potentially pathogen infection.

Acknowledgements

I would like to sincerely thank my supervisors Dr. Michele Loewen and Dr. Matthew Loewen for their unconditional support and guidance, and for being very patient with me throughout the course of my research program. I have learned many things from them and I will always value the mentorship from both Dr. Loewen's.

I would also like to thank my committee members Dr. George Forsyth, Dr. Patrick Covello, Dr. Christopher Todd, and my graduate chairs Dr. Karen Machin, and Dr. Daniel MacPhee, for their valuable comments and advice.

A special thanks to Dr. Kishore Rajagopalan and Dr. John Ching for teaching me many lab techniques, and helping me with my research experiments.

Thank you to the knowledgeable and friendly technicians at NRC Joe Hammerlindl, Yuping Lu and Yifang Tan for assisting me with the techniques required for my project.

Finally, I would like to thank my siblings and express my gratitude to my parents for their support through my journey as a student.

Table of contents

List of Tables

List of Figures

List of Abbreviations

AAPK – ABA -activated protein kinase

ABA – abscisic acid

ABC – ATP-binding Cassette

ABI – abscisic acid insensitive

ABRC – *Arabidopsis* biological resource center

ACA – autoinhibited calcium ATPase

AKT – *Arabidopsis* potassium transport system

ALMT – aluminum activated malate transporter

CaCC – calcium activated chloride channel

CaM - calmodulin

CAX – calcium exchanger

CBD – calmodulin binding domain

CBL – calcinerin B-like protein

Ch1H/ABAR/CCH/GUN5 – magnesium-chelatase H subunit/abscisic acid receptor/conditional chlorine/genome uncouple 5

CHX – cation/proton exchanger

CIM – callus initiation media

CIMMYT – International maize and wheat improvement center

CIPK – CBL-interacting protein kinase

CLC – chloride channel

CPA – cation proton antiporter

CPK or CDPK – calcium-dependent protein kinase

EGTA – ethylene glycol tetraacetic acid

GCR or GPCR - G-protein coupled receptor

GFP – green fluorescent protein

GORK – guard cell outward rectifying potassium channel

G-protein – guanine nucleotide binding protein

HAB – Homology to ABI

HEK293 – human embryonic kidney 293

HRP – horseradish peroxidase

IRES – internal ribosome entry site

ITC – isothermal titration calorimetry

KAT – potassium channel in *Arabidopsis thaliana*

KC – potassium rectifying channel

KCO – potassium channel opener (non-gated potassium channel)

KEA – potassium efflux antiporter

KT/HAK/KUP – potassium transporter/high-affinity potassium transporter/potassium uptake permease

NAR – nitrate accessory protein

NBS-LRR – nucleotide-binding sites-leucine rich repeats

NCBI – national center for biotechnology information

NHX – sodium, potassium /proton exchangers

NO_3^- - nitrate

NRT – nitrate transporters

OD – optical density

OSAK – osmotic stress activated protein kinase

OST1 – Open Stomata 1

PBS – phosphate buffered saline

PBST – phosphate buffered saline tween

PCR – polymerase chain reaction

PHOT – phototropin

PP2C – protein phosphatase 2C

PPase – pyrophosphatase

PPM – metal-dependent protein phosphatase

PPT – phosphinothricin

PVDF – polyvinylidene difluoride

PYR/PYL/RCAR – Pyrabactin resistance/ PYR-like/ regulatory component of ABA receptor

qPCR – quantitative polymerase chain reaction

QTL – quantitative trait locus

QUAC – quick anion channel

Rboh – respiratory burst oxydase

ROS – reactive oxygen species

R-type – rapid type

SDS-PAGE – sodium dodecyl sulfate-polyacrylamide gel electrophoresis

SKOR – Stelar postassium outward rectifier

SLAC – slow anion channel

SLAH – SLAC homolog

SNF – sucrose non-fermenting

SnRK – SNF related kinase

START – Steroidogenic Acute Regulatory Protein related lipid-transfer

S-type – slow type

TMEM16 – transmembrane member 16

TPC – two pore channel

TPK – tandem-pored potassium channel

TRK/HKT – potassium transporter/high-affinity potassium transporter

UBC18 – ubiquitin conjugating enzyme 18

CHAPTER 1. LITERATURE REVIEW

1.1. Plant biology and stomatal movement

1.1.1. Introduction to stomata

Like many forms of living organisms, plants also require nutrients, water, air, appropriate temperature and light for their basic needs to survive. While nutrients and water are obtained from roots, air is obtained from leaves through pores called "stomata" (Hetherington & Woodward, 2003). Oxygen and carbon dioxide are exchanged through open stomatal pores (Scheidegge et al., 2000). Plants use oxygen for respiration and carbon dioxide for photosynthesis, which is another source of energy for plants (Ziem-Hanck et al., 1980, Calvin, 1976). In addition, stomatal closure is critical in plant response against both biotic and abiotic stress, such as pathogen infection, drought and heat, respectively. Therefore, the movement of stomata is strictly regulated in plants.

Each stoma is a pore formed by two guard cells located on the leaf epidermis (Figure 1.1); guard cells are kidney-shaped in dicots, whereas, dumbbell-shaped in monocots (Sack, 1987). Opening and closing of stomatal pores depend on the turgor pressure of guard cells (Fischer, 1973). Turgor pressure is the pressure of the intracellular water pushing the plasma membrane against the cell walls. Change in the turgor pressure is caused by ions moving and drawing water with them in and out of guard cells (Meidner and Edwards, 1975, Zeiger, 1983). When ions move into guard cells and water follows by osmosis, the turgor pressure increases. Under high turgor pressure, guard cells swell and draw away from each other in dicots (Figure 1.2A) or the thick inner walls of guard cells are pulled away from each other in monocots (Figure 1.2B), and the pore is opened. Stomata are kept opened due to the non-osmotic movement of water triggered by the presence of

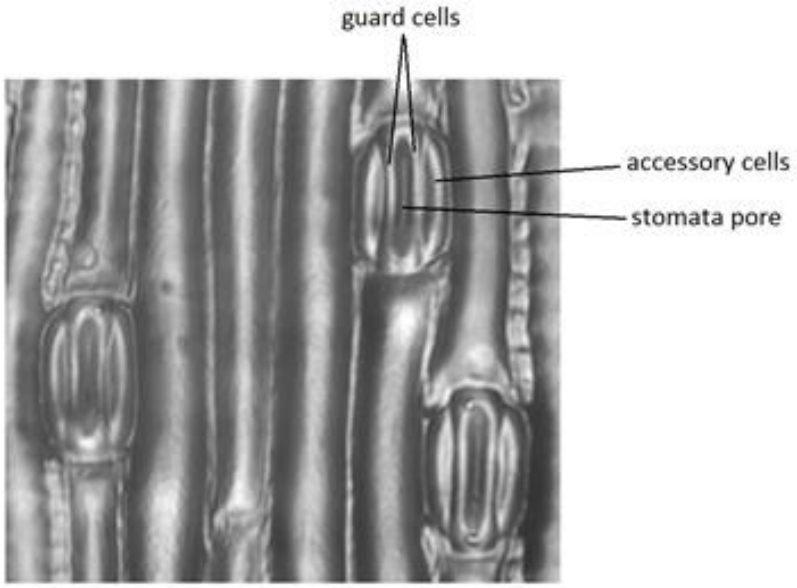

Figure 1. 1 The surface of a monocot *Hierochloe odorata* (sweet grass) leaf taken under the Zeiss Axiovert 135 inverted phase contrast microscope at 1000 x magnification

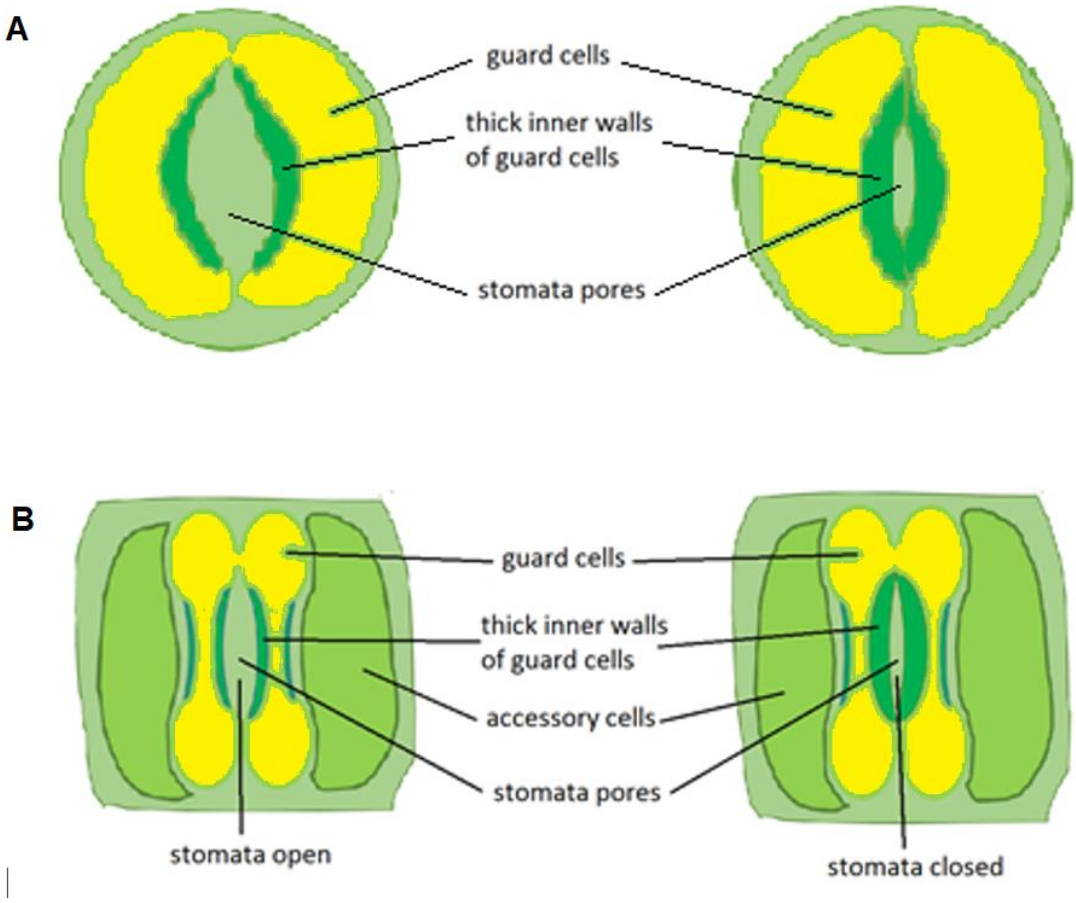

Figure 1. 2. **Typical structure of stomata**

A. Dicot stomata, formed by a pair of kidney-shaped guard cells. **B. Monocot stomata**, formed by a pair of dumbbell-shaped guard cells.

larger solutes (such as sugars) inside the guard cells. When ions and water efflux, the turgor pressure is reduced, resulting in shrinking of the guard cells and stomatal pore closure. Ultimately, the movement of stomata is controlled by ion channels in guard cells (Meidner and Edwards, 1975, Zeiger, 1983).

1.1.2. Movement of molecules across the cell membrane

Molecules, such as gases, water, sugars, amino acids, and ions, are able to move across the plasma and vacuolar membranes by several mechanisms which can be distinguished into two groups: passive transport and active transport. With passive transport, molecules move down the concentration gradient, from an area having higher concentration to an area with lower concentration without the requirement of exogenous energy. In active transport, energy is required and molecules move against the concentration gradient, from an area of lower concentration to an area of higher concentration (Epstein 1955, Epstein 1956, Bowling et al., 1966).

1.1.2.1. Passive transport

There are three types of passive transport across the membrane: simple diffusion, osmosis, and facilitated diffusion. Smaller molecules such as O_2 or CO_2 can move freely across the membrane by simple diffusion. Osmosis is the movement of water across the membrane, which occurs depending on the concentration of solute. Lastly, larger molecules and charged molecules are passively transported by facilitated diffusion via proteins called ‘channels’ and ‘uniporters’ (Figure 1.3A). Channel proteins include aquaporin channels and ion channels. Channels are generally selective and only allow the passage of certain substances. Aquaporin channels are major water channels. However, many aquaporin channels have been reported to transport both water and substrates, such as carbon dioxide, hydrogen peroxide, glycerol, urea, etc. (Pavlovic-Djuranovic et al., 2006. Bienert et al., 2007, Almasalmeh et al., 2014), and ion channels transport

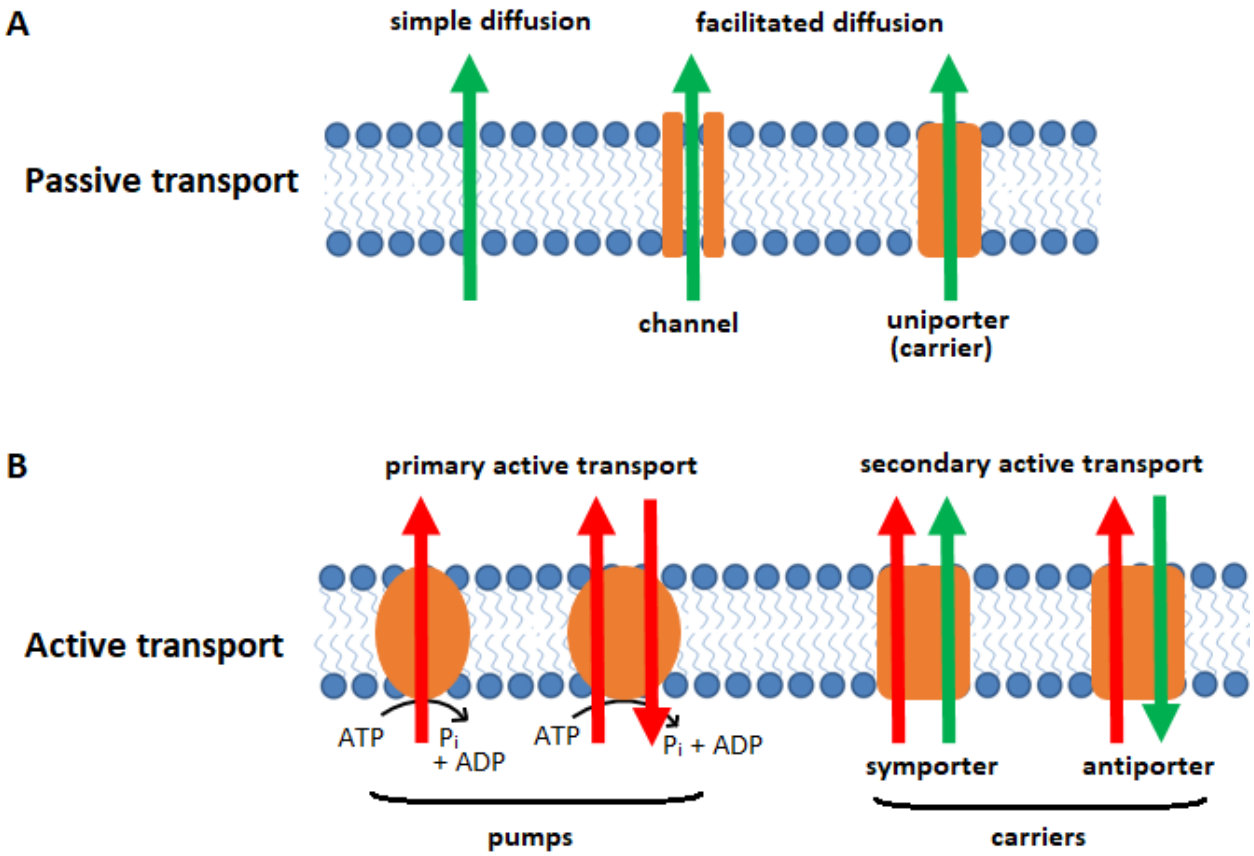

Figure 1. 3. Movement of molecules across the cell membrane.

Green arrows indicate molecules moving along the concentration gradient. Red arrows indicate molecules moving against the concentration gradient. **A.** Passive transport. **B.** Active transport.

only specific ions. Uniporters, also referred to as carriers, usually move molecules such as sugars or amino acids, one at a time, along the concentration gradient (Molnar and Jane, 2012).

1.1.2.2. Active transport

Larger or charged molecules can also move against the concentration gradient by active transport. There are two types of active transport: primary active transport and secondary active transport (Feher, 2012).

In primary active transport, the transporting proteins use adenosine triphosphate (ATP) as energy to pump the ions across the membrane. Thus, these proteins are referred to as 'pumps', or 'ATPases' interchangeably, for example, H^+ ATPase, or H^+ pump. An ion pump can transport one single type of ion, or co-transport two different types of ions such as the sodium-potassium pump (Figure 1.3B) (Feher, 2012, Stillwell, 2016).

In secondary active transport, ATP is not used as an energy source. Instead, the transporting protein couples the movement of an ion, usually Na^+ or H^+, to drive the transport. Free energy is generated due to ions moving down their electrochemical gradient. The electrochemical gradient for an ion consists of both the chemical gradient (concentration gradient), and the electrical gradient, which is the difference in charges across the membrane. Thus, the secondary active transport is also referred to as ion-coupled transport (Figure 1.3B), and the transporting proteins are generally referred to as carriers. If both the molecules and the coupling ions move in the same direction, the protein is called 'symporter'. If the molecules and the coupling ions move in the opposite direction, the transporting protein is called 'antiporter' (Feher, 2012, Stillwell, 2016).

1.1.3. Ion channels

Ions are atomic molecules that have gained or lost one or more electrons and therefore are carrying an electrical charge. A positively-charged ion is referred to as a cation, and a negatively-charged ion is referred to as an anion. As described in the previous sections, ions can move across the cell membrane by transporters such as ion channels, pumps, and other carriers including symporters and antiporters. Ions channels can be differentiated from other types ion transporters by two characteristics. First, ion channels do not require exogenous energy to function whereas other transporters rely solely on energy to move ions across the membrane. Secondly, ion channels have a pore and a gating system that controls the passage of ions by opening and closing of the pore (Barker et al., 2017).

All ion channels are transmembrane proteins. Channel proteins are composed of one or more subunits with transmembrane helices (Sigworth, 2003). These transmembrane helices come together and form a pore that allows ions to move across the hydrophobic membrane (Schumacher and Adelman, 2002). There are four main types of ion channels, classified by the gating property: voltage-gated channels, ligand-gated channels, mechanosensitive channels, and non-gated (leak) channels (Barker et al., 2017).

1.1.3.1. Voltage-gated ion channels

Voltage is the difference in electrical potential between two different places. In an electrical circuit, this difference is able to drive currents, which are movements of charges (carried by electrons), across a resistance. In cell biology, positively and negatively charged ions are not equally distributed on the inside and outside of membranes, thus generating an electrical potential difference, also known as membrane voltage, or membrane potential. Since membranes are selectively permeable to ions, the voltage across the membrane stays relatively constant. This

stable voltage is called the membrane resting potential. Due to the potential difference, the membrane is said to be polarized at resting potential. Movement of ions across the membrane can shift the membrane voltage to become more negative or positive, causing hyperpolarization or depolarization. If the membrane voltage becomes more negative than the resting potential, the membrane is said to be hyperpolarized. If the membrane voltage becomes less negative than the resting potential, the membrane is said to be depolarized.

Voltage-gated ion channels are activated by changes in the membrane voltage, and can exist in three main conformation states: closed, open, and inactivated (Catterall, 1995, Purves et al., 2001). At resting potential, the channels are closed. When there is a change in membrane voltage, such as depolarization or hyperpolarization, voltage-gated channels go through a conformational change, which opens the pore and allows ions to pass through the channels. In this state, the channels are considered open (Catterall, 1995). Within milliseconds after opening, the channel becomes inactivated by the mechanism called 'ball and chain' (West et al., 1992). 'Ball and chain' is a set of amino acids hanging by the pore of the channel on the cytosolic side of the membrane. Once the channels open, this "ball" of amino acids swings in and plugs the pore, blocking the passage of ions (Figure 1.4) (Demo and Yellen, 199, West et al., 1992). The channels remain in the inactivated state for some time before returning to the closed state.

1.1.3.2. Ligand-gated ion channels

Ligand-gated ion channels open in response to stimulating molecules called ligands. Ligands are chemical messengers that bind to proteins. Therefore, ligand-gated ion channels are also commonly known as ionotropic receptors. A ligand-gated ion channel can have one or multiple ligand-binding sites, and the binding sites are most often on the extracellular side of membranes. When ligands bind to the ligand-gated ion channel, it creates a conformational change,

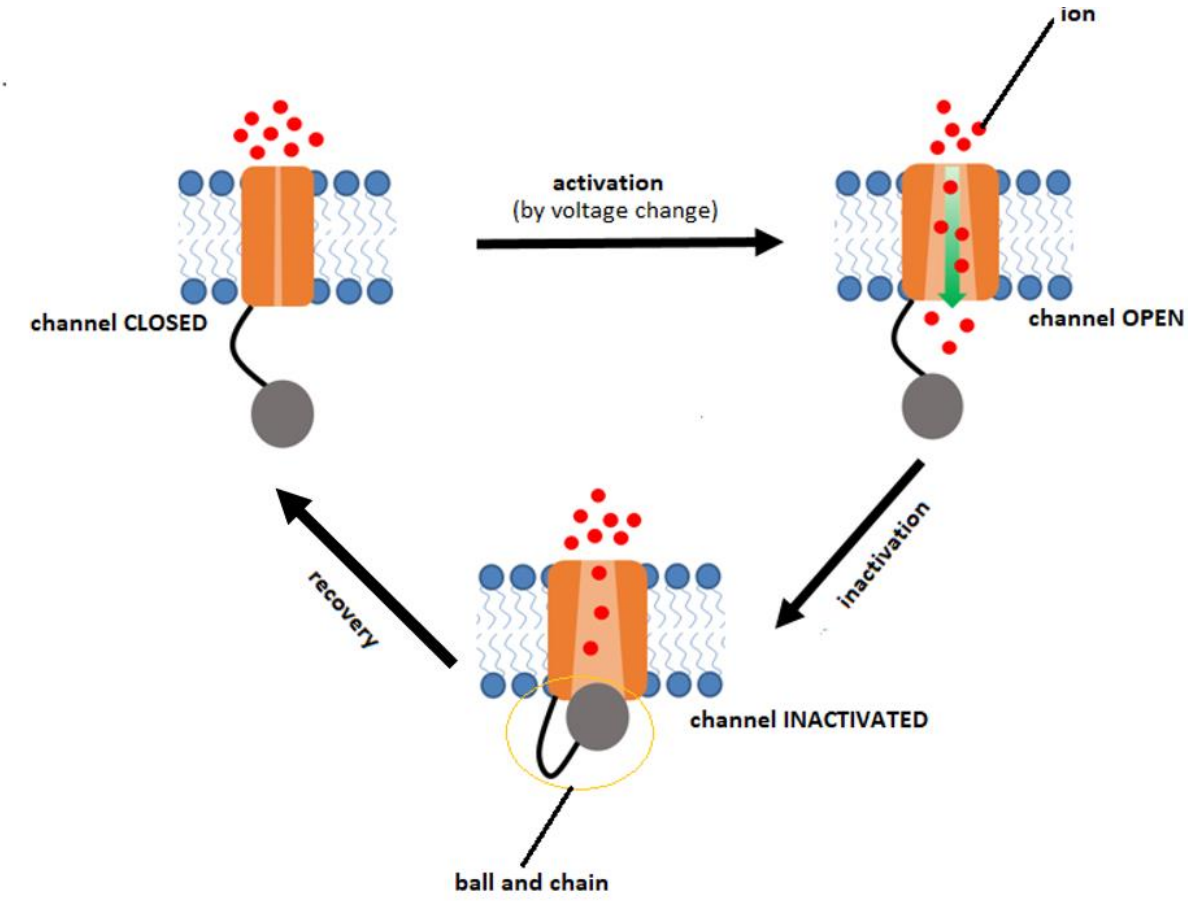

Figure 1. 4. The three main states of voltage-gated ion channels: closed, open, and inactivated.

At resting potential, the channel is closed. Shifts in membrane voltage activate and open the channel. At the open state, ions are able to pass through the channel. Shortly after opening, the channel becomes inactivated due to the 'ball and chain' blockage. The channel remains at the inactivated state for some time then returns to the closed state.

hiding the large hydrophobic amino acids and exposing the small and hydrophilic ones. This conformational change opens the channel and allows ions to move across. Ligand-gated ion channels have only two functional states: the open state and the closed state. (Figure 1.5) (Auerbach, 2013, Sauguet et al., 2014). Examples of ligand-gated ion channels include glutamate receptor and GABA receptors.

1.1.3.3. Mechanosensitive channels

Mechanosensitive channels open in response to mechanical force. They are also known by other names including mechanically-gated channels, stress-gated channels, or stretch-gated channels. These channels can sense and respond to the membrane tension change produced by mechanical stimuli such as osmotic pressure, gravity, environmental stress. Stress increases the lateral membrane tension and causes local lipid disordering (Perozo et al., 2002, Schulten and Gullingsrud, 2004). The channel, in response, favors the open conformation to reduce the local lipid disordering (Figure 1.6). Examples of mechanosensitive channels include the calcium-permeable non-selective cation channel TRPC6 or the potassium channel TREK-1.

1.1.3.4. Non-gated channels

Non-gated channels, also called leakage channels, are not controlled by a gating system. Unlike all other types of channels described above, these channels only exist in one state, the open state. There are only two kinds of non-gated ion channels: the K^+ channels and the Na^+ channels (Goldstein et al., 2001, Ren, 2011). Na^+ and K^+ can move passively down the non-gated channels along the concentration gradients, or against the concentration via Na^+/K^+ pump. Therefore, the channels play a crucial role in maintaining the cell resting membrane potential.

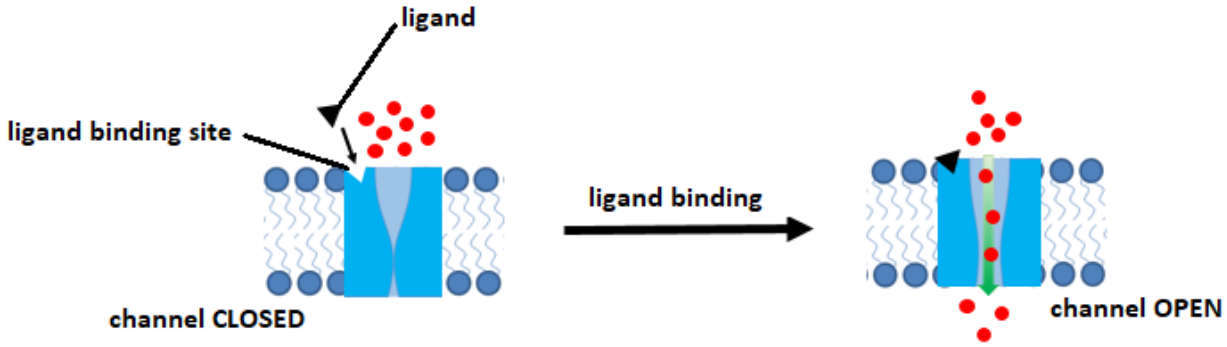

Figure 1. 5. The two states of ligand-gated ion channels: open state and closed state

The channel contains a ligand binding site. Binding of the channel to ligand opens the channel and allows ions to pass through.

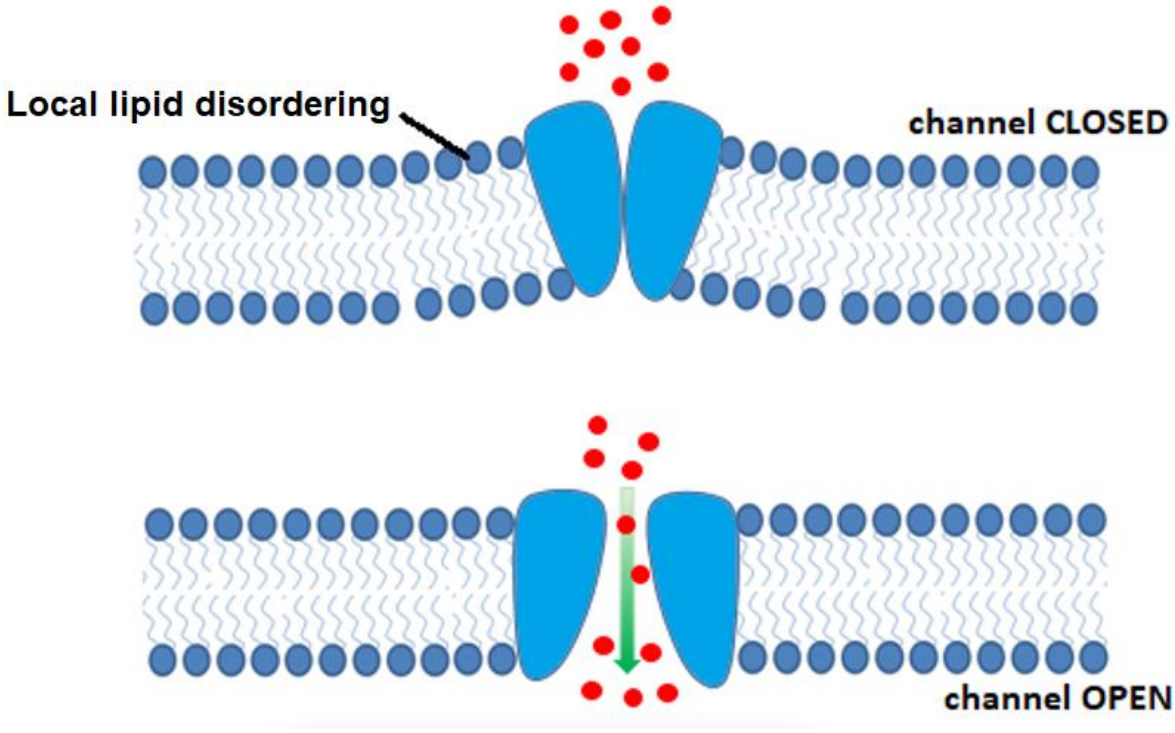

Figure 1. 6 Gating mechanism of the mechanosensitive channel

The channel changes its conformation to reduce the lipid disordering of the membrane.

1.1.3.5. Cation versus anion channels

Beside classification by gating, channels can also be classified by the type of ions they transport. Cation channels move positively charged ions, and anion channels move negatively charged ions.

Cations present in plant cells include Ca^{+}, Na^{+}, K^{+}, Mg^{+} and proton (H^{+}). Each type of ion channel will be described in more detail below. Beside cation channels which are specific to only one type of ions, there are also non-selective cation channels, which are permeable for most types of cations. To date, Mg^{+} and Na^{+} selective ion channels have not yet been identified, and the majority of these ions are likely moved across by other types of transporters.

Anions channels in plant cells have been classified into three groups: the Cl^{-} channels (CLC) family, the aluminum-activated malate transporters/quick anion channel (ALMT/QUAC) family, and the slow anion channels (SLAC). These channels together transport anions such as NO_3^{-}, Cl^{-}, $malate^{2-}$ and SO_4^{2-}.

1.1.4. Transporters involved in stomatal movement

Transporters that play a role in modulating the function of stomata include ions channels, pumps, symporters, and antiporters. Below are descriptions of ions involved in stomatal movement and their transporters.

1.1.4.1. Ca^{2+} transporters

Ca^{2+} channels. Since early days, scientists used patch clamp to prove the existence of Ca^{2+} channels in plant guard cells and root cells using protoplasts. In these studies, Ca^{2+} channels were activated by depolarization (Huang et al., 1994, Thuleau et al., 1994), hyperpolarization (Gelli et al., 1997, Véry et al., 2000, Hamilton et al., 2000), and the plant hormone abscisic acid (ABA)

(Hamilton et al., 2000). Thuleau et al. (1994) also showed that the channels were permeable not only to Ca^{+}, but also to K^{+}, Ba^{2+}, and Mg^{2+}, therefore they could possibly be non-selective cation channels. Although there is evidence of Ca^{2+} channels in plant cells, it has been a challenge for researchers to identify specific genes. To date, only one gene has been identified to encode a plant Ca^{2+} channel. Peiter et al., (2005) showed that the two-pore channel 1 (TPC1) gene which encodes for a slow vacuolar channel also encodes for a Ca^{2+}-dependent Ca^{2+} channel. Mutation of the gene leads to decrease in Ca^{2+} influx (Peiter et al., 2005). Beside Ca^{2+}, K^{+} and Na^{+} can also be transported through TPC1. From a study by Islam et al. (2010), the *Arabidopsis Attpc1* mutant neither induces stomatal closure in the presence of exogenous Ca^{2+}, nor activates S-type anion channel in the presence of high cytosolic Ca^{2+} (Islam et al., 2010). This suggests involvement of the Ca^{2+} channel, functioning upstream of the anion channels, at least the S-type channel, in stomatal closure.

Ca^{2+} pumps and carriers. Beside Ca^{2+} channels, Ca^{2+} can be transported by two other groups of transporters: the autoinhibited Ca^{2+} ATPase (ACA) family (Carafoli, 1992, Carafoli & Brini, 2000), and the Ca^{2+} exchanger (CAX) family (Hirschi et al., 1996). ACA is a family of Ca^{2+} pumps. ACAs are believed to promote plant growth and development as mutants of ACA genes caused reduced growth of pollen tubes and aborted fertilization (Schiott et al., 2004, Lucca and León, 2012, Iwano et al, 2014). However, the involvement of ACA in guard cell signaling is still unclear. The CAX family is a group of antiporters which exchange Ca^{2+} and H^{+} in the opposite direction. The first two CAX genes (CAX1 and CAX2), encoding polypeptides with sequence similar to microbial H^{+}/Ca^{+} antiporters, were isolated from *Arabidopsis*. Vesicles from AtCAX-transformed yeast cells showed significantly increased Ca^{2+} uptake, suggesting that the genes encode for H^{+}/Ca^{+} exchangers (Hirschi et al., 1996). Two different groups of researchers have

shown effects of knockdown of cax1, cax3 and cax1/cax3 on stomatal function. While Conn et al., (2011) showed constitutive stomatal closure in knockdown mutants *cax1/cax3*, Cho et al., (2012) showed that mutants *cax1, cax3* and *cax1/cax3* are impaired in light-induced stomatal opening, and the plant hormone auxin failed to inhibit ABA-induced stomatal closing in *cax1, cax3 and cax1/cax3* (Cho et al., 2012). However, when response to the hormone auxin was restored by lowering the apoplastic pH, stomata of the mutants remained more closed. At lower pH, the results were consistent with the other study. Thus the authors have suggested that the CAX genes act downstream of auxin in maintaining ion homeostasis and pH.

1.1.4.2. K^+ transporters

K^+ channels. In plants, K^+ channels can be divided into two groups: voltage-gated K^+ channels and non-gated K^+ channels. All voltage-gated K^+ channels share a common structure, with six transmembrane domains and a pore loop. The first four domains form a voltage sensor and the other two transmembrane domains together with the pore loop forms a K^+ permeable pathway (Figure 1.7A). These voltage-gated channels are found on plasma membrane with most channels moving K^+ inwardly, namely KAT, AKT, KC (Table 1.1). Presently, only two outward-rectifying K^+ channels have been identified: Stelar K^+ outward rectifier (SKOR) and Guard cell outward rectifying K^+ channel (GORK) (Gaymard et al., 1998, Ache et al., 2000). Knockout of the GORK gene in *Arabidopsis* causes a reduced stomatal response to ABA and darkness (Hosy et al., 2003). In *Arabidopsis*, fifteen K^+ channels have been identified with nine members being voltage-gated and six members non-gated (Table 1.1). All six members of the non-gated K^+ channels (KCO1 to KCO6) initially belonged to the K^+ channel opener (KCO) family. Beside KCO3 having a single subunit that forms the functional channel, the other five KCO channels assemble as dimers

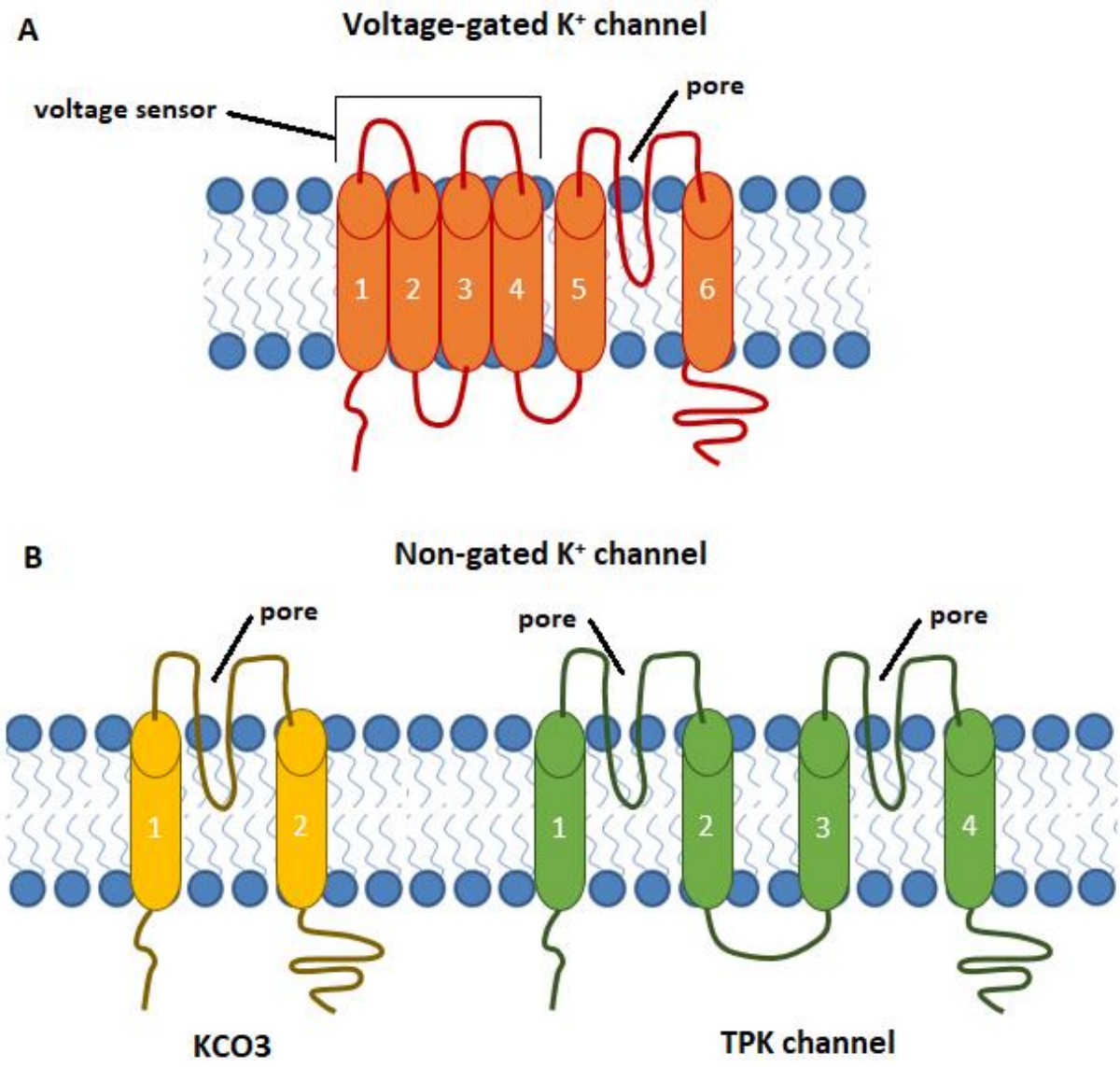

Figure 1. 7. The secondary structure of plant K+ channels

A. Voltage-gated K^+ channel with the first four transmembranes forming a voltage sensor, and the other two transmembranes forming an ion permeable pathway with the pore loop**. B.** Non-gated K^+ channel. KCO3 has a single subunit that forms a functional channel. TPK channels assemble as dimers by forming two identical subunits.

Channel class	Sub-family	Channel name (other names)	Full name
Voltage-gated (found in plasma membrane)	**Inward-rectifying K^+ channels**	KAT1	K^+ Channel in *Arabidopsis thaliana*
		KAT2	
		AKT1	*Arabidopsis* K^+ Transport system
		AKT2 (AKT3, AKT2/3)	
		AKT5	
		KC1 (KAT3/AKT4)	K^+ rectifying Channel
		SPIK (AKT6)	Shaker pollen inward K^+ channel
	Outward-rectifying K^+ channels	SKOR	Stelar K^+ Outward Rectifier
		GORK	Guard cell Outward-rectifying K^+ channel
Non-gated K^+ channels (found in vacuolar membrane except for TPK4)	**Tandem-pore K^+ channels**	TPK1 (KCO1)	Tandem-pore K^+ channels
		TPK2 (KCO2)	
		TPK3 (KCO6)	
		TPK4 (KCO4)	
		TPK5 (KCO5)	
	KCO family	KCO3	K^+ channel openers

Table 1.1. K^+ channels in *Arabidopsis*

by forming two identical "transmembrane-loop-transmembrane" subunits (Figure 1.7B). The five KCO channels were separated from KCO3 and later named tandem-pored K^+ (TPK) channels (Becket et al., 2004). Except for TPK4, located on the plasma membrane, the other non-gated K^+ channels are found on the vacuolar membrane (Czempinski et al., 2002, Schonknecht et al., 2002, Voelker et al., 2006, Dunkel et al., 2008). Nonetheless, the role of TPK channels in plants is still unclear.

K^+carriers. Beside K^+ channels, plants have three other K^+ transporter families: the KT/HAK/KUP (K^+ transporter/High-Affinity K^+ transporter/K^+ uptake permease) transporters, the TRK/HKT (K^+ Transporter/ High-affinity K^+ transporter) transporters and the CPA (Cation Proton Antiporter) transporters. Due to different authors using different names, the name KT/HAK/KUP was given to the family of symporters of K^+ and H^+, and the TRK/HKT family refers to symporters of K^+ and Na^+ (Quintero et al., 1997, Santa-Maria et al., 1997, Fu et al., 1998, Kim et al., 1998, Haro et al., 1999, Kato et al., 2001, Maser et al., 2002, Gierth and Maser, 2007). However, there has been no evidence that these two families of K^+ transporters are involved in stomatal function. Rather, they are found mostly in root cells taking up K^+ for plant growth and maintaining homeostasis under salinity and drought conditions (Rubio et al., 2000, Elumalai et al., 2002, Osakabe et al., 2013, Chen et al., 2015). Lastly, within the big family of CPA are three groups of antiporters: the Na^+, K^+ /H^+ exchangers (NHX), the K^+ efflux antiporter (KEA) and cation/H^+ exchangers (CHX). Like the other two families of transporters, CPA is also known for its role in maintaining homeostasis and assisting in salt tolerance (Almeida et al., 2017, Jia et al., 2018). However, several CPA genes including NHX1, NHX2 and CHX20 were found highly expressed in guard cells. Double mutants *nhx1/nhx2* showed impairment in plant growth and stomatal

function and mutants *chx20* showed reduced stomatal opening in response to light (Padmanaban et al., 2007, Barragán et al., 2012).

1.1.4.3. Anion transporters

Unlike in animals, where chloride is the most abundant anion, in plants, the two types of anions found most abundantly are malate and nitrate. There are four gene families encoding anion channels/transporters in plants: the CLC family, the ALMT/QUAC family, the SLAC family, and the nitrate transporters (NRT) family.

The CLC family. The CLC family in plants were identified based on homologs of the CLC genes in animals. Although being called the chloride channel, this family contains both Cl- channels and Cl^-/H^+ antiporters (Jentsch, 2008, Lisal and Maduke, 2009). In *Arabidopsis*, seven CLC genes were identified, from CLCa to CLCg. Interestingly, the CLCa protein in *Arabidopsis* was found to be a NO_3^-/H^+ antiporter (De Angeli et al., 2006). Since CLCa is highly similar to the other six CLC genes (up to 87%), it was suggested that they potentially share the same properties (Zifarelli and Pusch, 2010). CLCc was found highly expressed in guard cells and plays a role in regulating stomatal movement. In the *clcc* mutant, stomata failed to close in response to ABA and had reduced opening in response to light, thus demonstrating that CLCc plays a crucial role in stomatal movement (Jossier et al., 2010).

The ALMT family. The ALMT family was first identified in wheat (*Triticum aestivum*), and mostly found in root cells (Sasaki et al., 2004). As its name suggests, the *Ta*ALMT1 channel transports malate and is aluminum sensitive. This family was first thought to play significant roles in aluminum resistance (Sasaki et al., 2004). Under high aluminum soil conditions which are toxic to plants, malate is extruded from these channels to chelate the harmful cations. The ALMT1 gene in other species such as *Arabidopsis* (*At*ALMT1), canola (*Bn*ALMT1) and soybean (*Gm*ALMT1)

have also been shown to have similar functions (Hoekenga et al., 2006, Ligaba et al., 2006, Liang et al., 2013).

Other members of the ALMT family have been identified and studied extensively. Interestingly, unlike ALMT1, most other ALMT members are not involved in aluminum resistance, but in other functions such as fruit acidity and stomatal functions. This is consistent across many species including wheat, corn, rice, grape, apple, tomato, etc. (Sasaki et al., 2010, Meyer et al, 2011, Ligaba et al., 2012, Bai et al., 2012, De Angeli et al., 2013, Liu et al., 2017). Many of these ALMT genes are found located in other parts of plants rather than in root apices. In *Arabidopsis*, *At*ALMT4, *At*ALMT6, *At*ALMT9 and *At*ALMT12 are all found in guard cells and are involved in stomatal movement (Eisenach et al., 2017, Meyer et al., 2011, De Angeli et al., 2013, Meyer et al., 2010). Beside malate, channels of the ALMT family are also permeable to Cl^-, NO_3^- and even SO_4^{2-} (Pineros et al., 2008). Furthermore, the *At*ALMT12 gene was shown to be insensitive to aluminum salts (Meyer et al., 2010).

QUAC versus SLAC. Using the patch-clamp technique, Schroeder and Keller (1992) distinguished that there are at least two types of anion channels: the rapid type (R-type) and the slow type (S-type) present in the plasma membrane of guard cells. The R-type channels can be fully activated and rapidly inactivate within milliseconds, while the S-type channels can take up to several tens of seconds to be fully activated, followed by a slow inactivation of the channels. In 2008, the first S-type anion channel in guard cells was identified and named SLAC1 (Slow anion channel 1) (Vahisalu et al., 2008). Several SLAC1-homologous (SLAH) proteins, SLAH1 to SLAH4, have been identified since, and shown to accumulate and translocate Cl^- and NO_3^- from root to shoot (Maierhofer et al., 2014, Cubero-Font et al., 2016, Qiu et al., 2016). Additionally, SLAH3, along with SLAC1, were also shown to inhibit the inward K^+ channels KAT1 and KAT2

dramatically, thus functioning as negative regulators of stomatal opening (Deger et al., 2015, Zhang et al., 2016). In 2010, the *Arabidopsis* ALMT12 gene from the ALMT family was shown to encode an R-type anion channel in guard cells and renamed to QUAC1 (Quick anion channel 1) (Meyer et al. 2010). Details of the QUAC channel are described in the next section.

The NRT family. Nitrate is a nutrient that is vital for plant health and development. The NRT is a large family of NO_3^- and H^+ symporters, consisting of three subgroups: NRT1, NRT2 and NRT3. NRT1 genes encode for low-affinity nitrate transporters and NRT2 genes encode for high-affinity nitrate transporters. Most of the NRT2 genes have been shown to require a nitrate accessory protein (NAR) to function (Quesada et al., 1994, Zhou et al., 2000, Yong et al., 2010, Kotur et al., 2012.). Xenopus oocytes injected with NAR2 and NRT2.1 genes separately failed to produce nitrate currents (Zhou et al., 2000, Tong et al., 2005), indicating the NAR2 genes facilitate NRT2 transport activity. Thus, NAR2 was proposed to be named NRT3. Most NRTs are involved in the nitrate uptake from soil and transportation of nitrate from root to shoot. However, the NRT1.1 in *Arabidopsis* was reported to be expressed in guard cells, and the *nrt1.1* mutant impaired in stomatal opening in response to light (Guo et al., 2003).

1.1.4.4. H^+ transporters

H^+ in plants is actively transported by carriers (symporters, antiporters) and pumps. Proton carriers, including CAX, KT/HAK/KUP/, CPA, CLC, NRT, have been described in the above sections, as they cotransport H^+ and other ions.

Proton pumps. There are two main types of proton pumps: the H^+-ATPase and H^+-PPase (H^+ pyrophosphatase). Pyrophosphate is a by-product of several reaction processes such as polymerization of DNA and protein synthesis. While H^+-ATPase breaks down ATP for energy, H^+-PPase breaks down pyrophosphate for energy to pump protons across. H^+ pumps play

important roles in many plant activities, such as regulation for ion homeostasis, nutrient transporters, regulating plant growth, and regulating stomatal movement. The plasma membrane H^+-ATPase in guard cells is especially crucial for stomatal opening in response to blue light (Wang et al., 2014, Yamauchi et al., 2016, Inoue and Kinoshita, 2017).

Regulation of H^+-ATPase via blue light. Plants have blue light receptors called phototropins (PHOT1 and PHOT2). Phototropins contain a light sensing domain and a serine/threonine protein kinase domain. When the receptor senses blue light, it is stimulated by autophosphorylation and binds to 14-3-3 proteins (Tseng et al., 2012). The 14-3-3 proteins then bind to and activate H^+ATPase in guard cells by phosphorylation (Kinoshita and Shimazaki, 1999).

1.1.5. Regulation of stomatal movement

Current clamp recordings showed resting potentials between -60 and -160 mV for guard cells (Schroeder, 1987). Hyperpolarization and depolarization of the guard cell membrane trigger the activation of outward rectifying K^+ and inward rectifying K^+ channels, respectively. This, subsequently, results in the opening and closing of stomata.

1.1.5.1. Opening stomata

Stomata opening can be induced by light, especially blue light (Darwin 1989, Shimazaki et al., 2007). As described above, in the presence of light, the light receptor phototropin is stimulated and activates H^+-ATPase, which pumps H^+ out of guard cells (Assmann et al., 1985, Shimazaki et al., 1986, Kinoshita and Shimazaki, 1999). The efflux of H^+ hyperpolarizes the plasma membrane, leading to the activation of the voltage-gated inwardly rectifying K^+ channels, such as KAT1, KAT2, AKT1 (Schroeder et al., 1987). Ions moving into guard cells followed by osmosis increase the turgor pressure, causing stomata to open (Figure 1.8A). Since the influx of K^+ should be accompanied by the influx of anions, several research groups have proposed the

involvement of H^+/Cl^- symporters in stomatal opening (Assmann and Wang, 2001, Dietrich et al., 2001). Guo et al., (2003) showed that the H^+/NO_3^- symporter NRT1.1 is expressed on the plasma membrane of guard cells and functions in stomatal opening. In addition to activating the proton

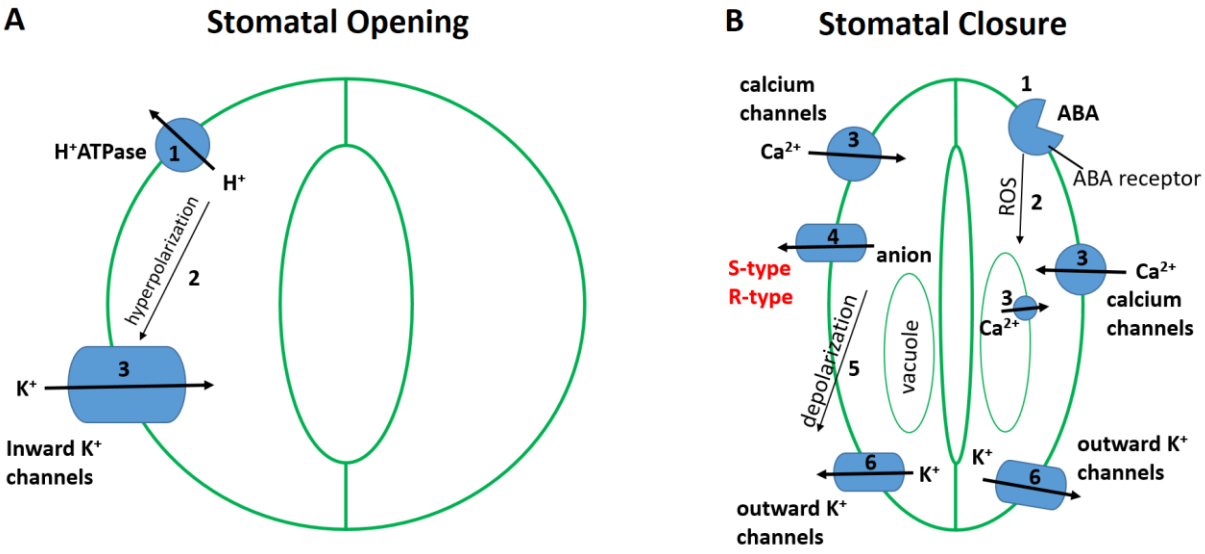

Figure 1. 8. Mechanism of stomatal movement

A. Stomatal opening. Protons leave guard cells through the proton pump H^+-ATPase (1), causing hyperpolarization of the plasma membrane (2), which in turn activates the inwardly rectifying potassium channels (3). Movement of the potassium ions and water (via osmosis) into guard cells increases the turgor pressure and opens stomata. **B. Stomatal closure.** ABA binding to its receptors (1) stimulates the production of reactive oxygen species (ROS) (2). Increased ROS stimulates release of Ca^{2+} from the vacuole into the cytosol and influx of Ca^{2+} across the guard cell membrane through Ca^{2+} permeable channels (3). High cytosolic Ca^{2+} concentration then stimulates the activation of membrane anion channels, resulting in an efflux of chloride and other anions (4). The efflux of anions depolarizes the guard cell membrane potential (5), which in turn activates the outward rectifying potassium channels (6). Outward movement of potassium ions decreases the turgor pressure of guard cells and closes stomata.

pump H^+-ATPase, phototropins also inhibit the activity of S-type anion channels, which prevents anions from leaving guard cells, maintaining a high turgor pressure (Marten et al., 2007).

1.1.5.2. Closing stomata

When photosynthesis is not occurring, and the CO_2 level is high, or if the air is too dry or hot, plants will signal for stomatal closure. One of the primary signaling pathways for stomatal closure involves the plant hormone ABA.

ABA is a hormone originally believed to be involved in the abscission process of plants, thus given the name abscisic acid. However, further studies showed it is the hormone ethylene, rather than ABA, that triggers abscission, and ABA only promotes abscission through ethylene (Morgan and Durham 1973, Brown, 1997). Nonetheless, ABA plays many important roles in plant developmental processes and plant responses to biotic and abiotic stress, such as dormancy, germination, cold, heat, drought tolerance, and stomatal function (Tuteja, 2007, Nakashima and Yamaguchi-Shinozaki, 2013, Sah et al., 2016, Huang et al., 2017, Vishwakarma et al., 2017). ABA can be synthesized in guard cells for rapid stomatal response, but mostly is synthesized in the vascular tissues in leaves, where many ABA biosynthesis enzymes are localized (Koiwai et al., 2004, Kuromori et al., 2014, Merilo et al., 2015). Since guard cells are in the epidermal layers of plants, and vascular tissues are inside the plant body, ABA has to be transported from vascular tissues to guard cells to signal stomatal closure. Following this hypothesis, researchers have identified ABA transporters on both the vascular tissues and guard cell membrane (Kang et al., 2010, Kuromori et al., 2010, Kuromori et al., 2014, Meriolo et al., 2015).

When plants are under stress, ABA accumulates in guard cells and initiates the signaling pathway for stomatal closure. ABA binding to its receptors inhibits the protein phosphatase 2C (PP2C), a negative regulator of the Open Stomata 1 (OST1) kinase. Inhibition of PP2C

phosphatase releases and activates OST1 through autophosphorylation (Vlad et al., 2009). From here, ABA signals by either a Ca^{2+}-independent or Ca^{2+}-dependent pathway. In the case of the Ca^{2+}-independent pathway, OST1 directly activates the S-type and R-type anion channels, resulting in an efflux of chloride, malate and other anions (Lee et al., 2009, Geiger et al., 2009, Imes et al., 2013). The efflux of anions depolarizes the guard cell membrane potential, which then activates the outward movement of potassium ions and decreases the turgor pressure of guard cells, resulting in the closure of the stomata (Ward et al., 2009, Hosy et al., 2003). In the case of Ca^{2+}-dependent signalling, the OST1 kinase phosphorylates and activates the reactive oxygen species (ROS)-generating enzyme NADPH oxidase, which stimulates the production of ROS (Sirichandra et al., 2009). ROS are unstable molecules containing oxygen, such as superoxide anion (O_2^-), hydrogen peroxide (H_2O_2) and hydroxyl radical ($^{\bullet}OH$), formed by the reductions of oxygen, and therefore can easily react with other molecules. Mutations of the NADPH oxidase encoding genes (RbohD and RbohF) impair ABA-induced stomatal closing (Kwak et al., 2003). ROS, more specifically H_2O_2, stimulates the elevation of cytosolic Ca^{2+} levels by activating Ca^{2+} permeable channels on the plasma membrane of guard cells (Pei et al., 2000, Zhang et al., 2001). Patch clamp studies showed an increase in the activities of the Ca^{2+} channel with increasing H_2O_2 concentrations (Pei et al., 2000). This is consistent with the findings that ABA triggers Ca^{2+} channel activities and increases cytosolic Ca^{2+} of guard cells (Schroeder and Hagiwara 1990, Hamilton et al., 2000, Kohler et al., 2003). The high cytosolic Ca^{2+} concentration in guard cells then stimulates the activity of Ca^{2+} -dependent protein kinases (CPKs), which in turn activate the same S-type and R-type membrane anion channels as in Ca^{2+}-independent pathway, resulting in stomatal closure (Mori et al., 2006, Geiger et al., 2010, Brandt et al., 2012, Scherzer et al., 2012).

On a side note, increases in cytosolic Ca^{2+} concentration also inhibit the activities of both the H^+-ATPase pump and the inward rectifying K^+ channels, which are required for stomata opening (Kinoshita et al., 1995, Schroeder & Hagiwara, 1989, Blatt et al., 1990).

1.2. Quick anion channel (QUAC)

1.2.1. The effect of QUAC1 on stomatal closure

As an R-type anion channel in guard cells, QUAC1 plays an important part in stomatal closure. Prior to the renaming of ALMT12 to QUAC1, the effects of ALMT12 on stomatal functions, including stomatal conductance and aperture in responses to light/darkness, ABA, and CO_2, were investigated in two separate studies. Sasaki et al. (2010) showed that loss-of-function of the *At*ALMT12 results in impaired stomatal closure. Knockdown mutation of *At*ALMT12, (*Atalmt12-1*) showed a larger aperture in response to darkness, Ca^{2+} and exogenous ABA compared to wildtype. Furthermore, the *atalmt12-1* plants had a higher rate of water loss and were more susceptible to drought (Figure 1.9) (Sasaki et al., 2010). Meyer et al., (2010) also showed the *atalmt12* knockdown plants had suppressed stomatal closure in response to ABA and CO_2, and a much slower decline of stomatal conductance in response to darkness. Taken all together, the ALMT12/QUAC1 gene is an essential component in regulating the function of stomata.

1.2.2. Molecular characteristics and functional domain of QUAC1

Like other members of the ALMT family, QUAC1 also contains an ALMT (PF11744) domain. In 2004, the first ALMT gene was first discovered in wheat by Sasaki et al. Since then, researchers had identified other members of the family by using either the wheat *Ta*ALMT1 gene or the UPF005 (uncharacterized protein family five) domain as a search sequence (Delhaize et al.,

Figure 1. 9. Wildtype and mutant of Arabidopsis plants in response to drought

Image from Sasaki et al., 2010. One-week-old *Arabidopsis* plants were subjected to water withholding for a further two weeks. Under drought, plants close stomata to prevent water loss. However, the knockdown mutant *almt12-1* impaired stomatal responses, thus became more susceptible drought.

2007, Hoekenga et al., 2006). The UPF005 domain has now been renamed to Bax1-I (Inhibitor of apoptosis-promoting Bax1, PF01027), and the ALMTs have been moved to their own group (Aluminum activated malate transporter, PF11744). The PF11744 domain has been shown to be highly conservative with five to seven transmembrane domains at the N-terminus, a WEP fingerprint motif (Trp-Glu-Pro) (Delhaize et al., 2007, Dreyer et al., 2012). The glutamate in the WEP-motif is thought to be involved in the ALMT channel activation (Furuichi et al., 2010), though the function of the motif remains unknown.

Predictions of the secondary structure of QUAC1 also show six alpha helix transmembrane domains at the N-terminus and a large soluble C-terminal domain (Figure 1.10). Aside from the ALMT domain, little information is available about the structure and functional domains of QUAC1.

1.2.3. The regulations of *At*QUAC1 activities

Although originating from the ALMT family, *At*QUAC1 is not aluminum sensitive, and the activation of the *At*QUAC1 channel does not require Al^{3+}. Instead, *At*QUAC1 activation is malate and voltage-dependent (Meyer et al., 2010). Both in the presence and absence of Al^{3+}, injection of malate into *At*ALMT12-expressing oocytes caused a significant increase in the recorded currents of oocytes (Meyer et al., 2010). Beside the *At*QUAC1 (*At*ALMT12) channel, the *At*ALMT9 channel has also been shown to be activated by cytosolic malate, but this channel transports mainly Cl^- ions (De Angeli et al., 2012). In addition to the regulation by malate, co-expression of *At*QUAC1 and OST1 in oocytes showed a much pronounced activation compared to expression of *At*QUAC1 alone, and the QUAC1-type currents of guard cell protoplasts were shown to be induced by ABA (Imes et al., 2013).

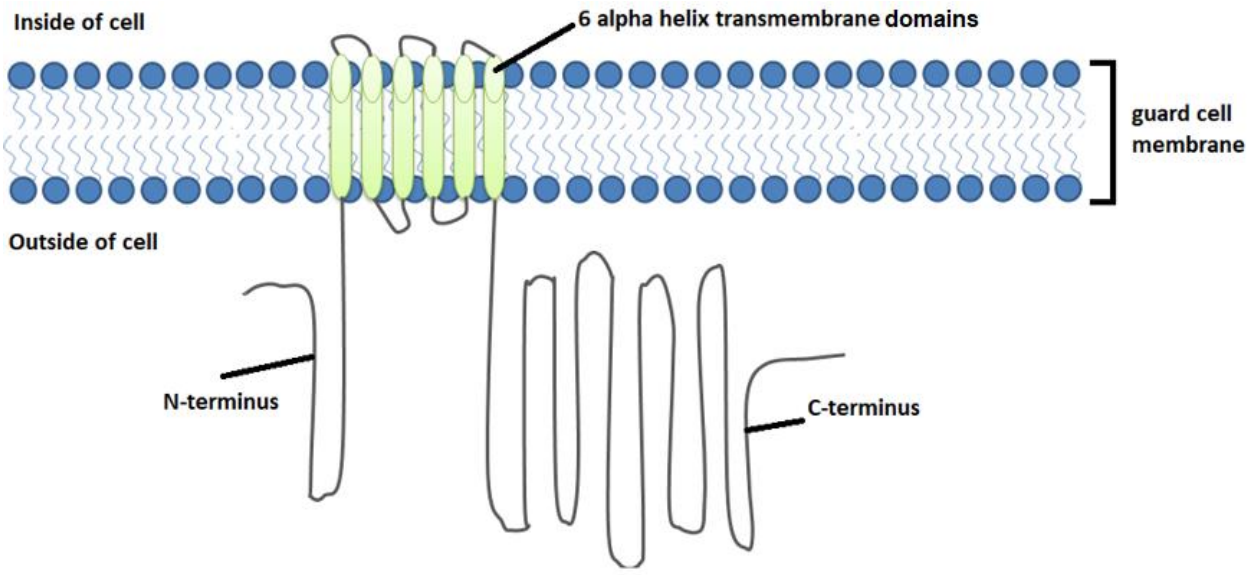

Figure 1. 10. Secondary structure of QUAC1

Both the S-type and R-type channels are regulated through ABA signaling pathways, which have been described briefly in the closing stomata section. Main components in this pathway include: ABA, ABA receptors, PP2C phosphatases, OST1, CPK, ROS, Ca^{2+} channels, and anion channels (SLAC and QUAC).

ABA receptors are the first main component in the pathway by which QUAC1 is regulated. There are three types of ABA receptors grouped together based on their subcellular locations: on the chloroplast envelope, on the plasma membrane, and in the cytosol. The first receptor ChlH/ABAR/CCH/GUN5 (Mg^{2+}-chelatase H subunit/Abscisic Acid Receptor/Conditional Chlorina/Genome Uncoupled 5) localized on the chloroplast is an ABA-binding protein and was shown to mediate ABA responses such as seed germination, and stomatal movement (Zhang et al., 2002, Shen et al., 2006, Wu et al., 2009). The second group of ABA receptor consists of GCR2 (G-protein coupled Receptor 2) and GTG (GPCR-type G proteins), both localized on the plasma membrane. Whether GCR2 is an ABA receptor is still controversial. The protein was initially reported to interact with the G protein α subunit and proposed to be involved in all ABA responses including the expression of ABA-responses genes, stomatal movement, and seed germination, and identified as an ABA receptor (Liu et al., 2007). However, in further studies, *gcr2* mutants did not show insensitivity to ABA, and double mutants of *gcr2* and its homolog showed wild-type phenotype in response to ABA (Gao et al., 2007, Guo et al., 2008). The GTG proteins were also identified due to their sequence similarity to the (G-protein coupled receptor) GPCR protein and interaction with the G protein α subunit (Pandey et al., 2009). The same authors showed that GTG bound to ABA and the knockout *gtg1/gtg2* mutant caused ABA hyposensitivity in seed germination, thus suggesting the GTG proteins to be ABA receptors. Additionally, in an independent study, ABA was again shown to bind the GTG1 protein in both *Sacaromycese*

cerevisiae and *in vitro* (Kharenko et al., 2013). The last group of ABA receptors is the PYR/PYL/RCARs (Pyrabactin Resistance / PYR-like / Regulatory Component of ABA Receptor) localized in the cytosol. Pyrabactin is an ABA agonist and was isolated as a seed germination inhibitor (Zhao et al., 2007). The PYR genes were found and isolated through screening for pyrabactin-resistant mutant alleles in *Arabidopsis* (Park et al., 2009). At the same time, the RCAR genes were identified based on their ability to bind to ABA, and regulate the ABA signaling pathway by inhibiting PP2Cs (Ma et al., 2009). Thus, the family of PYR/RCAR proteins was recognized as ABA receptors (Park et al., 2009, Ma et al., 2009). Since then, other research groups have also shown that PYRs are major PP2C-interacting proteins and play an important role in ABA signalling (Nishimura et al., 2010, Antoni et al., 2013).

PP2C, which acts downstream of ABA receptors, belongs to the large family of protein serine/threonine phosphatases in animals and plants. In animals, the phosphatases are classified into four groups: PP1, PP2A, PP2B, and PP2C based on their target substrates and inhibitors (Ingebritsen and Cohen, 1983). However, there are only three groups in plants: the PP1, PP2A and PP2C as the homologs of mammalian PP2B have not yet been found. PP1, PP2A and PP2B have similar amino acid sequences in the catalytic subunit, and therefore form their own family referred to as the PPP (Phospho-protein phosphatases) family of protein serine/threonine phosphatases. PP2C by itself forms a PP2C family, also known as the PPM (metal-dependent protein phosphotase) family since PP2C phosphatases require either Mg^{2+} or Mn^{2+} for their enzymatic activities (Cohen, 1989). In plants, PP2C is the largest family of phosphatases, accounting for up to 65% of phosphorylases (Singh et al., 2010). PP2C phosphatases are known to negatively regulate ABA signaling since the discovery and isolation of the ABA-insensitive 1 (ABI) and ABA-insensitive 2 (ABI2), phosphatases that has high sequence homology with PP2Cs

(Leung et al., 1994, Meyer et al., 1994, Leung et al., 1997, Gosti et al., 1999). Mutations of ABI1 and ABI2 causes ABA insensitivity (Leung et al., 1997, Gosti et al., 1999). To date, other PP2C phosphatases that regulate ABA signal transduction have also been identified, such as HAB1, HAB2 (Homology to ABI1), HAI1, HAI2, and HAI3 (Highly ABA-induced PP2C) (Rodriguez et al., 1998, Saez et al., 2004, Yoshida et al., 2006).

OST1, a target of PP2C is a kinase belonging to the SnRK2 [SNF1 (sucrose non-fermenting-1)-related protein kinase 2] family. Members of this family are serine/threonine kinases involved in ABA responses including stress responses and plant development. Some of the earlier-identified members of SnRK2 include the NtOSAK (*Nicotiana tabacum* osmotic stress-activated protein kinase) kinase and the AAPK (ABA-activated protein kinase) kinase (Mikolajczyk et al., 2000, Li et al., 2000). Mutation of AAPK in *Arabidopsis* blocks ABA-activation of anion channels and impairs stomatal closure in response to ABA (Li et al., 2000). To date, ten members of the SnRK2 family have been identified in *Arabidopsis* as well as in rice. The OST1 kinase, also called SnRK2.6) has been recognized as one of the main components in regulating stomatal response (Mustilli et al., 2002, Yoshida et al., 2002).

In the absence of ABA, PP2C phosphatases, such as ABI1 and ABI2, bind to and inhibit the activities of CPK and OST1 by dephosphorylation (Yoshida et al., 2006, Geiger et al., 2010, Zhou et al., 2012, Soon et al., 2012). In the presence of ABA, ABA receptors PYL/PYR/RCAR upon binding to ABA, interact with and inhibit the activities of PP2Cs (ABI1, ABI2, ABI3) (Park et al., 2009). This initiates the Ca^{2+}-dependent and Ca^{2+}-independent ABA signalling pathways as described in section 1.1.5.2 (Figure 1.11). SLAC proteins, including SLAC1, SLAH3, have been reported to be regulated by both the CPK and OST1 kinases (Geiger et al., 2010, Brandt et al.,

2012). Although the association between QUACs and CPK remains unexplored, it is very possible that the protein CPK also regulates QUAC1 activity (Figure 1.11).

1.3. The role of Ca^{2+} and CaM in stomatal aperture

1.3.1. A brief overview of Ca^{2+} and plant CaM

Ca^{2+} dependent anion channels have been studied extensively in mammalian systems. In recent years, increasing numbers of studies have reported the link between CaM and anion channels (Yang and Colecraft, 2016, Tian et al., 2010). Ca^{2+} is a critical intracellular secondary messenger in plants. It is involved in many signal transduction pathways that regulate daily activities such as stomatal functions and transpiration to plant defense responses against pathogen invasion and abiotic stresses. As such, the cytosolic Ca^{2+} level is increased in response to many environmental and physiological stimuli such as cold, heat, drought, light, dark, high CO_2, wounding, pathogen elicitors, and plant hormones. Elevation in cytosolic Ca^{2+} levels can be quickly detected by Ca^{2+} sensors. Most Ca^{2+} sensors can bind to Ca^{2+} using the EF-hand motif, which has a helix-loop-helix structure. Ca^{2+} sensors bound to Ca^{2+} undergo a conformational change which allows their interactions with other proteins or changes in their enzymatic activities, which can begin Ca^{2+} -mediated signal transduction. In plants, Ca^{2+} sensors have been clustered into three major classes: CaM, Ca^{2+} -dependent protein kinase (CPK) and calcineurin B-like protein (CBL).

CaM. CaM is a small messenger protein made of 148 amino acid residues. The protein has a simple structure - two globular domains connected by a central alpha-helix. Each globular domain has three alpha-helices, forming two Ca^{2+} -binding EF-hands (Chattopadhyaya, 1992)

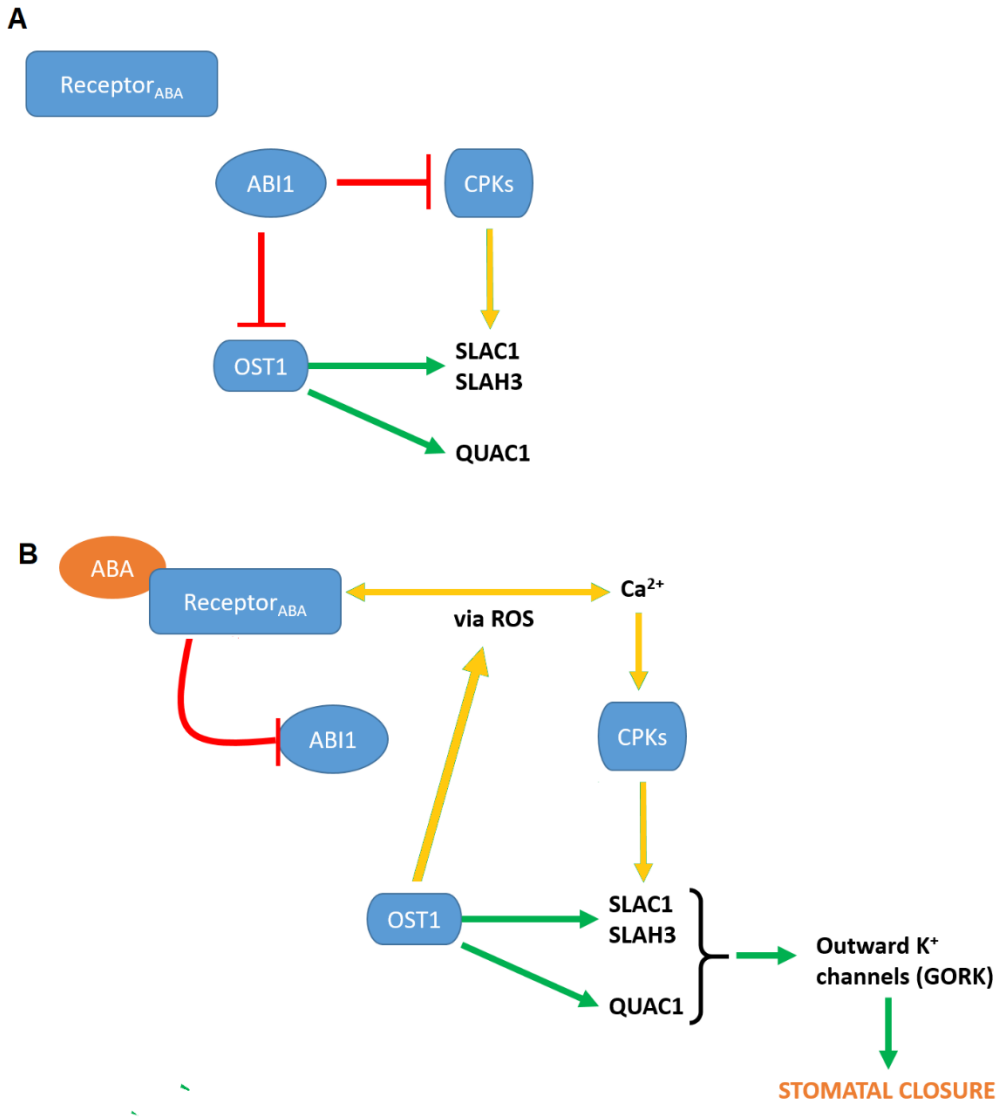

Figure 1. 11. Regulation of QUAC1/SLAC1 through ABA signaling pathways

Red arrows indicate inhibition. Green and yellow arrows indicate activation under Ca^{2+} -independent and Ca^{2+} -dependent pathway, respectively. A) In the absence of ABA, ABI1 (PP2C) inhibits CPKs and OST1. B) In the presence of ABA, ABA binding to its receptors inhibits the activities of PP2C phosphatase ABI1. CPKs and OST1 kinases are released from ABI1 inhibition. In the Ca^{2+} -independent pathway, OST1 phosphorylates and stimulates the activation of anion channels QUAC1, SLAC1 and SLAH3. In the Ca^{2+} -dependent pathway, beside ABA, OST1 also stimulates ROS production through phosphorylation of the NADPH oxidase. ROS in turn activates Ca^{2+} permeable channels on the membrane of guard cells which results in an elevation of cytosolic Ca^{2+} level (Pei et al., 2000, Zhang et al., 2001). The cytosolic Ca^{2+} then stimulates the activity of CPKs which phosphorylate the same anion channels, leading to stomatal closure.

CBLs and CPKs. CBLs are Ca^{2+} sensors that have been identified only in plants. Unlike CPKs and CaM which have four Ca^{2+} binding EF hands, CBLs only have three EF hands. There have not yet been any studies regarding the conserved domains and motifs of CBLs. Nonetheless, CBLs are well known for their role in the CBL-CIPK (CBL-interacting protein kinase) network, which plays a vital role in Ca^{2+} signaling in response to stress (Luan, 2009, Mao et al., 2016).

CPKs are a large family of serine/threonine kinases in plants. The CPK proteins are much larger proteins compared to CBLs and CaM, and contain a kinase domain which CBLs and CaM do not possess. The CPK kinases contain four domains: the protein kinase domain, the Ca^{2+} -binding domain, the N-terminus variable domain and the autoinhibitory junction. (Harmon et al., 2001). Like other Ca^{2+} sensors, there has been increasing evidence supporting the important role of CPK in various physiological processes including plant stress responses and plant growth (reviewed in Arimura and Maffei 2010, and Gardette et al., 2014).

1.3.2. The structure of CaM binding domains

As an important component in the Ca^{2+} signal transduction pathways, CaM as well as its targets, CaM binding domains, have been studied extensively and are well characterized. CaM-binding proteins contain a basic amphiphilic alpha helix. This helix is the CaM binding domain, which CaM binds to specifically (Figure 1.12). Most CaM-binding domains have been identified as 15 to 20 amino acid peptides, in the form of an alpha helices with one side being hydrophobic and the other having basic residues predominantly (O'Neil & DeGrado, 1990, Dash et al., 1997).

1.3.3. The mechanism of CaM binding to target proteins

CaM, after binding to Ca^{2+} ions, undergoes conformational changes such that the hydrophobic methyl groups of the methionine residues become exposed to the surface (LaPorte et

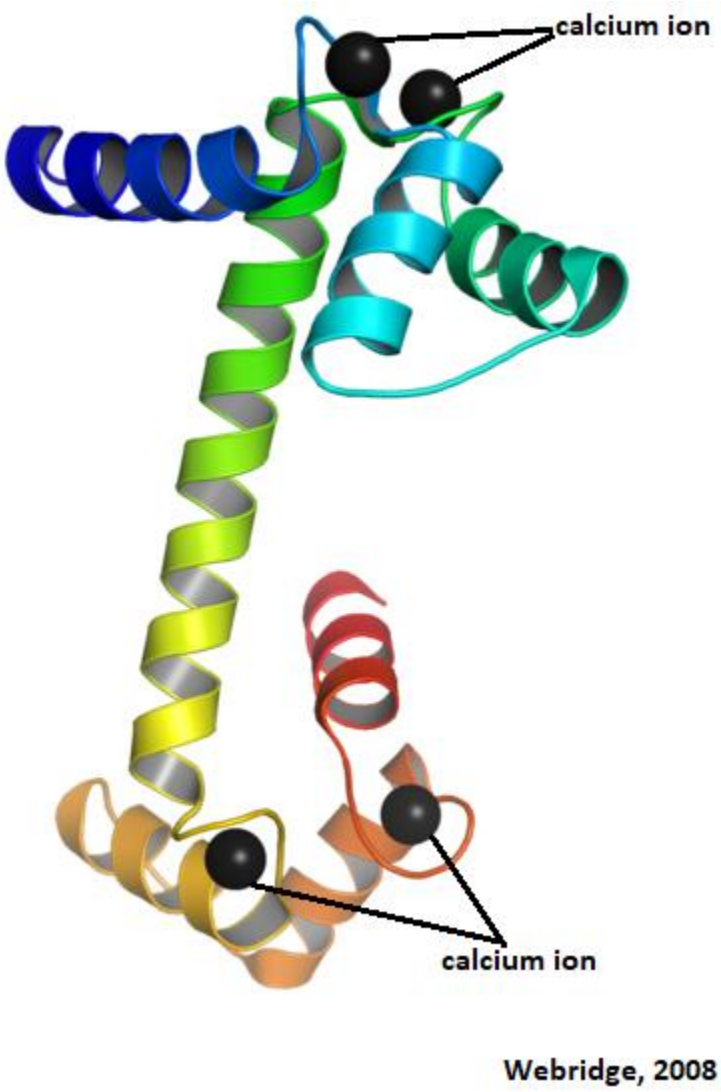

Figure 1. 12. The structure of CaM

Two globular domains are connected by a central alpha-helix. Each globular domain has three alpha-helices, forming two EF-hands for Ca^{2+} binding.

al., 1980, Siivari et al., 1995). This hydrophobic side then binds to the basic amphiphilic alpha helix of the target protein and stimulates activities of the protein (Cox, 1985) (Figure 1.13).

1.3.4. The effect of Ca^{2+} and CaM on stomata

As described in previous sections, stomatal aperture is modulated mainly through the ABA signaling pathways. For decades, extensive research has been done to investigate the involvement of Ca^{2+} and CaM in response to ABA. Ca^{2+} ions, Ca^{2+} ionophores and Ca^{2+} -channel blockers, CaM binding drugs and CaM inhibitors have all been shown to affect stomatal movement (Donovan et al., 1985, De Silva et al., 1985a, De Silva et al., 1985b, Nejidat et al., 1987, Schwartz et al., 1988, Gilroy et al., 1991). De Silva et al., 1985a showed that stomata closure could be triggered by simply incubating the leaf epidermis in $CaCl_2$ solution. In *Commelina communis*, stomata failed to close in response to ABA upon treatment with either the Ca^{2+} channel blockers Verapamil, Nifedipine, and Lanthanum or the CaM antagonists Trifluoperazine, W-7 and Compound 40/80. The authors had tested a variety of Ca^{2+} and CaM inhibitors in the studies, nonetheless, the outcome from the experiments was consistent (De Silva et al., 1985b, Donova et al., 1985). Additionally, the inward rectifier K^+ channels required for stomatal opening and the anion channels required for stomatal closure have been shown to be regulated by cytosolic Ca^{2+} (Schroeder & Hagiwara, 1989, Keller et al., 1989). As mentioned above, studies in mammalian systems have shown CaM regulating anion channels, particularly chloride channels, such as TMEM16A and 16B (Yang and Colecraft, 2016). However, to date, whether CaM directly interacts with or regulates anion channels in plants remains unexplored.

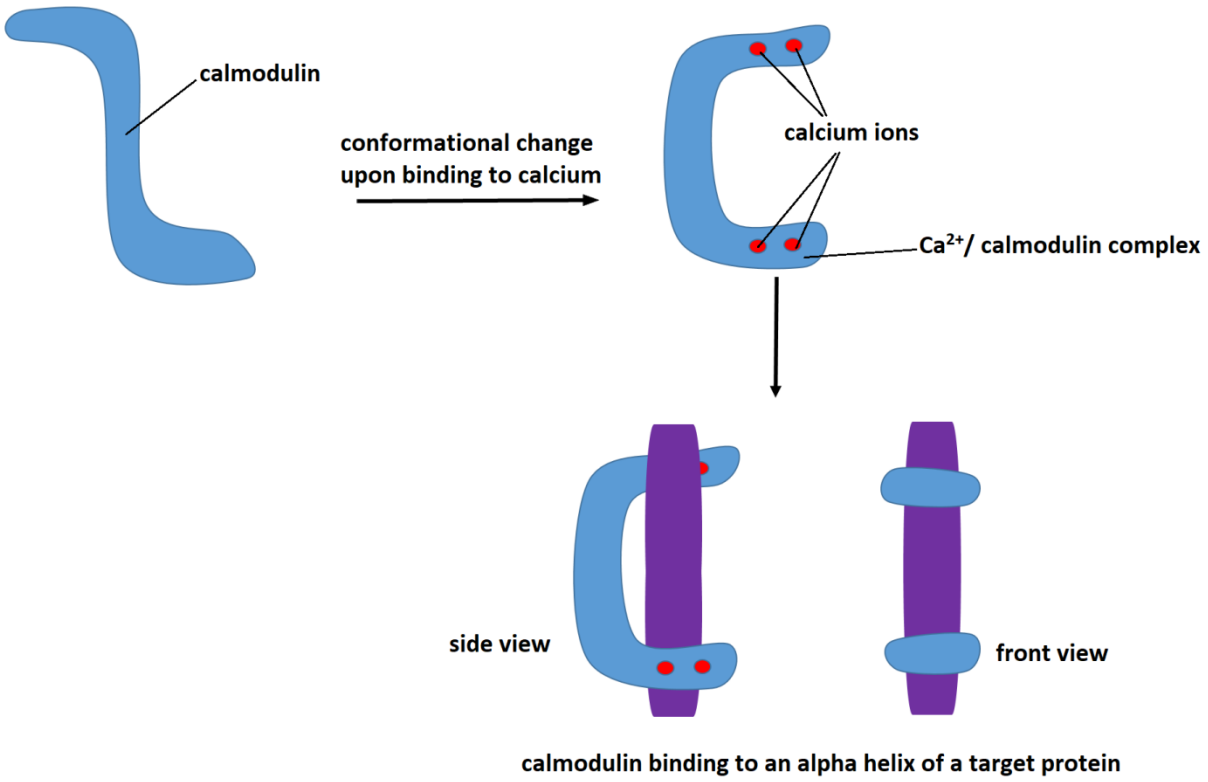

Figure 1. 13. Mechanism of CaM binding

Figure adapted from Das et al., 2013. CaM has 2 EF hands on each terminus for Ca^{2+} binding. After binding to Ca^{2+}, CaM goes through a conformational change and becomes an active Ca^{2+} - CaM complex which binds to the target protein and stimulates its activities.

1.4. Stomata and Wheat rust infection

1.4.1. Wheat rust diseases and the three types of wheat rusts

Although stomata play a crucial role in plants' adaptation to the environment, they are also responsible for being the route of entry for disease infections. Most pathogens infect plants through stomata openings, including rusts. Wheat rust diseases are one of the oldest diseases recognized in plants and have been known to cause devastating crop loss. Epidemic sites of wheat rust have been observed in South and Central America, Europe, Central Asia, East and Northern Africa, with most recent outbreaks in Argentina (2017) and in Ethiopia (2016), according to the International Maize and Wheat Improvement Center (CIMMYT) Rust tracker. Rust infection is favored by warmer climates and high humidity environments for infection. Once successfully infected, the disease can destroy the entire wheat crop, thus, wheat rust disease has been a global concern for decades. According to the American Phytopathological Society, it is estimated that more than 5 billion dollars are lost due to cereal rusts each year, globally.

There are three types of rust diseases in wheat: leaf rust, stem rust, and stripe rust, caused by the fungus *Puccinia triticina, Puccinia graminis and Puccinia striiformis*, respectively. Rusts are biotrophic pathogens as they take nutrients from the host plants via haustoria. All three types of rust diseases have similar symptoms, which are pustules producing rust spores. However, each type of rust can be distinguished by the sites of infection, and the colors and sizes of pustules. Pustules of leaf rust are smaller, reddish-orange and are generally observed on the leaves of infected plants (Figure 1.14A). Stem rust occurs primarily on the stems of infected plants, but can also be found on leaves and spikes. While leaf rust is more clustered, stem rust appears scattered and has a brownish-black color (Figure 1.14B). Stripe rust occurs on the leaves and spikes of

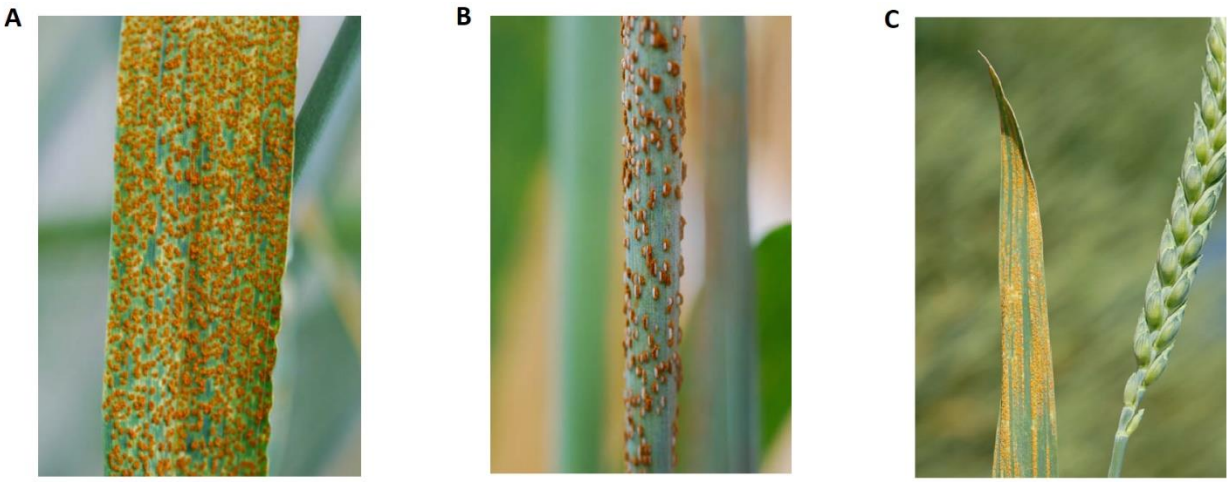

Figure 1. 14. Pustules caused by rust diseases

A. Leaf rust. **B.** Stem rust. **C.** Stripe rust.

infected plants and is distinguished by its light-yellow pustules arranged into stripes (Figure 1.14C).

1.4.2. Life cycle of rusts

The life cycle of wheat rusts includes five different types of spores formed on two host plants: a primary host, wheat, and an alternate host, such as barberry (Bolton et al., 2008). After infection, thousands of urediniospores are produced inside a pustule. Urediniospores can be spread by wind to a neighboring plant or another wheat field. Each urediniospore is capable of infecting another wheat plant and producing another pustule. At the end of the wheat growing season, instead of urediniospores, the fungus produces overwintering spores called 'teliospores'. As teliospores mature, the two haploid nuclei inside fuse together and spore-walls thicken, which allow their survival through the fall and the winter. In the spring, teliospores germinate and produce haploid spores called 'basidiospores' through meiosis. These basidiospores don't infect wheat but instead infect another alternate host such as barberry. Upon infection, basidiospores produce reproductive spores called 'pycniospores' and receptive hyphae on the upper surface of barberry leaves. Once fertilized by pycniospores, hyphae continued to grow and produce pustules containing aeciospores, on the lower side of barberry leaves. Aeciospores travel by wind to other wheat fields and directly infect wheat plants, generating thousands of urediospores and pustules, and thus the cycle continues (Figure 1.15) (Alexopoulus et al., 1996).

1.4.3. The process of infection and interaction with host-plant

Infection is initiated by a germinated aeciospore or urediniospore. Upon contact with moisture such as dews, urediniospores develop germ tubes which grow along the leaf surface until a stomata is reached. The germ tube then forms an appressorium on top of the stomata and the

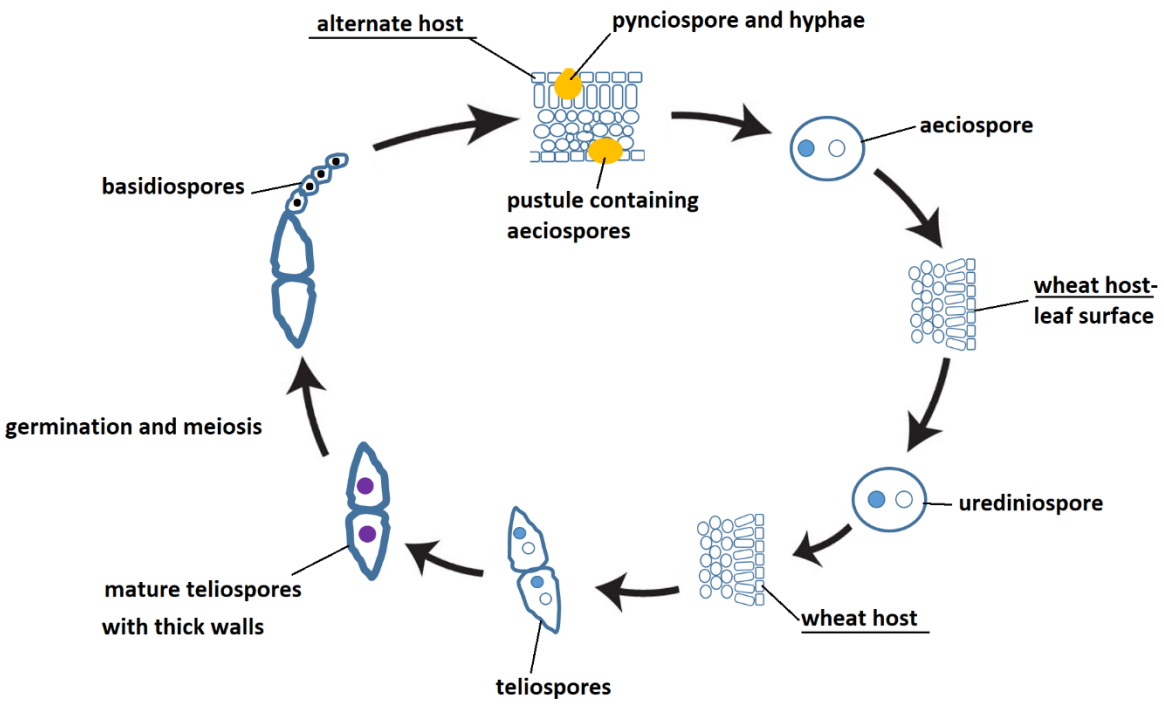

Figure 1. 15. The life cycle of wheat rust

Adapted from Alexopoulus et al., 1996. Aeciospores after infecting wheat plants produce thousands of urediniospores. A single urediniospore can again infect nearby plants. At the end of wheat seasons, teliospores are produced instead of urediniospores. As teliospores mature, the spore-walls thicken, which allow the fungus to survive through the fall and the winter. In the spring, teliospores germinate and produce the haploid basidiospores through meiosis. Basidiospores infect the alternate host and produce the reproductive pycniospores and receptive hyphae on the upper surface of leaves. Once fertilized by pycniospores, hyphae continued to grow and produce pustules containing aeciospores, on the lower side of leaves. Aeciospores directly infect wheat plants and continue the cycle.

appressorium develops a penetration peg through the stomata. Once the penetration peg is inside the living plant cells, a substomatal vesicle is formed, followed by formation of haustoria cells which indicates successful infection (Figure 1.16) (Grambow 1977, Harder 1986a, Harder 1986b). Haustoria contain amino acid and sugar transporters which are used to transport nutrients from the plants to nourish the fungus (Staples, 2001, Voegele and Mendgen, 2003). The fungus continues invading the plant by forming haustoria and start producing urediniospores. Within two weeks of initial infection, pustules are formed containing thousands of urediniospores. These urediniospores can travel for miles by wind, infecting neighboring plants and plants from another wheat field, causing an epidemic level of infection.

To successfully infect plants after penetration, rusts are known to release toxins that force stomata to stay open or closed (Grimmer et al., 2012). The infection process and physiology of rust host-pathogen interactions have been studied extensively. Hart (1929) showed that stem rust could not enter through closed stomata. The number of infections was significantly lower when plants were kept in the dark right after rust-inoculation (Hart 1929). In contrast, Caldwell and Stone (1936) showed that leaf-rust is able to penetrate through both opened and closed stomata. In 1963, Yirgou and Caldwell again showed that the number of stem rust penetration increased significantly when plants were incubated in a CO_2-free environment right after rust treatment and decreased significantly in 5%-CO_2 or dark environment. Although the authors did not relate these conditions to stomatal behavior, other studies have shown that high atmospheric CO_2 and darkness are factors causing stomata closure, linking these latter correlations to the stomatal condition (Young 2006). In the same study, leaf rust penetration was reported to be independent of light and CO_2 (Yirgou and Caldwell, 1963). This outcome is consistent with Caldwell and Stone 1936 which had shown that leaf rust was able to penetrate through both opened and closed stomata.

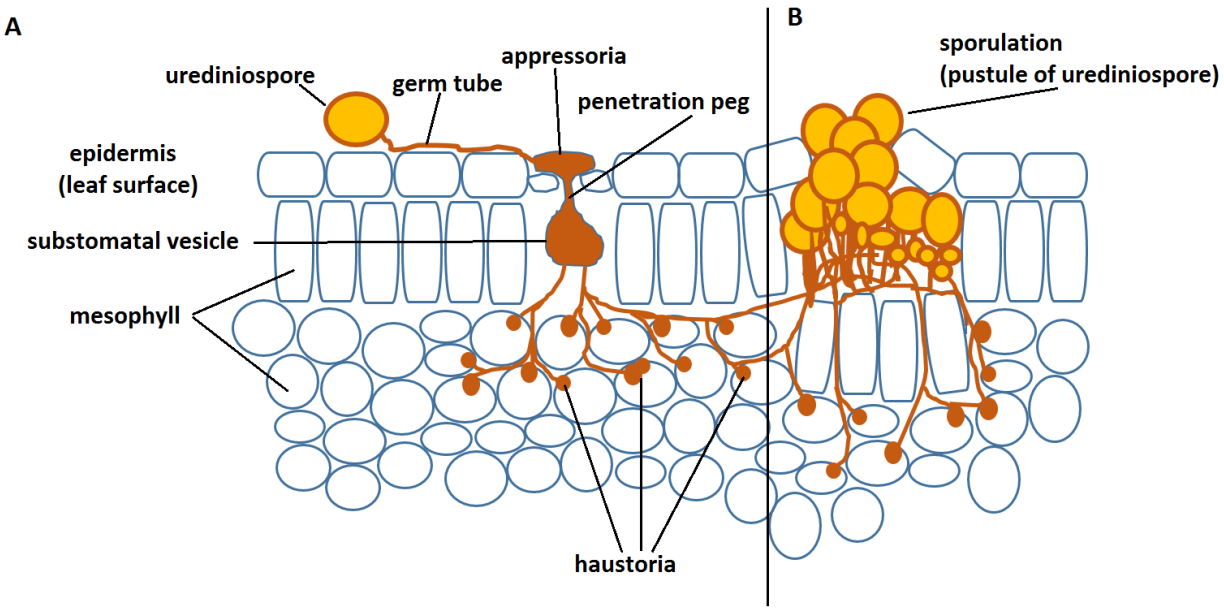

Figure 1. 16. The infection process of rust

A. Infection is initiated by a germinated urediniospore. Once the germ tube finds a stomata, an appressorium is formed on the epidermis. The appressorium then develops a penetration peg through the stomata. Once the penetration peg is inside the living plant cells, a substomatal vesicle is formed, followed by haustoria. The fungus continues to grow and spread until sporulation. **B**. Sporulation.

In contrast, there have not been any reports showing the ability of stripe rust to penetrate through closed stomata. However, stripe rust is quite different from both stem and leaf rust. Moldenhauer (2006) showed that stripe-rust does not form appressoria during penetration. Instead, germ tubes penetrate through stomata directly, then form substomatal vesicles. Nevertheless, Garnica et al. (2013) stated that although penetration often occurs without the formation of appressoria, stripe-rust is able to form appressoria over stomata prior to leaf penetration.

1.4.4. Rust resistance genes in wheat

Research scientists have spent much effort in identifying and characterizing rust-resistance genes. Some of the earlier resistance genes were discovered from rust-resistant cultivars almost 100 years ago (Mains et al., 1926, Ausemus et al., 1946). To date, nearly 200 resistance genes among the three rust types have been found derived from wheat cultivars (Aktar-Uz-Zaman et al., 2017), and these genes have been identified using PCR-based molecular markers and QTL mapping. The majority of proteins encoded by resistance genes belong to one of the following three families: cytoplasmic protein receptors with an NBS-LRR (nucleotide-binding sites-leucine-rich repeats) domain, lipid-transfer proteins with a START (Steroidogenic Acute Regulatory Protein related lipid-transfer) domain, or ABC (ATP-binding Cassette) transporters (Brueggeman et al., 2008, Liu et al., 2014, Krattinger et al., 2009, Krattinger et al., 2011). Mur et al., (2013) suggested that resistance genes and their signaling cascades could affect stomatal functions. Of the three mentioned domains, notably, the broader START protein family includes the ABA receptors belonging to the PYL/PYR family (Bhatla and Lal, 2018). This supports the hypothesis that ABA signalling events play an important part in rust resistance. Since a major route for pathogen entry

is arguably through opened stomata, components that are downstream of ABA receptors in signaling pathways of stomata closure, such as QUAC1, could affect pathogen infection.

2. HYPOTHESIS AND OBJECTIVES

2.1 Objectives

1. To determine whether *Brachypodium* QUAC1 activation is Ca^{2+} -dependent and involves binding to CaM.
2. To determine whether the activation of *Brachypodium* QUAC1 affect stomatal function and rust infection.

2.2 Hypotheses

1. *Brachypodium* QUAC1 channel is activated by malate and Ca^{2+}.
2. CaM effect *Brachypodium* QUAC1 activities.
3. CaM binds directly to *Brachypodium* QUAC1 and the binding affects the channel's activities.
4. QUAC1 affects rust infection through regulating stomatal opening.

This work has been published in The Journal of Biological Chemistry, titled 'The malate-activated ALMT12 anion channel in the grass *Brachypodium distachyon* is co-activated by Ca^{2+}/calmodulin'. doi: 10.1074/jbc.RA118.005301.

3. MATERIAL AND METHOD

3.1. Chemicals: All chemicals were purchased from Sigma-Aldrich unless otherwise noted below.

3.2. Plant materials and growth conditions

Brachypodium distachyon (Bd21) (BioResource Research Center) wild-type plants were used for the study. *Brachypodium distachyon* is widely used as a monocot model system due to its smaller size and ease of cultivation (Brkljacic et al., 2011, Scholthof et al., 2018). The seed-to-seed cycle of *Brachypodium* is shorter compared to other cereal crops, and therefore, is an advantage for generating transgenic plants. Importantly, genomic studies showed close evolutionary relationships between *Brachypodium* and other monocot species such as rice, wheat, corn (Draper et al., 2001). The plants were grown in chambers with the following conditions: 60 % humidity, with 16-hour photoperiod (full light), at 25 °C in the light and 20 °C in the dark.

3.3. RNA isolation and cDNA synthesis from *Brachypodium* leaves

Total RNA was extracted from fresh *Brachypodium* leaves using the RNeasy Plant Mini Kit (Qiagen), according to the manufacturer's protocol. For each sample, two *Brachypodium* leaves were placed in liquid nitrogen then ground thoroughly. The buffer RLT (containing β-ME) was added to the tissue powder. The lysate was vortexed, transferred to the provided QIAshredder spin column and centrifuged for two min at full speed. The supernatant of the flow-through was carefully collected. One half volume of 100% ethanol was added to the supernatant, and the mixture was transferred to the RNeasy spin column and centrifuged for one min. The column was rinsed with buffer RW1 then buffer RPE by centrifuge for 15 s each time. RNase-free water was then added directly to the membrane and RNA was collected by centrifuge for one min at full

speed. The RNA was reverse transcribed for cDNA synthesis using Superscript III Reverse Transcriptase (Thermo Fisher), according to the manufacturer's protocol. Oligo$(dT)_{20}$ and dNTP mix was added to total RNA of *Brachypodium.* The mixture was heated to 65°C for 5 min. The provided First-strand buffer, DTT, RNaseOUT and Superscript III RT were then added to the mixture. The reaction was incubated at 50°C for 30 min and inactivated by heating at 70°C for 15 min.

3.4. *BdQUAC1* expression plasmid construction

The *Bd*QUAC1 amplification primers were designed for Gateway (Thermo Fisher) cloning and traditional cloning with restriction sites NheI and SacII. Fwd: 5'-GCC GACAAGTTTGTACAAAAAAGCAGGCTTAATAGCTAGCGAGGCCACC**ATGGCTTGCA CTCTACATTCC**-3', Rev: 5'-GCCGACCACTTTGTACAAGAAAGCTGGGTACCGCGG **TTA TTATTCAGCTGCAGTAGAAACTGT**-3'. The yellow highlighted regions in the Fwd and Rev primers are attB1 and attB2 sequences, respectively, for the purpose of Gateway cloning. Sequences were found in the Gateway Technology user guide (Thermo Fisher). The green highlighted regions in the Fwd and Rev primers are the restriction sites NheI and SacII, respectively. The underlined nucleotides in the Fwd primer are the Kozak sequence. Since this plasmid was prepared for the expression of *Bd*QUAC1 in the mammalian HEK293 cell, the Kozak sequence was included at the N terminus. The bolded regions in the Fwd and Rev primers are the beginning and ending of the *Bd*QUAC1 coding sequence, respectively. Full length *Bd*QUAC1 cDNA was amplified from *Brachypodium* cDNA (in section 3.3), using High Fidelity Phusion polymerase (New England BioLabs) with the thermocycling conditions in Table 3.1. The PCR products were cloned into Gateway pDonor221 vector (Thermo Fisher) using Gateway BP Clonase

II enzyme mix (Thermo Fisher) according to the manufacturer's protocol. Cloning was carried out by mixing *Bd*QUAC1 PCR product, pDonor 221, and BP clonase II enzyme mix in an 1.5 mL microcentrifuge tube and incubating at 25°C for 1 h. The pDonor221 vector carrying *Bd*QUAC1 and the pIRES2-eGFP vector (Clontech) were digested with NheI and SacII enzymes (New England BioLabs). The *Bd*QUAC1 cDNA was then cloned into the pIRES2-eGFP vector by ligating the NheI ends and the SacII ends of *Bd*QUAC1 and pIRES2-eGFP vector using T4 DNA Ligase (New England BioLabs). The ligated clone was named pIRES2-eGFP-*Bd*QUAC1. The construct was transformed into competent DH5α *E. coli* cells (Thermo Fisher) for propagation and selection.

The transformation was carried out by adding the pIRES2-eGFP-*Bd*QUAC1 construct into 50 µl of competent *E.coli* cells. The cells were incubated on ice for 30 min, then heat shocked for 1 min at 42 °C and cultured at 37 °C with the addition of 1 mL LB broth (5 % tryptone powder, 2.5 % yeast extraction, and 5 % NaCl) for 40 min. The culture was then spread onto kanamycin resistance agar plate and incubated overnight at 37 °C. Colonies formed on the plate were cultured in LB broth for plasmid propagation, and plasmids were isolated using QIAprep Spin Miniprep kit (Qiagen) according to manufacturers' protocols. Pellet of transformed *E.coli* cells were collected by centrifugation. The pellet was resuspended in buffer P1. Buffer P2 was then added to the *E.coli* cells and incubated for 5 min, followed by buffer N3. Once buffer N3 was added, the mixture was centrifuged for 10 min at 13,000 rpm. Supernatant was carefully collected and transferred to QIAprep spin column. The column was centrifuged, then rinsed with buffer PB and buffer PE by centrifugation for 30 s each. RNase-free water was then added directly to column and DNA plasmids were collected by centrifuge for one min at full speed. Cloning of *Bd*QUAC1 into the pIRES2-eGFP vector was confirmed by sequencing.

STEP	TEMPERATURE	TIME
Initial Denaturation	98 °C	30 s
30 Cycles	98 °C 56 °C 72 °C	15 s 30 s 2 min 30 s
Final Extension	72 °C	10 min

Table 3. 1 Thermocycling conditions for PCR

The pIRES2-eGFP vector was chosen as it allows the expression of both the target gene and GFP on one transcript. This is due to the IRES (Internal Ribosome Entry Site) sequence forming a complex structure that allows the translation of any mRNA located immediately downstream of the IRES sequence. The pIRES-eGFP vector carrying *Bd*QUAC1 was expressed in HEK293 cells for patch clamp. Green fluorescing HEK293 cells indicate successful transfection and translation of *Bd*QUAC1 and the cells were chosen for the experiments (section 3.6).

3.5. Site-directed mutagenesis of plasmid and C-terminal Myc-tag fusion by PCR

The codons encoding three basic residues of *Bd*QUAC1 R335, R338, and K342, which are responsible for binding CaM, were changed to encode alanine in the pIRES2-eGFP-*Bd*QUAC1 plasmid. Mutated plasmids are listed in Table 3.2. The mutated plasmid pIRES2-eGFP-*Bd*QUAC1(R338A) was made by PCR amplification using the plasmid pIRES2-eGFP-*Bd*QUAC1 as template and the primers Fwd-R338A and Rev-R338A (Table 3.2). The PCR products were treated with DpnI (New England BioLabs) to digest all parental plasmids, then transformed into DH5α for propagation. The plasmid pIRES2-eGFP-*Bd*QUAC1(R338A) was then used as a template to generate pIRES2-eGFP-*Bd*QUAC1(R335A/R338A) and pIRES2-eGFP-*Bd*QUAC1(R335A/R338A/K342A) with pairs of primers Fwd-R335A/R338A with Rev-R335A/R338A and Fwd-R335A/R338A/K342A with Rev-R335A/R338A/K342A, respectively (Table 3.2). The plasmid pIRES2-eGFP-*Bd*QUAC1(R335A/R338A/K342A) was then used as a template to make pIRES2-eGFP-*Bd*QUAC1(R335A/K342A) and pIRES2-eGFP-*Bd*QUAC1(R338A/K342A) using the pairs of primers Fwd-R335A/K342A with Rev-R335A/K342A and Fwd-R338A/K342A with Rev-R338A/K342A, respectively (Table 3.2). Mutants were confirmed by sequencing. Myc-tag was also fused to the C-terminus of wildtype

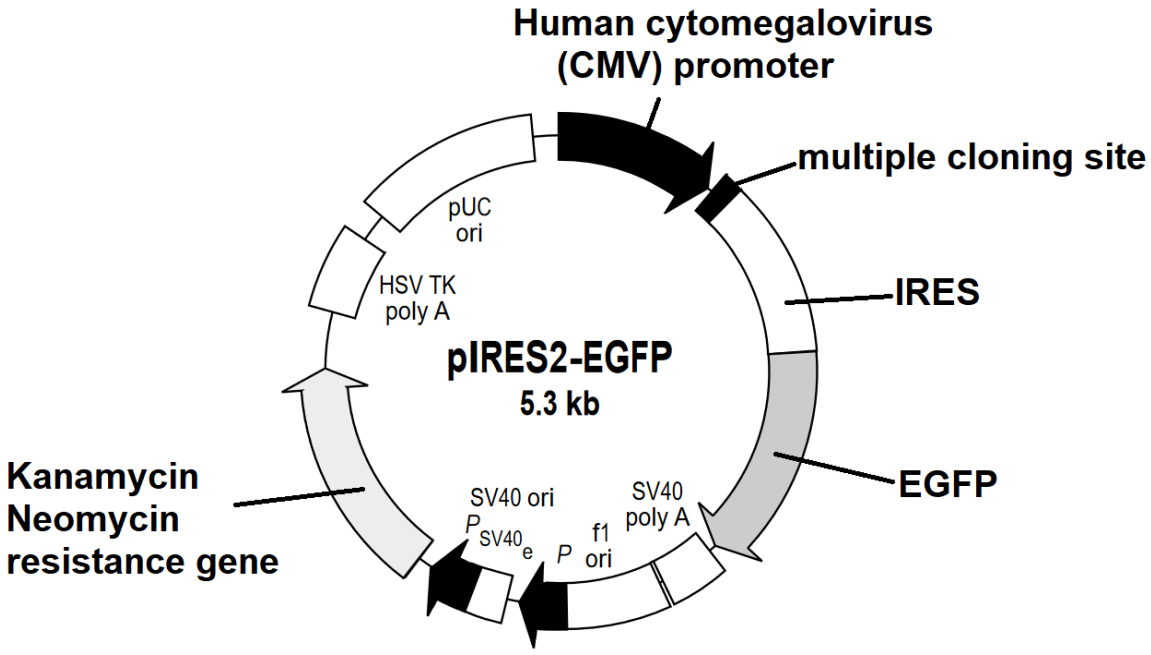

Figure 3. 1 The pIRES-eGFP vector.

The EGFP sequence is located downstream of the IRES sequence. The target protein is cloned into the vector at the multiple cloning site. Successful expression of the target protein also allows expression of the eGFP protein.

Primer	Primer Sequence	Generated plasmid
Fwd-R338A	5'-CCATGCACT**AGA**GTAGCA**GCG** GAAGTGGCC**AAG**GTTTGC–3'	pIRES2-eGFP-*Bd*QUAC1(R338A)
Rev-R338A	5'- GCAAAC**CTT**GGCCACTTC**CGC**T GCTAC**TCT**AGTGCATGG–3'	
Fwd-R335A/R338A	5'- CGAAATCCATGCACT**GCA**GTAG CA**GCG**GAAGTGGC-3',	pIRES2-eGFP-*Bd*QUAC1(R335A/R338A)
Rev-R335A/R338A	5'- GCCACTTC**CGC**TGCTAC**TGC**AG TGCATGGATTTCG-3'	
Fwd-R335A/R338A/K342A	5'- CGAAATCCATGCACT**GCA**GTAG CA**GCG**GAAGTGGCC**GCG**GTTCTA CAAGAGCT-3'	pIRES2-eGFP-*Bd*QUAC1(R335A/R338A/K342A)
Rev-R335A/R338A/K342A	5'- AGCTCTTGTAGAAC**CGC**GGCCA CTTC**CGC**TGCTAC**TGC**AGT GCATGGATTTCG-3'	
Fwd-R335A/K342A	5'- CCATGCACT**GCA**GTAGCA**CGA** GAAGTGGCC**GCG**GTTCTA-3'	pIRES2-eGFP-*Bd*QUAC1(R335A/K342A)
Rev-R335A/K342A	5'- TAGAA**CCG**CGGCCACTTC**TCG**T GCTAC**TGC**AGTGCATGG-3'	
Fwd-R338A/K342A	5'- CGAAATCCATGCACT**AGA**GTAG CA**GCG**GAAGTGGCC-3'	pIRES2-eGFP-*Bd*QUAC1(R338A/K342A)
Rev-R338A/K342A	5'- GGCCACTTC**CGC**TGCTAC**TCT**A GTGCATGGATTTCG-3'	
Fwd-Myc-tag	5' – GATATACCGCGGGCCCGGGAT CCGCCCCTCTCC -3'	pIRES2-eGFP-*Bd*QUAC1-myc pIRES2-eGFP-*Bd*QUAC1(R335A/R338A)-myc pIRES2-eGFP-*Bd*QUAC1(R335A/K342A)-myc pIRES2-eGFP-*Bd*QUAC1(R338A/K342A)-myc pIRES2-eGFP-*Bd*QUAC1(R335A/R338A/K342A)-myc
Rev-Myc-tag	5'-GATATACCGCGGTTATAGGTCC TCTTCGCTGATTAGCTTTTGTTCTT CAGCTGCAGTAGAAACTGTGTGGC TGCC -3'	

Table 3. 2 Primer sequences used for site-directed mutagenesis and Myc-tag fusion

The bolded and underlined letters are the codons at amino acid 335, 338, and 342. The yellow highlighted codons are the bases that have been mutated to encode Alanine. Of the reverse myc-tag primer, the blue highlighted region is the 3' end of the *Bd*QUAC1 ORF. The myc-tag, highlighted in green, was inserted at the 3' end of *Bd*QUAC1 ORF before the stop codon highlighted in red. The remaining bases of the reverse myc-tag primer and the forward primer are the multiple cloning site sequence present in the pIRES-eGFP vector.

*Bd*QUAC1 and mutants in pIRES-eGFP in the same manner using the primers Fwd-Myc-tag with Rev-Myc-tag and confirmed by sequencing.

3.6. Cell culture and transfection

The human embryonic kidney 293 cells (HEK293) (ATCC) were cultured in 35mm cell culture dishes (Thermo Fisher) in Dulbecco's Modified Eagle Medium (DMEM), (Thermo Fisher) supplemented with 10 % fetal bovine serum (FBS) (Thermo Fisher), 1 % Penicillin-Streptomycin (Thermo Fisher), and 1 % L-Glutamine (Thermo Fisher) at 37 °C in 95 % / 5 % CO_2. Once 80 % confluent, HEK293 cells were transfected with 3.5 µg (per 35mm dish) of the plasmid piRES2-eGFP-*Bd*QUAC1 or one of the mutated plasmids using Fugene HD Transfection Reagent (Promega), according to the manufacturer's protocol. DNA plasmids, transfection reagent, and optiMEM (Thermo Fisher) were added to a 1.5 mL tube, and incubated for 10 min. The mixture was added to confluent dish of HEK293 cells. The 35mm dish was then returned to the incubator for 24 h. Transfected cells were used either in patch clamp or for western blot analysis the following day. DNA plasmids used for transfection were propagated in DH5α *E. coli* cells (Thermo Fisher) and isolated using Qiagen Plasmid Maxi kit (Qiagen), as described in section 3.4.

3.7. Measurement of QUAC1 currents by patch clamp

HEK293 cells transfected with pIRES2-vector carrying either *Bd*QUAC1 or one of the mutants were used for the experiments. HEK293 cells transfected with the empty pIRES2-eGFP was used as a negative control. Cells were placed in the solution containing (in mM): 150 NaCl, 1 $CaCl_2$, 1 $MgCl_2$, 10 glucose, 10 mannitol, 10 HEPES, pH 7.3, adjusted with N-methyl-d-glucamine. Only green fluorescing cells, which indicated successful transfection, were chosen for

patch clamp experiments under a Zeiss inverted fluorescence microscope. The pipette solution contained (in mM): 130 CsCl, 10 EGTA, 1 $MgCl_2$, 10 HEPES, pH 7.3 with NMDG, and $CaCl_2$ providing various free Ca^{2+} concentrations; free Ca^{2+} concentration was calculated with WEBMAXC software. The pipette solution was made in volume of 100 mL then aliquoted into 1.5 mL Eppendorf tube and stored at -80 °C. In experiments using inhibitors such as W-5, W-7, Staurosporine, the inhibitors were added to the solution at the start of the experiment. Whole cell patch clamp was performed with a HEKA EPC 10 amplifier (Figure 3.1). Membrane voltage was clamped to +60 mV followed by 15 mV decrements from +60 mV to -195 mV. The holding potential was -20 mV (Figure 3.3). Once currents were recorded at voltages described above, the standard external solution was gently replaced with malate solution (in mM): 120 NaCl, 1 $CaCl_2$, 1 $MgCl_2$, 10 glucose, 10 mannitol, 10 Hepes, 30 malic acid at pH 7.3, and currents were again recorded in the same manner. Total currents can be influenced by different cell sizes, due to bigger cells having a larger surface area. To account for this, activities of *Bd*QUAC1 are more accurately presented in the units of current density (pA/pF). Current densities are the division of the recorded currents in picoAmperes (pA) to the cell membrane capacitance in picoFarads (pF). The cell membrane is so thin that ions line against the cell membrane on both sides, thus creating the membrane capacitance which is proportional to the cell surface area. The cell membrane capacitance value is calculated and provided by the patch clamp system.

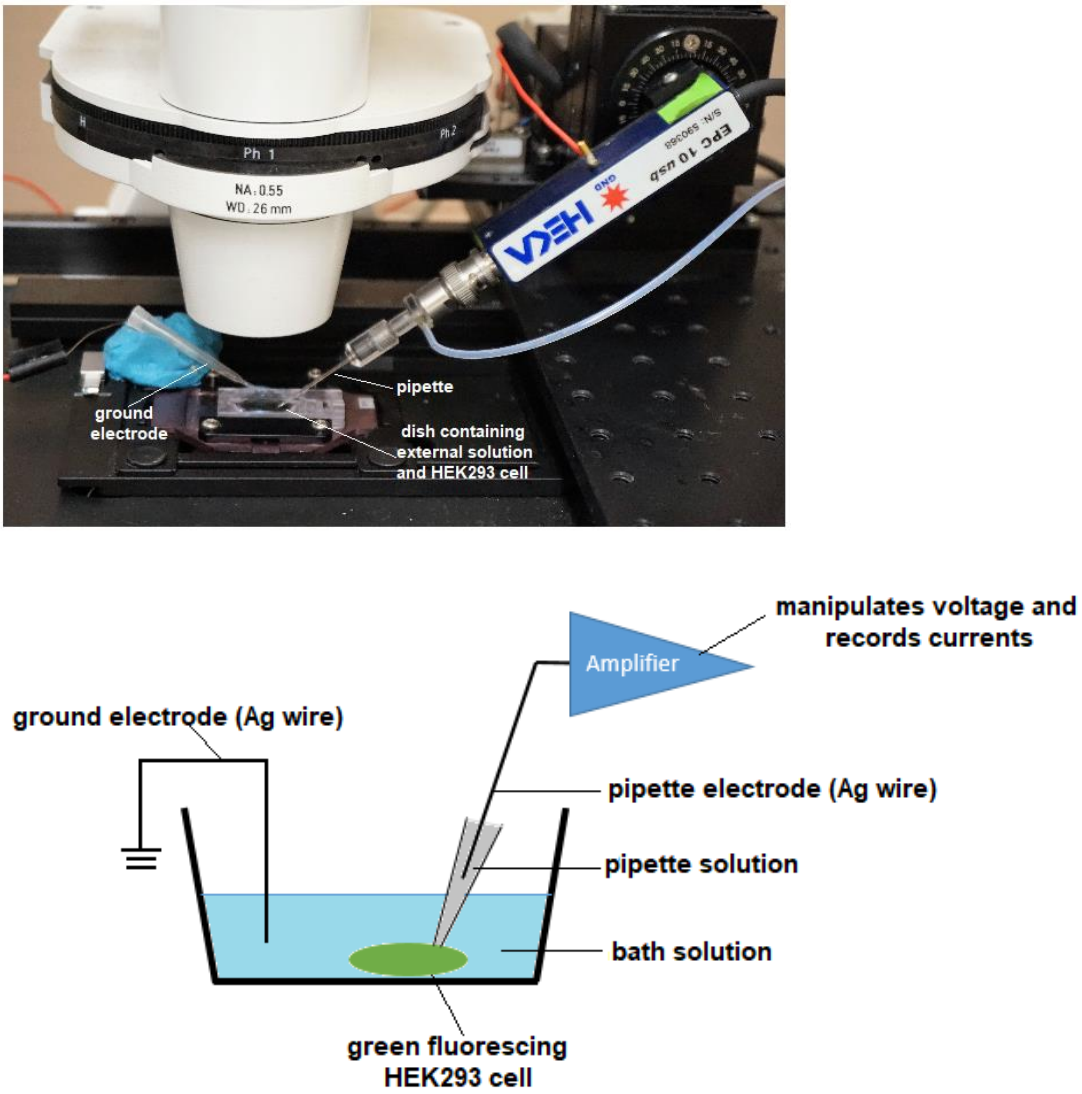

Figure 3. 2 Whole cell patch clamp apparatus.

This system allows the measurement of currents, which indicate the movement of ions across the HEK293 cell membrane. A pipette filled with internal (pipette) solution was placed against the cell membrane at its tip. By applying weak suction, the glass pipette tip and the cell membrane form a very tight seal. When the seal reached a resistance greater than 1 gigaohm, applying another gentle suction ruptured the membrane patch, creating the whole cell patch. Here, the pipette solution can freely diffuse, controlling the osmolality of the cytoplasm. Ions can move across the HEK293 cell membrane through opened channels expressed on the cell membrane. The net movement of ions is represented by the currents recorded. This system allows the measurement of currents, which indicate the activities of the expressed channels, such as QUAC1, at different voltages or in the presence of channel agonists and blockers.

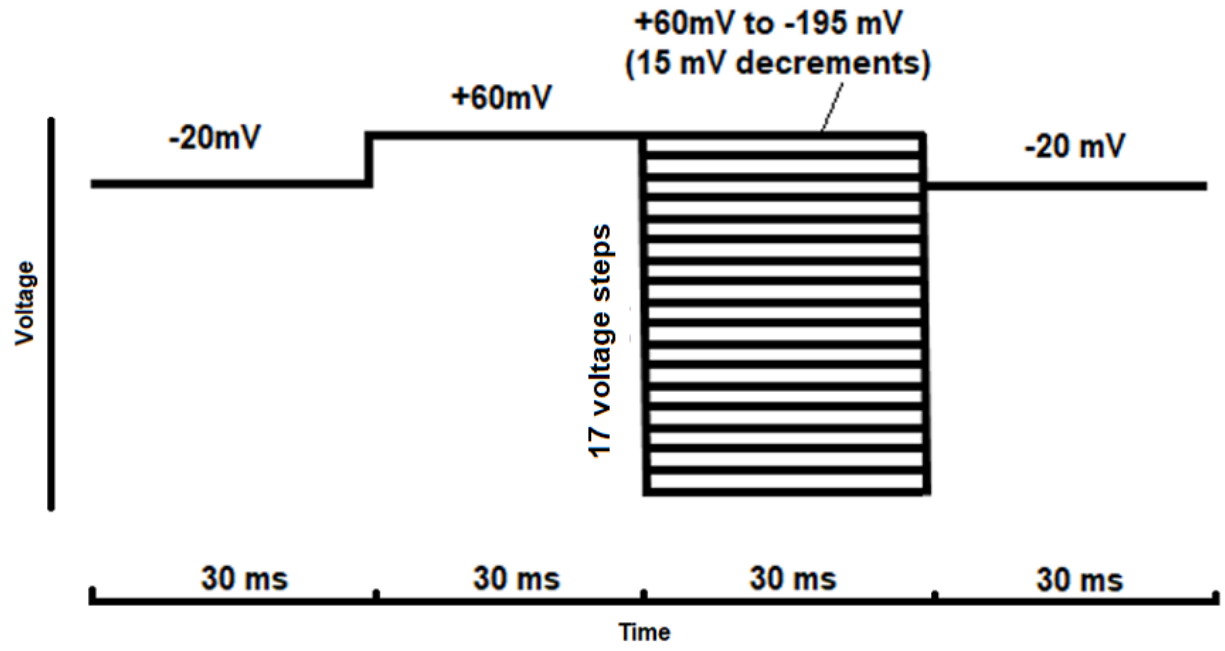

Figure 3. 3 Voltage protocol used for patch clamp experiments.

The membrane voltage was held at -20mV. The protocol consists of a series of 17 steps. In each reading, the voltage was first held at -20 mV, then clamped to +60 mV followed by the voltage desired for the study (between +60 mV and -195 mV), and returned to the holding voltage

3.8. Protein extraction and western blot analysis

Wildtype *Bd*QUAC1 and mutant proteins fused with Myc-tag were isolated from HEK293 cells transfected with the plasmid pIRES2-eGFP-*Bd*QUAC1-myc, pIRES2-eGFP-*Bd*QUAC1(R335A/R338A)-myc, pIRES2-eGFP-*Bd*QUAC1(R335A/K342A)-myc, pIRES2-eGFP-*Bd*QUAC1(R338A/K342A)-myc, or pIRES2-eGFP-*Bd*QUAC1(R335A/R338A/K342A)-myc. For each replicate of the western blot analysis, two T75 flasks HEK293 cells (approximately 7.5 x 10^6 cells per flask) were used per plasmid. Extraction was performed using Pierce Cell Surface Protein Isolation Kit (Thermo Fisher), according to manufacturer's protocol. HEK293 cells were gently rinsed twice with ice-cold PBS while attached to the T75 flasks. The cells were then incubated with Sulfo-NHS-SS-Biotin solution for 30 min at 4°C. After biotinylation of the cell surface, cells were gently scraped off and transferred to a 50 mL conical tube. Pellets of HEK293 cells were collected and rinsed two times by centrifuge at 500 x g for 3 min. Lysis buffer was then added to the pellets and cell lysate was incubated for 30 min on ice. The cell lysate was mixed with NeutrAvidin Agarose gel and incubated for 60 min. The mixture was transferred to a 1.5 mL spin column and centrifuged to remove unbound proteins. The column was rinsed twice with the provided wash buffer. SDS-PAGE Sample Buffer (Thermo Fisher) containing 50 mM DTT was then added to the column. The reaction was incubated for 60 min at room temperature and cell surface proteins were eluted by centrifuge. Proteins were analyzed immediately after by western blotting.

Proteins were first separated based on their molecular weight in 10 % SDS-PAGE (sodium dodecyl sulfate-polyacrylamide gel electrophoresis) with running buffer (25 mM Tris, 192 mM glycine, 0.1 % SDS). Proteins on the polyacrylamide gel were then electroblotted on PVDF membrane (Thermo Fisher) with transfer buffer (25 mM Tris, 192 mM glycine, 20% methanol).

Once transferred, membranes were blocked at room temperature with Rapidblock solution 10x (Amresco) for 15 min and subsequently probed at room temperature with anti-Myc tag HRP-conjugated (Abcam) and the loading control anti-Sodium Potassium ATPase HRP-conjugated (Abcam) for 2 h with gentle agitation. After antibody incubation, the membranes were washed with PBST buffer (0.1 % Tween in PBS solution (Thermo Fisher)) three times for ten min each time then treated with Amersham ECL Western Blotting Detection Reagent (GE Life Sciences). Membranes were scanned using the ChemiDoc Imaging system and protein bands were quantified using the software ImageLab (Bio-rad).

3.9. Isothermal titration calorimetry

Isothermal titration calorimetry (ITC) is a technique used to assess the interactions between molecules. The ITC instrument is made up of two cells: the sample cell which allows users to set up for mixing one type of molecule with another, and reference cell which contains distilled water. When binding between molecules occurs, the reaction either releases or absorbs heat. The instrument is a sensitive calorimeter that can detect differences in temperature between the two cells and supply heat to maintain equal temperature between the cells. The experiments were performed on a Nano-ITC (TA-instrument) with the following settings: 20 injections, 2.5 µL per injection, waiting period of 120 s between injections. Peptides representing the predicted CaM binding site of *Bd*QUAC1 (AA334 – AA355), as well as double mutants R335D/R338D, R335D/K342D, R338D/K342D, and triple mutants R335D/R338D/K342D were synthesized with > 90% purity by Genscript. The peptides and bovine CaM (BioOcean) were dialyzed with 0.1-0.5 kD MWCO Float-A-Lyzer (Spectrum) overnight with three changes of buffer containing 20 mM HEPES, 100 mM KCl, and 5 mM $CaCl_2$ at pH 7.4. After dialysis, peptide concentrations were

measured using Bio-rad protein assay and adjusted to 400 μM for the experiment. Peptides were titrated into the Nano-ITC cell containing either 60 μM CaM, 60 μM CaM with 60 μM W-7 or just dialysis buffer. Since W-7 inhibits by competing with the peptides and binds to CaM, W-7 was mixed with CaM 30 min prior to the ITC experiment to ensure CaM was fully inhibited. The 'no Ca^{2+}' sample was prepared exactly as described above, except that peptide and CaM were dialyzed overnight with 3 buffer changes, into buffer containing 20mM HEPES, 100mM KCl, and 1.5 mM EGTA at pH 7.4. The data was processed using the NanoAnalyze software by subtracting the background heat obtained from titrating the peptides into dialysis buffer to the heats obtained from titrating the peptides into the CaM-containing solutions.

3.10. CaM agarose affinity pull-down

Wildtype *Bd*QUAC1 and mutant R335A/K342A Myc-tag proteins were expressed in HEK293 cells. Cells were rinsed with PBS, pH 7.4 (Thermo Fisher) and gently scraped off the bottom of the flask into PBS. Cell pellets were collected by centrifuge at 500 x g for 3 min then re-suspended in lysis buffer (50 mM Tris-HCl, pH 7.4, 150 mM NaCl, 1mM EGTA, 1% Triton X-100, 10% glycerol and 1 x Halt protease inhibitor cocktail (Thermo Fisher)) and incubated at 4 °C for 30 min. The total cell lysate was clarified by centrifugation at 10,000 x g for 2 min. $CaCl_2$ was added to the cell lysate to make a final concentration of 8 mM $CaCl_2$.

CaM-Sepharose beads (Biovision) were transferred to mini spin columns (VWR BIOV6572-50) and equilibrated with wash buffer (50mM Tris-HCl pH 7.4, 150 mM NaCl, 0.25 % Triton X-100, 10 % glycerol, 1 x Halt protease inhibitor cocktail) by centrifugation at 1000 x g for 1 min, repeated two times. The cell lysate was added to the CaM beads and incubated for 8 h at 4 °C. All unbound proteins were removed by centrifuge at 1000 x g for 1 min and the columns

were rinsed four times with wash buffer at 1000 x g for 1 min each time. SDS-PAGE sample buffer containing 20 mM EGTA (62.5 mM Tris-HCl, pH 6.8, 1 % SDS, 10 % glycerol, 20 mM EGTA) was then added to the columns and incubated for 2 h at room temperature. Bound proteins were eluted by centrifuge at 1000 x g for 2 min and loaded onto the SDS-page gel for QUAC1 detection by western blotting as described above (Kaleka et al., 2012). Western bands were quantified by normalization against total (eluted) protein stain with Image Lab.

3.11. Generation of QUAC1 knockdown plants

QUAC1 knockdown plants were generated by the RNA interference (RNAi)-mediated gene suppression method using pANIC-8D vector (ABRC) (Figure 3.4) (Mann et al., 2012). A fragment of *Bd*QUAC1 and its inverted repeat were cloned into the vector so that the two cloned fragments, at the RNA level, pair with one another, creating a hairpin loop. The short hairpin RNA fragments are recognized as double-stranded RNA, which signals the RNAi process in plants. A 400bp fragment of the *Bd*QUAC1 cDNA (nucleotide 919 to 1293) was amplified with the primers: Fwd 5' –CACCGCCGACAAGTTTGTACAAAAAAGCAGGCTTAATAACTGTTGCTGCACT TCATGG- 3' and Rev 5' – GCCGACCACTTTGTACAAGAAAGCTGGGTACATTGCGTTCT GGTGGTTGA- 3'. The PCR product was subcloned into the pDonor221 vector (Thermo Fisher) using Gateway BP clonase II enzyme mix (Thermo Fisher), according to manufacturer's protocol, followed by transformation of DH5α and selection, as described in (section 3.4). The plasmid was named pDonor221-*Bd*QUAC1 (Figure 3.4). The plasmid pANIC-8D-*Bd*QUAC1 was generated by mixing pDonor221-*Bd*QUAC1 with the vector pANIC-8D (Figure 3.5) and LR clonase II enzyme mix (Thermo Fisher), and transformed into DH5α.

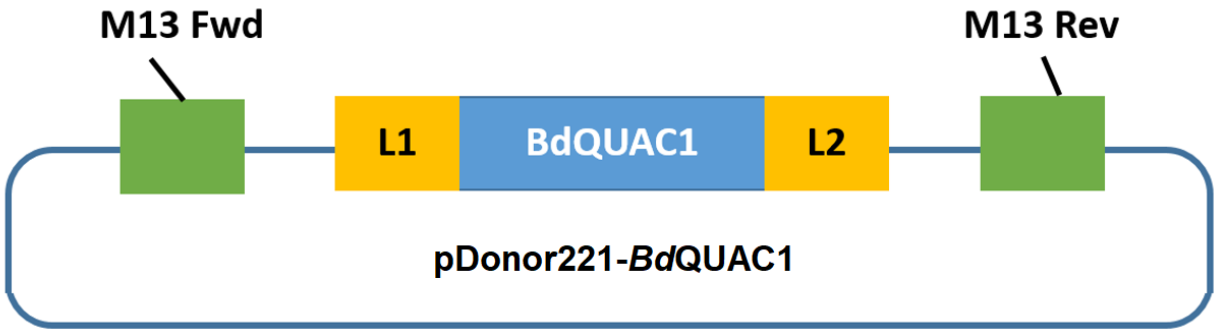

Figure 3. 4 The plasmid pDonor221-*Bd*QUAC1

pDonor221 is an entry clone vector of the Gateway cloning system. *Bd*QUAC1 was amplified with primers containing the Gateway attB1 and attB2sequences, as mentioned in 3.4, and cloned into the pDonor 221 vector using the BP clonase. The two yellow boxes L1 and L2 are the two flanking sites used for cloning of *Bd*QUAC1 into the destination vector. Destination vectors are vectors containing the AttR site (R1 and R2), such as the pANIC-8D vector below. The *Bd*QUAC1 was cloned into pANIC-8D using the LR clonase. The two universal primers M13 Fwd and M13 Rev were used for sequencing to confirm successful cloning.

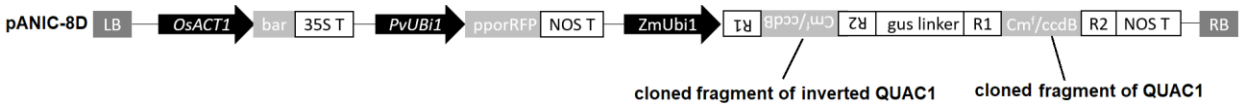

Figure 3. 5 pANIC-8D vector

Once QUAC1 was cloned into the pANIC-8D, the plasmid was used for generating transgenic plants. This figure shows half of the circular vector with LB and RB boxes at both ends representing left border and right border of the vector. The other half of the vector contains the T-DNA backbone, used for transferring DNA into *Agrobacteria*. The bar gene is used as a selectable marker. Transformed calluses having the bar gene are resistant to phosphinothricin (PPT). The pporRFP allows the constitutive expression of red fluorescent protein. Since PCR cannot be performed on calluses and young shoots, pporRFP is used as a quick screen for transgenic plants. OsACT1, PvUBi1, ZmUBi1 are promoters for bar, pporRFP, and *Bd*QUAC1, respectively. NOS, and 35S, are transcription terminators.

The vector pANIC-8D carrying a fragment of QUAC1 was then transformed into *Agrobacterium tumefaciens* strain EHA105 using the Triparental Mating method. 1 mL DH5α *E. coli* carrying the pANIC-8D plasmids, 1 mL of the helper strain E.coli RK2013, and 1 mL of *Agrobacterium* strain EHA105 were cultured overnight then rinsed with 1 mL 10 mM $MgSO_4$ 3 times by centrifuging and removing the supernatant and resuspended with 1 mL of 10 mM $MgSO_4$. The three cultures were then combined and centrifuged. After the supernatant was discarded, the pellet was resuspended with 500 µL of 10 mM $MgSO_4$ and pipetted onto an antibiotic free agar plate, and incubated overnight at 28 °C. The plate was washed with 1 mL of 10 mM $MgSO_4$ to collect all bacteria and streaked onto rifampicin agar plates for selection of transformed *Agrobacterium.* Subsequently, immature *Brachypodium* seeds were collected. After removal of the lemma, seeds were sterilized by soaking in a solution of 10 % bleach and 0.1 % Triton X-100 for 4 min and washed three times in sterile water. Embryos were then dissected out of immature seeds and placed on callus initiation media (CIM) (4.43 g Linsmaier and Skoog Medium, 30 g sucrose, 1 mL of 0.6 mg/mL $CuSO_4$, pH 5.8 with KOH, 2 g phytagel, 0.5 mL of 5 mg/mL 2,4-D stock solution (2000x) and distilled water to 1 liter) and incubated at 28 °C in the dark. Calluses produced from embryos were spread onto Petri plates every 2 weeks until there were enough calluses for transformation. Transformed Agrobacterium was cultured in 20 mL of CIM at 28 °C to 0.6 OD. Then 200 µL of 10 % Synperonic PE/F68 (Sigma) and 20 µL of 200 mM acetosyringone were added to the Agrobacteria suspension and 6 grams of callus pieces were then added to the suspension and incubated for 5 min. The calluses were then poured onto Petri dishes with filter papers and incubated at room temperature in the dark for 3 days. Calluses were then transferred to CIM plates containing 150 mg/L Timentin and 10 mg/L Phosphinothricin (so that only transformed calluses are selected) and incubated at 25 °C. Calluses with green shoots were considered T_0 plants

and transferred to soil and propagated as per growth conditions described above. Seeds collected from T_0 plants were used for further experiments (Alves et al., 2009). The expression of *Bd*QUAC1 was determined by real-time PCR described below.

3.12. Real-Time Quantitative PCR (RT-qPCR).

The expression of *Bd*QUAC1 was determined with real-time PCR. *Brachypodium* cDNA was synthesized as described in 3.3. Each cDNA was amplified using PerfeCTa SYBR Green supermix low ROX (QuantaBio) on the Stratagene Mx3000P qPCR system (Agilent Genomics). The *Brachypodium* UBC18 gene was used as a housekeeping gene. Primers for UBC18 and *Bd*QUAC1 qPCR are listed in Table 3.2. All primers used for qPCR were tested and had an efficiency between 90% and 110%. Relative expression of QUAC1 was calculated by normalizing to the housekeeping gene (UBC18) with the following equation: fold differences = $2^{-\Delta\Delta Ct}$.

$$\Delta\Delta Ct = [\Delta Ct_{(Bd\text{QUAC1})} - \Delta Ct_{(\text{UBC18})}]_{\text{knockdown } Brachypodium} - [\Delta Ct_{(Bd\text{QUAC1})} - \Delta Ct_{(\text{UBC18})}]_{\text{wildtype } Brachypodium}$$

Ct is the number of cycles required for the fluorescent signal to be detected, representing the results of qPCR.

3.13. Wheat rust infection

Wheat stripe rust spores (mixed race) were heat shocked for 5 min at 42 °C prior to inoculation. Approximately 0.01 g of rust spores were mixed with 2 mL of Bayol oil and paint-brushed on to 4 – 6-week old *Brachypodium* leaves. The plants were moved into a 100 % humidity chamber for 24 h then moved to standard conditions (60 % humidity, with 16-hour photoperiod, at 25 °C in the light and 20 °C in the dark). Rust infection symptoms appeared at two weeks after inoculation.

Gene name	Forward primer (5'-3')	Reverse primer (5'-3')
***Bd*QUAC1**	ACTGTTGCTGCACTTCATGG	CATTGCGTTCTGGTGGTTGA
UBC18	GGAGGCACCTCAGGTCATTT	ATAGCGGTCATTGTCTTGCG

Table 3. 3 qPCR primers of UBC18 and *Bd*QUAC1

3.14. Measurement of stomatal aperture

Detached leaves from 4 to 8-week old plants were soaked in opening buffer (50 mM KCl, 10 mM Mes, pH 6.1) for 2 h. Leaves were then soaked for another 3 h in control buffer (10 mM Mes, 25 μM $CaCl_2$, pH 6.1) or control buffer with the addition of malic acid (pH 6.1), Ca^{2+} ionophore A23187, and CaM inhibitor W-5 or W-7, as indicated in the results. Leaves were removed from the buffer and immediately dried by gentle blotting with Kim-wipe and then painted with a layer of clear nail polish, a process taking less than 30 s. The dried nail polish peel was used for microscopy using a Zeiss Axiovert 135 microscope (Khidir and Randall, 1984). Stomata width were measured from the obtained images using Image J. Blind measurement of stomata was performed by relabelling of the image files by a third party.

3.15. Count of appresoria formation

Fluorophore-conjugated wheat germ agglutinin (WGA) (Thermo Fisher) was used for visualization of appressoria formed on inoculated leaves. At three days after rust inoculation, detached *Brachypodium* leaves were soaked for 10 min in PBS solution containing 0.05% Tween and 1% fluorophore-conjugated WGA. The number of appressoria on each leaf was counted under the fluorescent microscope Zeiss Axiovert 135.

3.16. Statistical analysis

All data are expressed as mean with standard error of the mean. Significant was determined as $p < 0.05$.

Electrophysiology. Statistical significance is presented with lower case letters. Matching notations indicate no significant difference. Overall current densities or Δ current densities were

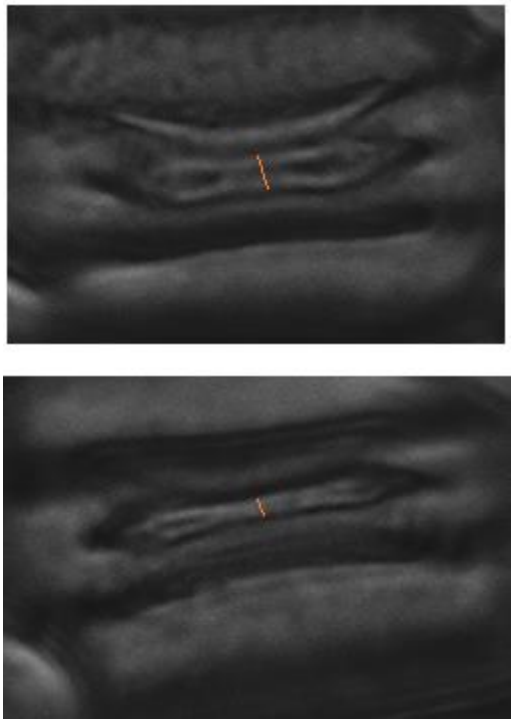

Figure 3. 6 Representative images of replicas of *Brachypodium* stomata.

The orange lines in the center are measurement of stomatal width.

analyzed by 2-way repeated measure ANOVA, where voltage points were the repeated factor and either the concentrations of Ca2+, malate, the presence of inhibitors or the type of QUAC1 (wildtype, mutants, eGFP vector) expressed were the second factor. The significance is presented with lower case letters. Matching notations indicate no significant difference. Peak current of each cell was used to determine current density, Δ current density and conductance. The Δ current density was calculated by subtracting current density recorded before adding malate to the current density recorded after adding malate to the bath solution. Conductance was calculated by division of peak current (after addition of malate) to the driving force. The driving force is the difference between the clamped voltage and the chloride equilibrium potential. Chloride equilibrium potential is calculated based on the concentrations of chloride in the pipette and bath solutions, with the following equation $V_{Eq} = RT/(zF)\ \ln([Cl^-]_{bath}/[Cl^-]_{pipette})$ (R is the universal gas constant, T was set to 296.15 K, which is equivalent to 23 °C, z is the valence of chloride, F is the Faraday's constant, $[Cl^-]_{bath}$ is the concentration of chloride in the bath solution and $[Cl^-]_{pipette}$ is the concentration of chloride in the pipette solution.). The channel conductance was normalized to maximum (G/G_{max}) and fit with the Boltzmann equation. Only Δ current densities more negative to -100 mV were used in statistical analyses. Time constant (tau) was calculated with the following equation: $\tau = Cm^*(Rss - Ro)$ where τ (ms) is the time constant, Cm (pF) is the membrane capacitance, Rss (mV/pA) is the resistance at steady state, and Ro is the resistance at peak.

Western blotting and RT-qPCR. The average of protein expression or gene expression of wildtype was normalized to 1. Significance was determined using one sample t-tests with the mean set as 1. The number of repetitions are included in the figure legends.

Stomatal aperture. Detached leaves from a tray of 15 *Brachypodium* plants were randomly assigned to each tested condition, approximately 4 leaves per condition. 100 stomata were

measured for each condition. The significance of differences was determined by 1-way ANOVA with Fisher's LSD *post-hoc*.

Germ tubes and appressoria formation. This experiment was carried out twice. Results were statistically analyzed using mixed model analysis in randomized blocked design, with wildtype or KD2 being the fixed factor, and each individual experiment being the random (block) factor. Four leaves from four rust inoculated plants of wildtype and of KD2 *Brachypodium* were randomly chosen for each experiment.

4. RESULTS

4.1. *Brachypodium* QUAC1 is co-activated by malate and Ca^{2+}

4.1.1. *Bd*QUAC1 channel is activated by malate

The *Brachypodium distachyon* ALMT12 (BdALMT12) gene sequence was found on the NCBI database (NCBI accession # XP_003574370.1; predicted BdALMT12). Based on the identification and renaming of the AtALMT12 gene to AtQUAC1 (Meyer et al., 2010), the putative BdALMT12, from here on, is referred to as *Bd*QUAC1. That said, despite the NCBI annotation, sequence alignments performed by NCBI BLAST showed only 56 % identity between the monocot *Bd*QUAC1 and dicot AtQUAC1, at the amino acid level. Alignments of several QUAC1s from different species show approximately 55 to 75 % identity between dicot and monocot, and up to 95 % identity within the dicot QUAC1s only or monocot QUAC1s only. Though QUAC1 of both dicot and monocot species share the same conserved transmembrane regions and the WEP-fingerprint motif (Trp-Glu-Pro) which present in all ALMTs (Figure 4.1), it is unclear whether the monocot QUAC1s maintain the same properties and function as the dicot QUAC1s, and *At*QUAC1, in particular. To assess this, whole cell patch clamp was performed on HEK293 cells expressing *Bd*QUAC1 to see whether the channel is voltage dependent and malate activated as reported for AtQUAC1.

.

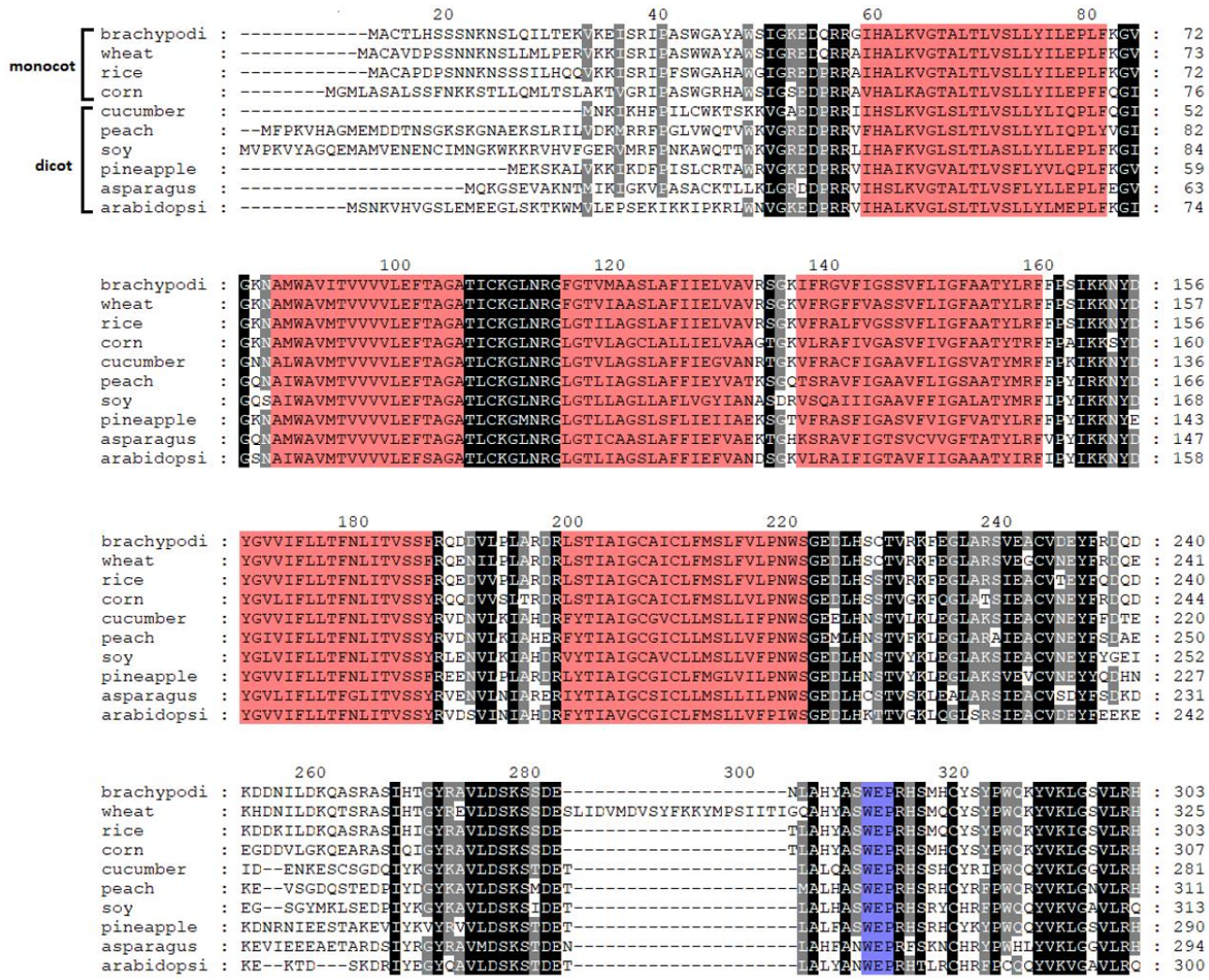

Figure 4. 1 Sequence alignments of QUAC1 proteins in monocot and dicot species.

QUAC1 sequences [NCBI accession numbers: XP_003574370.1 (brachypodium), EMS57711.1 (wheat), XP_015614622.1 (rice), PWZ19427.1 (corn), KGN60407.1 (cucumber), XP_007209894.1 (peach), XP_003538776.1 (soy), OAY77120.1 (pineapple), XP_020261302.1 (asparagus), O49696.1 (Arabidopsis)], were aligned by ClustalW multiple sequence alignment software (Larkin, 2007) and visualized in Genedoc (Nicholas, 1997). The pink boxes indicate the six transmembrane segments and the blue boxes indicate the location of the WEP-motif. The six transmembrane helices were predicted by the TMHMM server of the Technical University of Denmark (Krogh et al., 2001). The different shades of black and grey indicate the level of similarity between different QUAC1s, with the lightest grey being the least similar and black being the most similar.

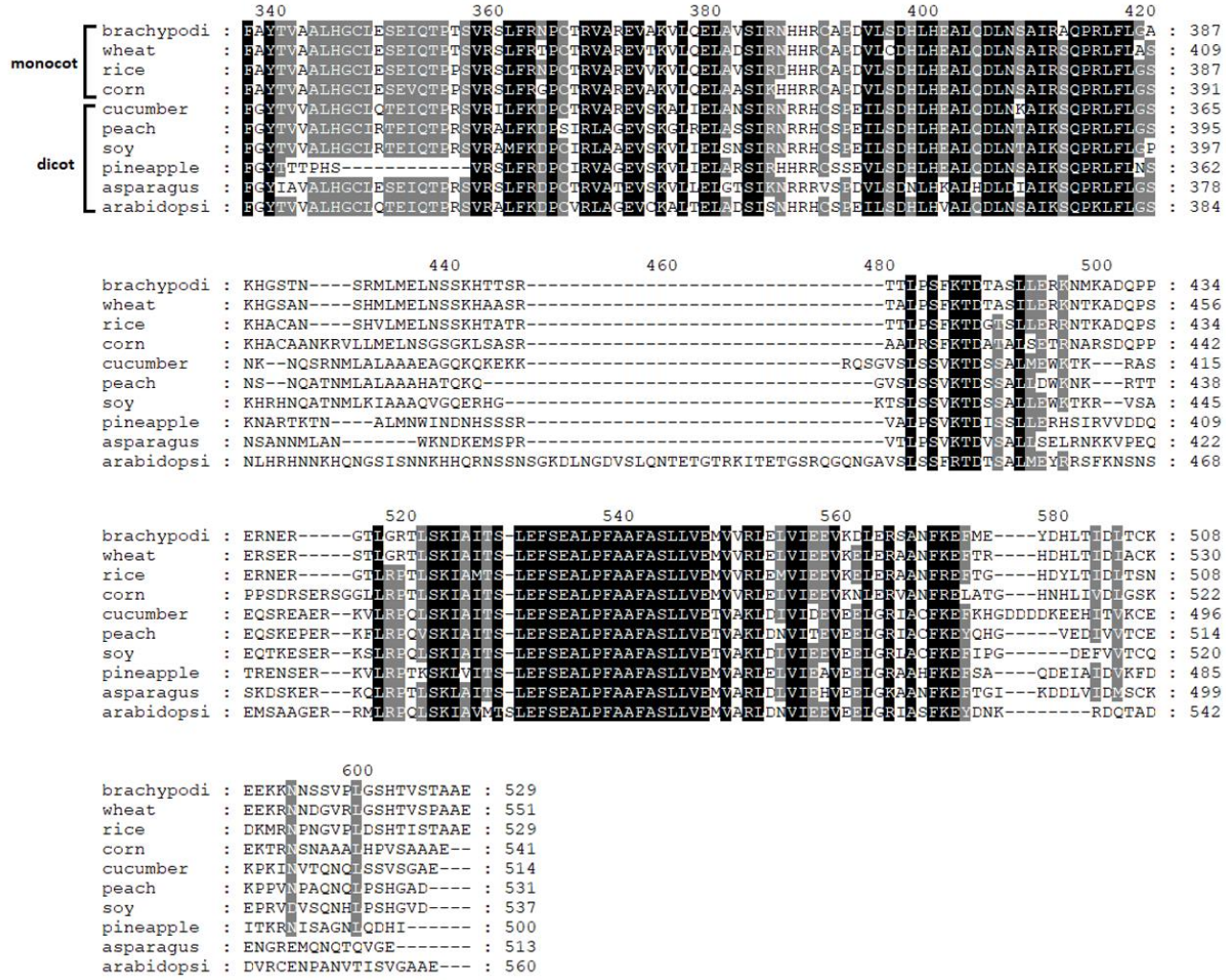

Figure 4.1 continued

Currents were recorded from *Bd*QUAC1-HEK293 cells (HEK293 cells transfected with the plasmid pIRES2-eGFP-*Bd*QUAC1) and compared to GFP-HEK293 cells (HEK293 cells transfected with the plasmid pIRES2-eGFP). GFP-HEK293 cells were used as a negative control representing the endogenous currents. The activities of *Bd*QUAC1 are presented in the units of current density (pA/pF), as explained under the material and method chapter, section 3.7.

The activation of *Bd*QUAC1 was observed at voltages in the range of -100 mV and lower (Figure 4.2). With the addition of 30 mM malate, the current densities of *Bd*QUAC1 (negatively) increased significantly, while GFP current densities stayed unchanged regardless of the absence and presence of malate (Figure 4.2). This result indicates that the *Bd*QUAC1 channel is voltage dependent and activated by malate.

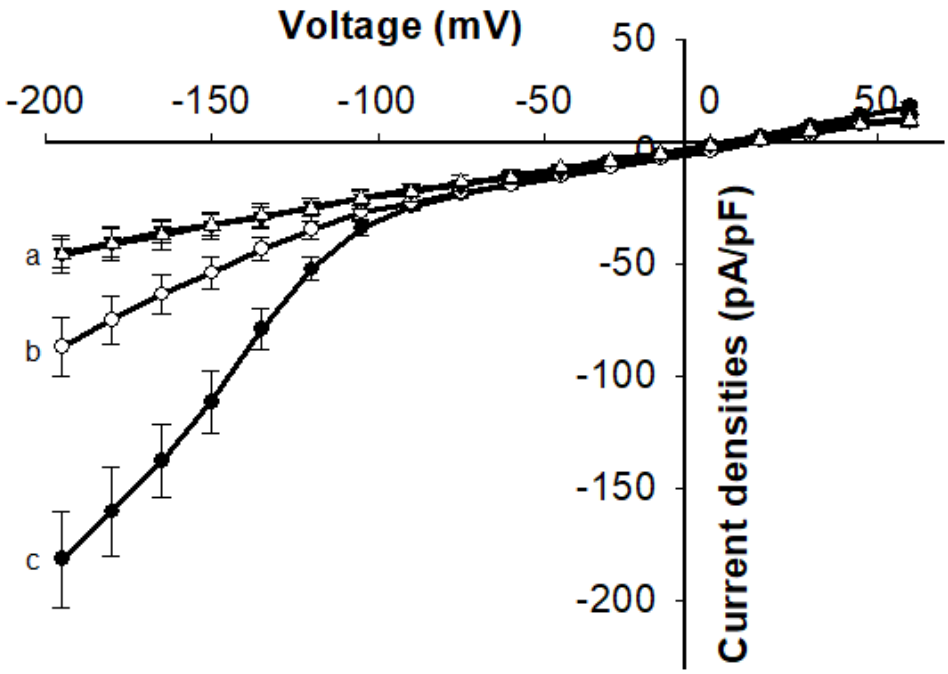

Figure 4. 2 Effect of malate on activation of *Bd*QUAC1.

Currents of *Bd*QUAC1-HEK293 cells (circles) or GFP-HEK293 cells (triangles) were recorded at different clamped voltages in the absence (white) and presence (black) of malate. GFP was used as a negative control and baseline for endogenous currents. Black triangles are obscured by overlapping white triangles. Lower case letters indicate significant differences. n = 12 for *Bd*QUAC1 and n = 6 for GFP.

4.1.2. *Bd*QUAC1 activation is Ca^{2+} -dependent

Since Ca^{2+} plays such a big part in the mechanism and signaling events for stomatal closure, the malate-activation of *Bd*QUAC1 was further tested for Ca^{2+} -dependence. With the whole cell patch clamp technique allowing control of internal solutes via pipette solution, *Bd*QUAC1 currents were recorded in the presence of different cytosolic Ca^{2+} concentrations (0 µM, 0.05 µM, 0.1 µM, 0.5 µM, and 5 µM free Ca^{2+}), before and after the addition of malate to the bath solution. Activation by malate is presented as Δ current densities, calculated by subtracting the current densities after malate addition from the current densities before malate addition. Increased concentrations of Ca^{2+} were found to increase the activation in a dose-dependent manner in cells expressing *Bd*QUAC1 (Figure 4.3A). Currents of GFP-HEK293 cells were also recorded as a negative control, and no changes were observed in response to different cytosolic Ca^{2+} concentrations (Figure 4.3B).

In addition, the conductance of the *Bd*QUAC1 channel was also calculated and normalized to maximum (G/G_{max}), as described in section 3.7. This value indicates the permeability of a channel at applied voltages. Though Ca^{2+} concentration affected the current densities of *Bd*QUAC1, no change was observed in the voltage dependence of conductance (Figure 4.3C). This result suggests that cytosolic Ca^{2+} is regulating only the malate-activation of the channel and not the voltage-dependent properties of the channel.

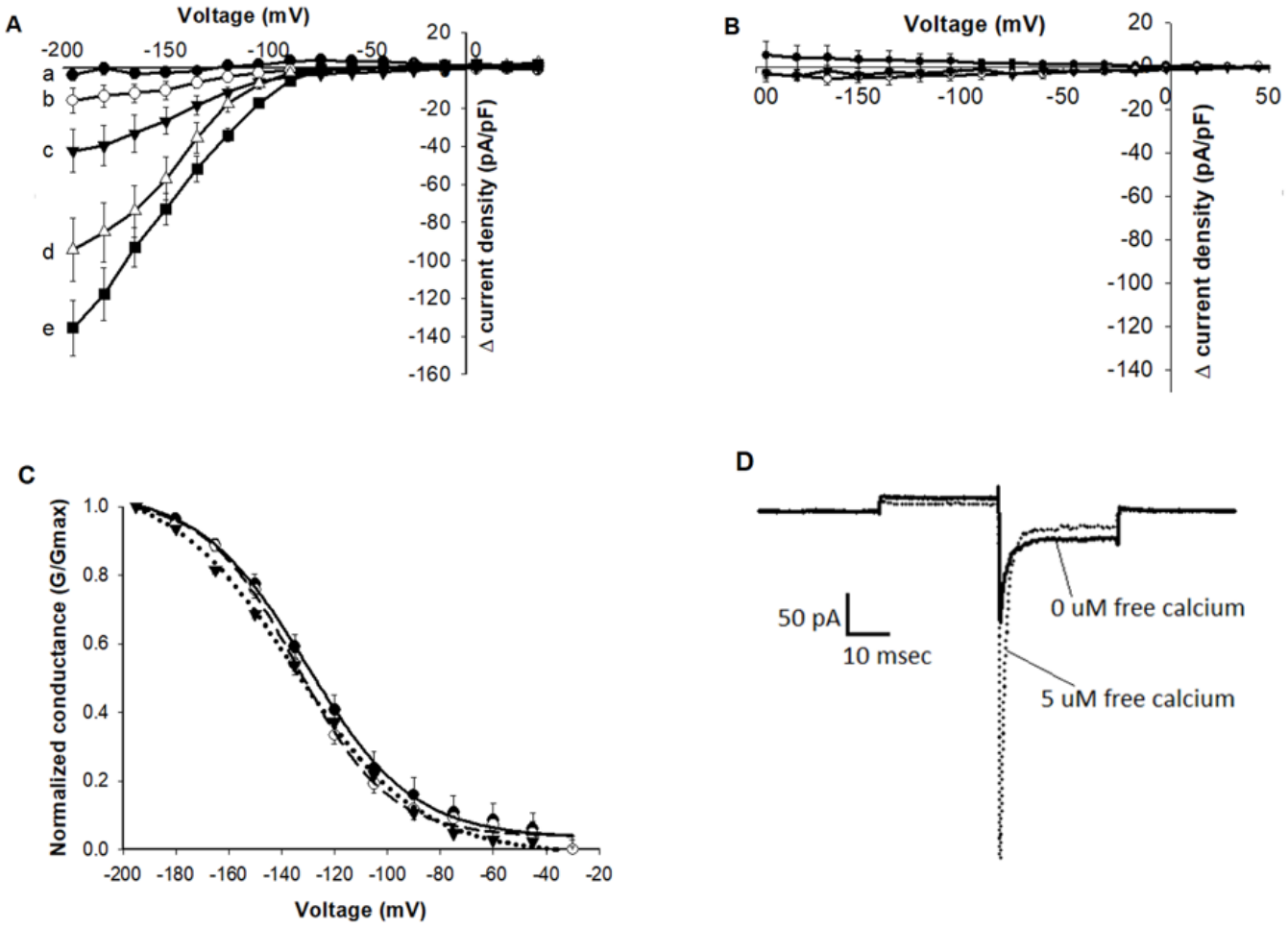

Figure 4. 3 Effect of Ca^{2+} on activity of *Bd*QUAC1 after malate activation.

A) Ca^{2+} -dependent Δ current density (± 30 mM malate) of *Bd*QUAC1-HEK293 cells. Currents of *Bd*QUAC1-HEK293 cells were recorded at different Ca^{2+} concentrations in the pipette solution including 0 µM (black circles), 0.05 µM (white circles), 0.1 µM (black triangles), 0.5 µM (white triangles) and 5 µM (black squares) free Ca^{2+}, $n \geq 8$ for each concentration. Lower case letters indicate statistical differences. B) Negative control - effect of Ca^{2+} on Δ current density of GFP-HEK293 cells. Currents of GFP-HEK293 cells were recorded at different Ca^{2+} concentrations in the pipette solution including 0 µM (black circles), 0.1 µM (white circles), 0.5 µM (black triangles) and 1 µM (white triangles) free Ca^{2+}, n = 3 each concentration. C) Conductance of BdQUAC1 channels (normalized to maximum) at different Ca^{2+} concentrations including 0.1 uM (solid line), 0.5 uM (broken line), 5 uM (dotted line) free Ca^{2+}. No statistical differences were detected ($p > 0.05$). D) Representative traces of *Bd*QUAC1-HEK293 cells at -180 mV with 0 or 5 µM free Ca^{2+} in the pipette solution.

4.2. The Ca^{2+} -dependent mechanism of activation of *Bd*QUAC1

With data suggesting the activation of *Bd*QUAC1 channel is Ca^{2+} -dependent, further patch clamp experiments were performed to determine whether the Ca^{2+} activation is mediated through a kinase or CaM-dependent mechanisms.

4.2.1. The effect of kinase on *Bd*QUAC1 activation

To examine whether kinases might be involved in the Ca^{2+} activation of *Bd*QUAC1, the non-specific kinase inhibitor staurosporine was included in the pipette solution for patch clamp experiments. Staurosporine inhibits kinase activity by preventing ATP from binding to the kinase, thus preventing the phosphorylation events from occurring. Surprisingly, the addition of 60 nM staurosporine to the patch clamp pipette solution, containing 0.1 μM free Ca^{2+}, did not reduce the activities of *Bd*QUAC1, but resulted in an increase in Δ current densities (Figure 4.4). Additionally, the conductance curve also showed a slight shift to the left (Figure 4.4), suggesting the channel requires more hyperpolarization for the activation in the presence of staurosporine.

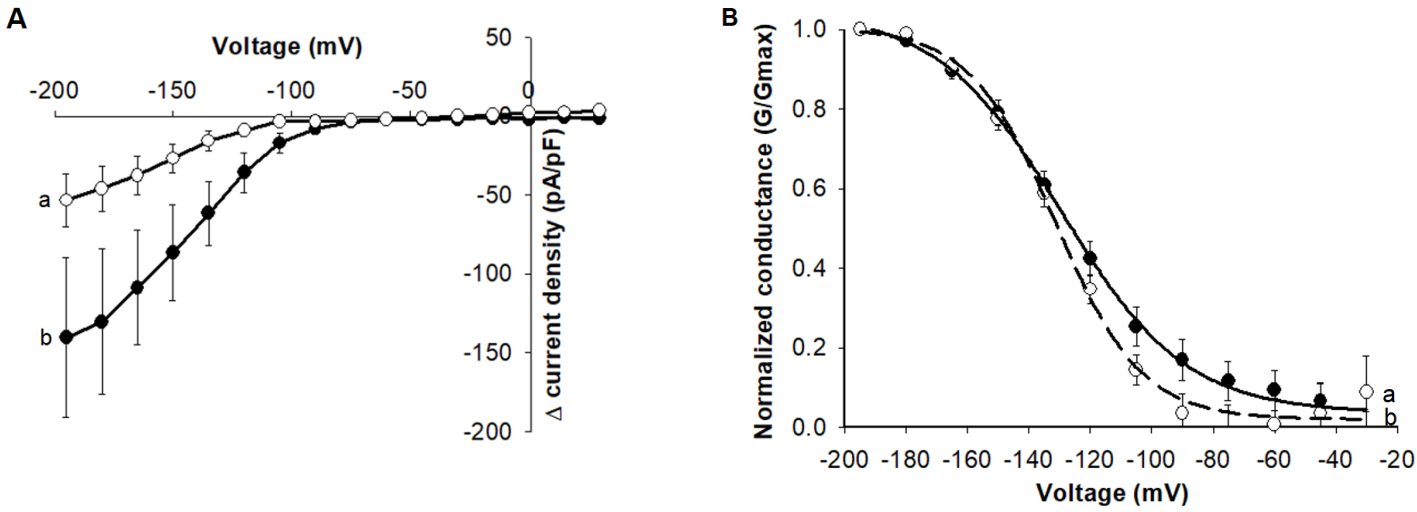

Figure 4. 4 Effect of Staurosporine on *Bd*QUAC1 activation.

A) Δ current density (± 30 mM malate) of *Bd*QUAC1-HEK293 cells. Currents of *Bd*QUAC1-HEK293 cells were recorded with pipette solutions containing 0.1 μM free Ca^{2+} (white circles) or 0.1 μM free Ca^{2+} and 60 nM staurosporine (black circles) with n = 9 for each treatment. B) The voltage dependence of conductance of *Bd*QUAC1 channels with the addition of staurosporine in the pipette solution. Pipette solutions contained 0.1 μM free Ca^{2+} (solid line) or 0.1 μM free Ca^{2+} and 60 nM staurosporine (dotted line).

4.2.2. *Bd*QUAC1 activation is CaM-dependent

To examine whether CaM effects the activation of *Bd*QUAC1, CaM inhibitors W-5 and W-7 were used. Both W-5 and W-7 are naphthalene sulfonamide derivatives and inhibit CaM activities by binding to CaM which prevents the binding of CaM to target proteins. W-5 is generally a much weaker antagonist compared to W-7. The effect of CaM inhibition was first tested using the weaker inhibitor,W-5, at 500 μM in the pipette solution (containing 0.1 mM free Ca^{2+}), resulting in significantly decreased peak current and Δ current density for *Bd*QUAC1 (Figure 4.5A and 4.5E). Subsequently, the stronger inhibitor W-7 was used to examine *Bd*QUAC1 activation at several lower doses, in a dose-response manner (at 1 μM, 5 μM and 10 μM). The peak currents and Δ current densities decreased significantly as the dose of W-7 increased. With the addition of 10 μM W-7, the Δ current density is statistically the same as Δ current density of *Bd*QUAC1 patched in the absence of free Ca^{2+} (Figure 4.5B and 4.5F). There was no significant change in channel conductance with both the addition of W-5 and W-7 (Figure 4.5C and 4.5D), suggesting calmodulin modulates only the malate- Ca^{2+} activation but not the voltage activation of the *Bd*QUAC1.

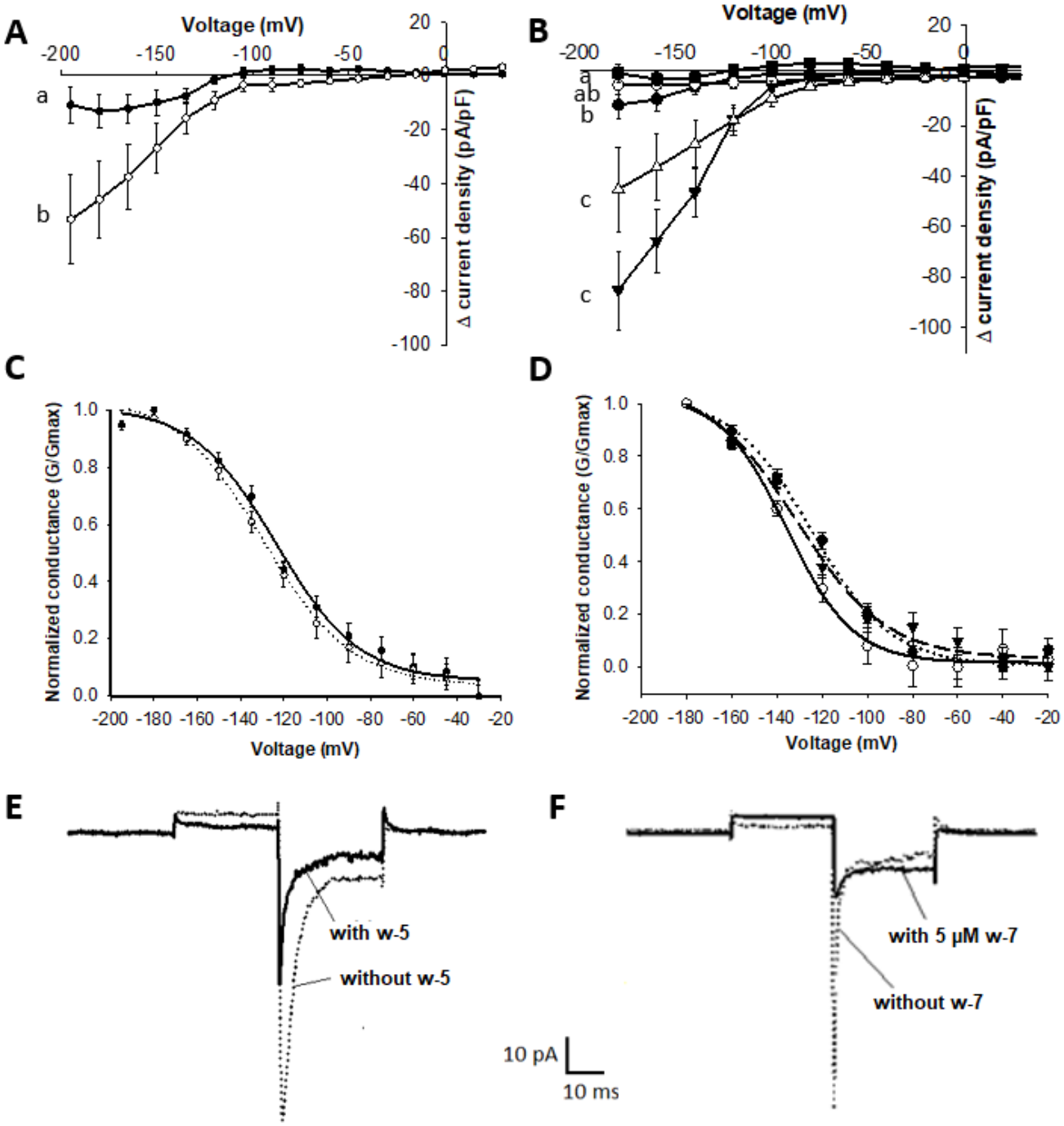
A
Voltage (mV)
-200
-150
-100
-50
0
20
a
b
-20
-40
-60
-80
-100
Δ current density (pA/pF)
B
Voltage (mV)
-200
-150
-100
-50
0
20
a
ab
b
c
c
-20
-40
-60
-80
-100
Δ current density (pA/pF)
C
Normalized conductance (G/Gmax)
1.0
0.8
0.6
0.4
0.2
0.0
-200 -180 -160 -140 -120 -100 -80 -60 -40 -20
Voltage (mV)
D
Normalized conductance (G/Gmax)
1.0
0.8
0.6
0.4
0.2
0.0
-200 -180 -160 -140 -120 -100 -80 -60 -40 -20
Voltage (mV)
E
with w-5
without w-5
10 pA
10 ms
F
with 5 μM w-7
without w-7

Figure 4. 5 Effect of W-5 and W-7 on malate activation of *Bd*QUAC1.

A) Δ current density of *Bd*QUAC1-HEK293 cells with the addition of W-5. Currents of *Bd*QUAC1-HEK293 cells were recorded with pipette solutions containing 0.1 μM free Ca^{2+} (white circles) or 0.1 μM free Ca^{2+} and 500 μM W-5 (black circles), with $n \geq 6$ for each treatment. B) Δ current density of *Bd*QUAC1 with the addition of W-7. Pipette solutions contained 0.5 μM free Ca^{2+} (black triangles), 0.5 μM free Ca^{2+} and 1 uM W-7 (white triangles), 0.5 μM free Ca^{2+} and 5 μM W-7 (black circles), 0.5 μM free Ca^{2+} and 10 μM W-7 (white circles), and 0 μM free Ca^{2+} (black squares) with $n \geq 6$ for each treatment. Same letters indicate statistical similarity. C) The conductance of HEK cells expressing *Bd*QUAC1 with the addition of W-5 in the pipette solution. Pipette solutions contained 0.1 μM free Ca^{2+} (dotted line) or 0.1 μM free Ca^{2+} and 500 μM W-5 (solid line). D) The conductance of *Bd*QUAC1 channels with the addition of W-7 in the pipette solution. Pipette solutions contained 0.5 μM free Ca^{2+} (broken line), 0.5 μM free Ca^{2+} and 1 μM W-7 (dotted line), or 0.5 μM free Ca^{2+} and 5 μM W-7 (solid line). E) Representative traces of *Bd*QUAC1 current at -180 mV with 0.1 μM free Ca^{2+} and the presence or absence of 500 μM W-5. F) Representative traces of *Bd*QUAC1 current at -180 mV with 0.5 μM free Ca^{2+} and the presence or absence of 5 μM W-7. Lower case letters indicate statistical differences.

4.2.3. Regulation of stomatal closure by malate, Ca^{2+} and CaM

To validate the role of malate, Ca^{2+} and calmodulin in stomatal regulation, the widths of stomatal pores in *Brachypodium* leaves were measured after being soaked in solutions containing malate, Ca^{2+} ionophore A23187 (which allows Ca^{2+} to pass the cell membrane resulting in higher Ca^{2+} in the cytosol), and/or CaM inhibitors W-5 and W-7 (Figure 4.6). Stomata treated solely with malate or A23187 showed no significant difference compared to untreated stomata, while stomata treated with both malate and A23187 yielded significantly smaller pores (Figure 4.6). However, with the separate addition of CaM inhibitors W-5 and W-7 (along with malate and A23187), the widths of stomatal pores increased, as the concentration of CaM inhibitors increased, eventually returning to the untreated sizes. This result is consistent with the patch clamp data above, which showed the effects of W-7 on *Bd*QUAC1 activity in a dose-dependent manner. That W-7-alone does not increase stomatal widths in the absence of malate and A23187 further emphasizes that this effect of CaM seen in stomata regulation is likely associated with the *Bd*QUAC1 channel.

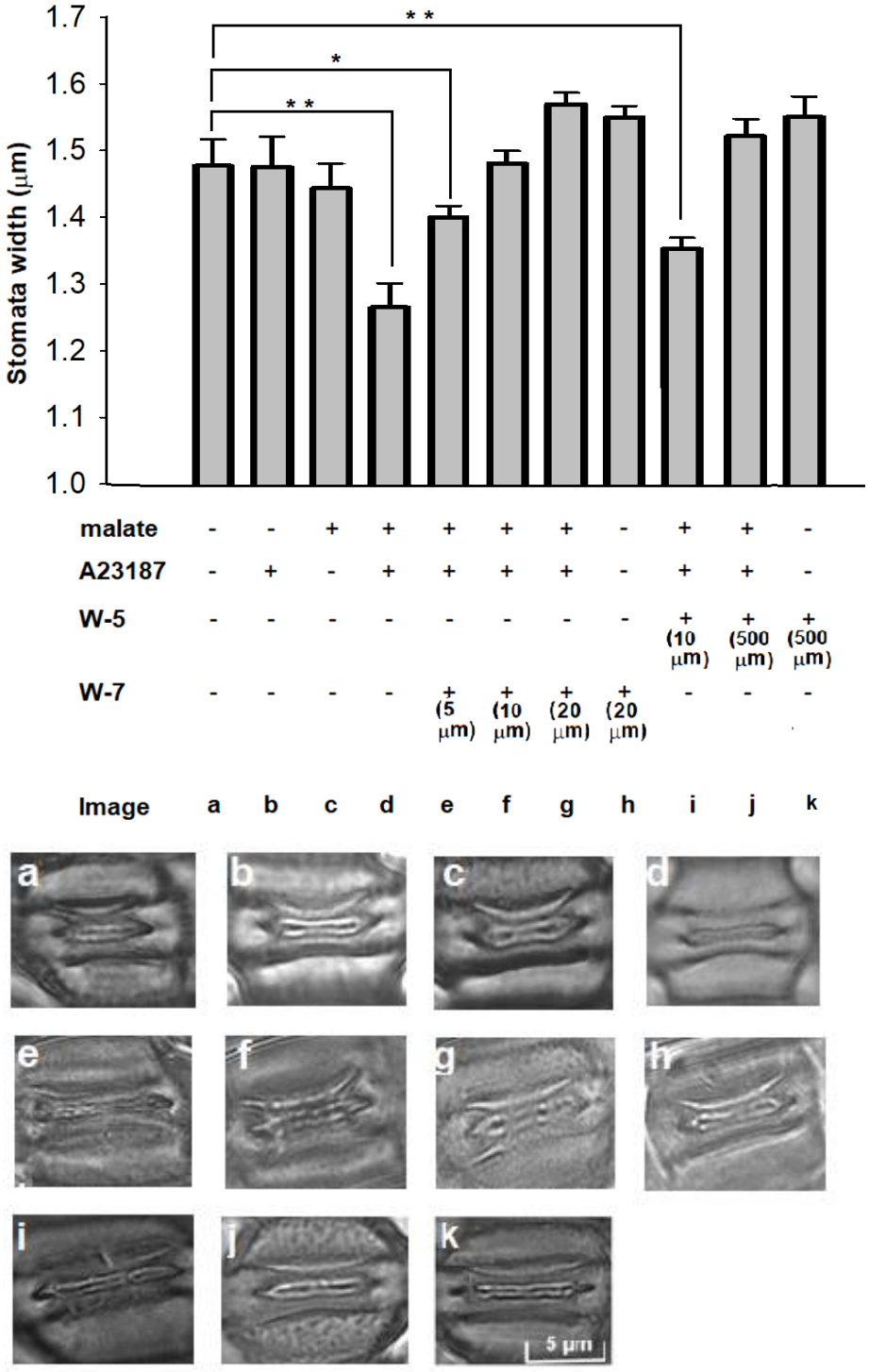

Figure 4. 6 Effect of malate, a Ca^{2+} ionophore and CaM inhibitors on stomatal aperture in *Brachypodium dystachion* wildtype.

Statistical symbols * indicates p≤0.05, and ** indicates p ≤ 0.01. Average stomata width of 100 stomata and representative stomatal images for each treatment. n = 100 stomata from 4 randomly chosen plants for each treatment.

4.3. *Brachypodium* QUAC1 contains a CaM-binding domain and is regulated by CaM binding

4.3.1. Identification of the putative *Bd*QUAC1 CaM-binding domains (CBD)

To further investigate the mechanism involving CaM, the *Bd*QUAC1 sequence was analyzed using the CaM-binding domain (CBD) prediction server MI-1 (Minhas 2012). *Bd*QUAC1 regions with high CBD prediction scores were analyzed for secondary structure using the Jpred3 server. Several regions having higher scoring for CBD were analyzed for secondary structure. However, of those, only the sequence from amino acid 334 to amino acid 351, having the second the highest CBD score, showed the structure of a basic amphiphilic alpha-helix (Figure 4.7), which is a common property of CaM-binding domains (Dash et al., 1997).

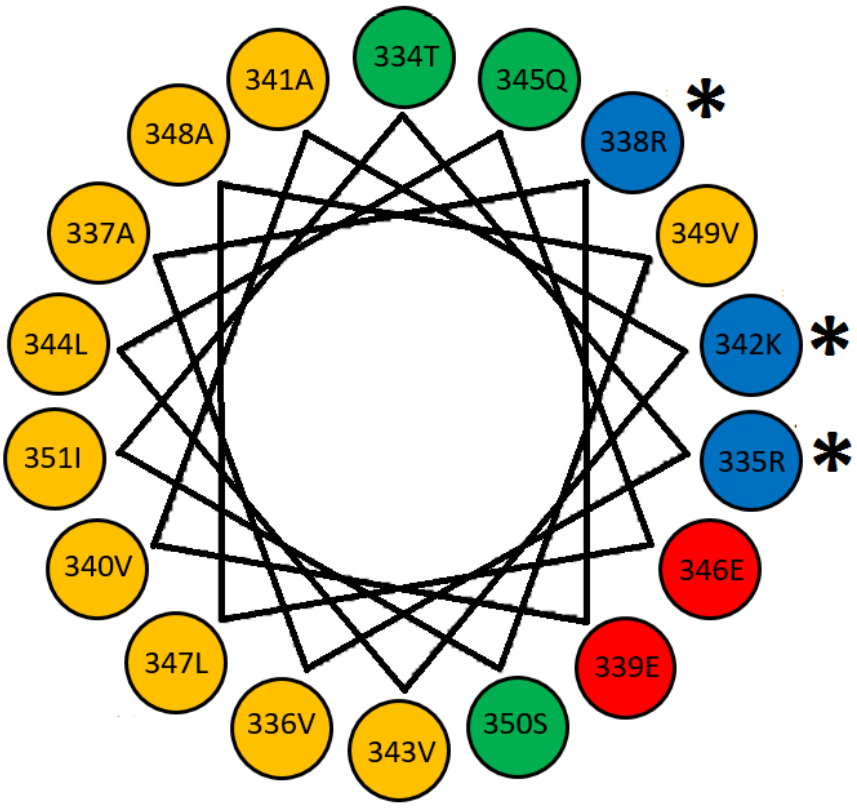

Figure 4. 7 Helical wheel depiction of the putative CaM-binding domain in *Bd*QUAC1 (amino acids 334 to 351)

Non-polar, hydrophobic residues are yellow, uncharged polar residues are green, polar acidic residues are red and polar basic residues are blue. Residues selected for mutagenesis are indicated with an asterisk.

4.3.2. Mutations in the putative CBD affect the *Bd*QUAC1 activity

Since the basic residues of CBD are known to be crucial for binding to CaM, the three basic amino acids of the *Bd*QUAC1 CBD (Arg 335, Arg 338, and Lys 342) were mutated to Ala in double and triple mutants for patch clamp studies. Patch clamp analysis of HEK293 cells expressing *Bd*QUAC1 showed that the triple mutant 335A/338A/342A had Δ current density close to 0, suggesting a lack of malate dependency in this mutated channel (Figure 4.8A). The two double mutants 335A/338A and 335A/342A had significantly smaller peak current and Δ current density compared to wildtype, however, there was no significant difference between the mutant 338A/342A and wildtype (Figure 4.8A and D). Additionally, the double mutants 335A/338A and 335A/342A showed significantly longer inactivation time constants while mutant 338A/342A had a similar inactivation time constant compared to wildtype (Figure 4.8C).

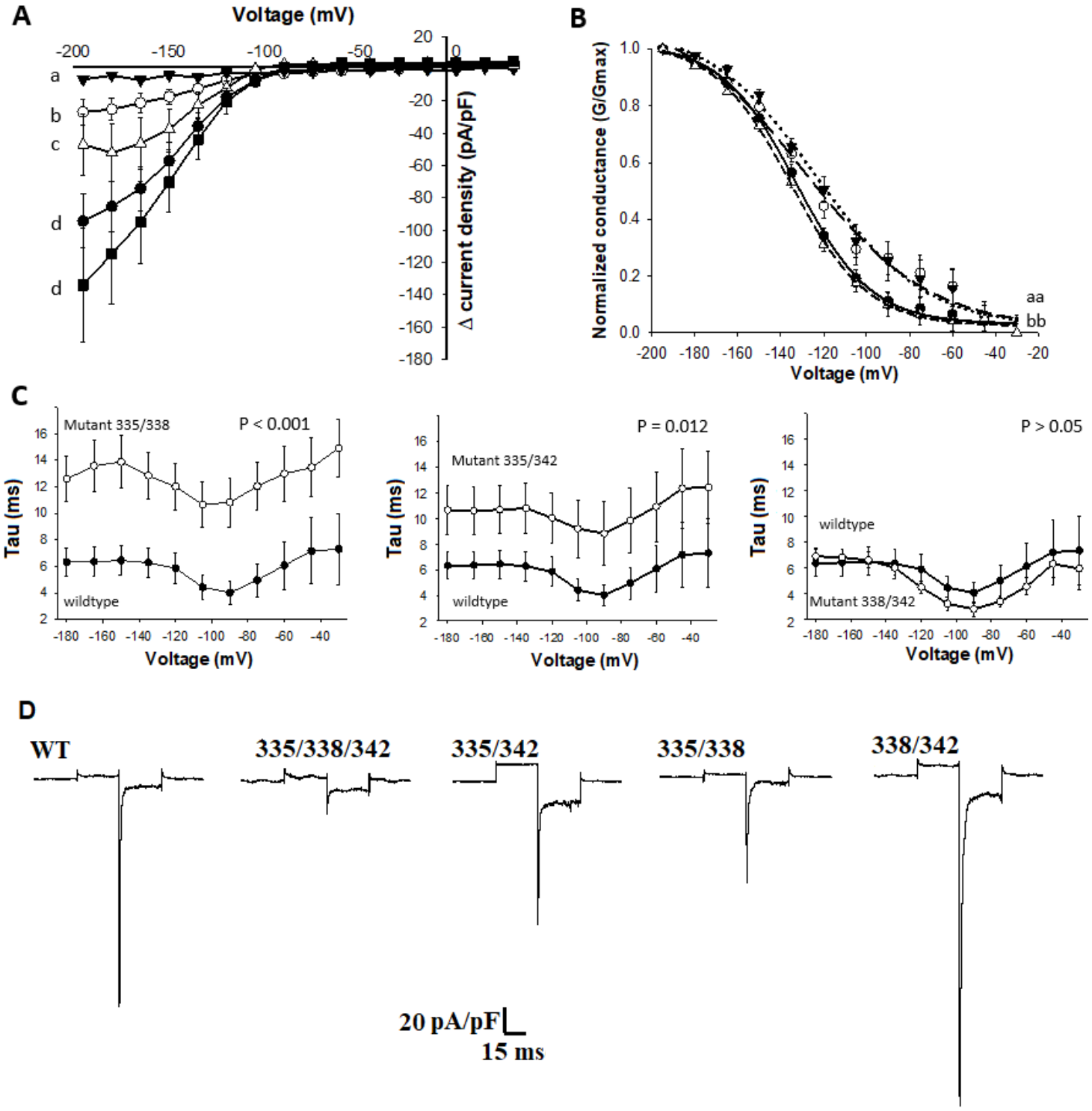
A
Voltage (mV)
-200
-150
-100
-50
0
20
-20
-40
-60
-80
-100
-120
-140
-160
-180
a
b
c
d
d
Δ current density (pA/pF)
B
Normalized conductance (G/Gmax)
1.0
0.8
0.6
0.4
0.2
0.0
-200 -180 -160 -140 -120 -100 -80 -60 -40 -20
Voltage (mV)
aa
bb
C
Mutant 335/338
P < 0.001
wildtype
Tau (ms)
Voltage (mV)
Mutant 335/342
P = 0.012
wildtype
Tau (ms)
Voltage (mV)
P > 0.05
wildtype
Mutant 338/342
Tau (ms)
Voltage (mV)
D
WT
335/338/342
335/342
335/338
338/342
20 pA/pF
15 ms

Figure 4. 8 Effect of mutations in the putative *Bd*QUAC1 CaM binding domain on *Bd*QUAC1 channel activity.

A) Δ current density of *Bd*QUAC1 and *Bd*QUAC1 mutants. Transfected HEK cells were patched with 0.5 μM Ca^{2+} in the pipette solution. Wildtype (black circles), mutant 335A/338A (white circles), mutant 335A/342A (white triangles), mutant 338A/342A (black squares), mutant 335A/338A/342A (black triangles), with $n \geq 8$ for each mutant or wildtype. Same letters indicate no significant difference. B) Normalized conductance of HEK cells expressing *Bd*QUAC1 or *Bd*QUAC1 mutants including wildtype (solid line), mutant 335/338 (long broken line), mutant 335/342 (dotted line) and mutant 338/342 (short broken line). C) Inactivation time constants of each double mutant compared to wild-type *Bd*QUAC1. D) Representative traces of mutant and wildtype QUAC1 currents at -180 mV.

.

Though patch clamp data showed that mutations at the predicted CBD reduced the channel's currents, it is important to confirm that wildtype *Bd*QUAC1 and mutants were expressed equally on HEK293 cell membranes and that the effect was not due to low expression of the mutant proteins. To confirm the protein expression, Myc-tagged *Bd*QUAC1 or Myc-tagged mutants of *Bd*QUAC1 were expressed in HEK293 cells, and membrane proteins were isolated for western blot analysis. The double mutant 335A/338A and triple mutant 335A/338A/342A which had shown significantly smaller currents in patch clamp (Figure 3.8A), also showed significantly lower protein expression on the cell membrane compared to wildtype *Bd*QUAC1 (Figure 4.9A). To compensate for the low or different amount of protein expression, Δ current densities of wildtype and mutant *Bd*QUAC1 were normalized to the level of protein expressed on HEK cell membrane (Figure 4.9B). Even so, the statistical results after normalization remain unchanged (Figure 4.9B), compared to the Δ current density data before normalization (Figure 4.8A). This suggests that the reduced activities seen in mutants represent effects caused by mutations in the CBD and are not simply due to the lower expression of the proteins.

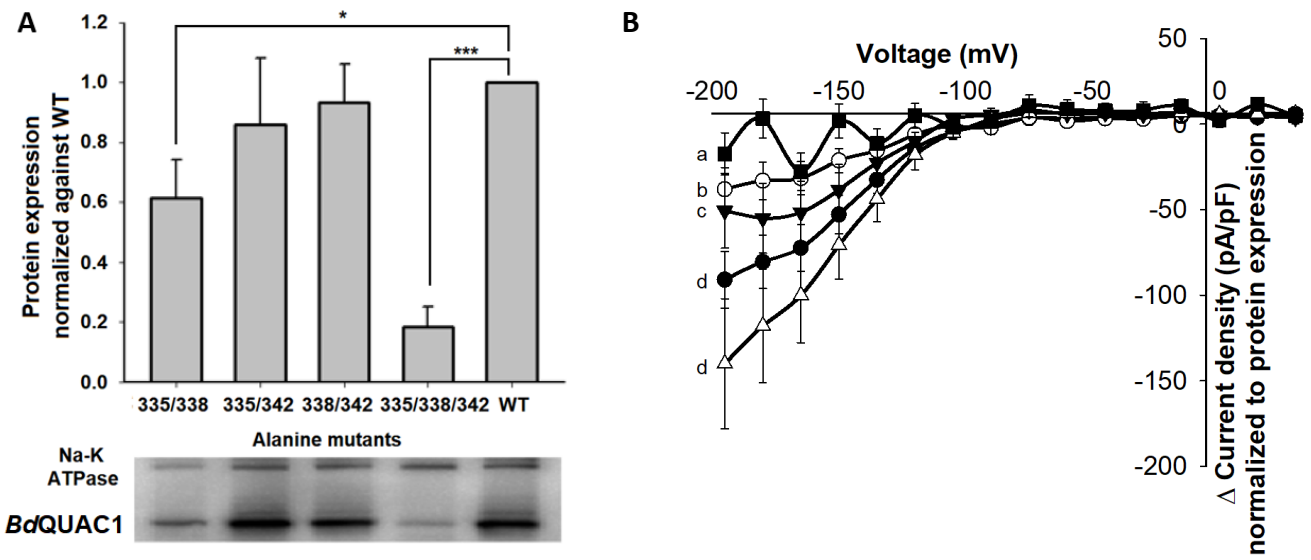

Figure 4. 9 Protein expression of mutants and wildtype Myc-tagged *Bd*QUAC1.

A) Protein expression of mutants and wildtype Myc-tagged *Bd*QUAC1in HEK293 cell membranes. Total isolated cell membrane proteins were analysed by Western Blot using an anti-Myc-tag antibody, with $n \geq 6$ for each mutant and wildtype. Wildtype expression was normalized to 1. * indicates p-value < 0.05, *** indicates p-value < 0.001. Representative Western Blot image showed the detection of *Bd*QUAC1 and the loading control Na-K ATPase. *B*) Δ current density of *Bd*QUAC1 and *Bd*QUAC1 mutants after normalization to protein expression. Normalized Δ current density was calculated by subtraction of the background Δ current density (Δ current density of GFP-HEK293 cells) to the Δ current density *Bd* QUAC1 or mutants, then dividing by protein expression for wildtype (black circles), mutant 335/338 (white circles), mutant 335/342 (black triangles), mutant 338/342 (white triangles), and mutant 335/338/342 (black squares). Same letters indicate statistical similarity.

4.3.3. Interaction between *Bd*QUAC1 CBD peptide and CaM shown by ITC

4.3.3.1. Binding of wildtype BdQUAC1 CBD peptide to CaM and inhibition by W-5 and W-7

With patch clamp results showing the involvement of CBD in regulating *Bd*QUAC1 activity, isothermal titration calorimetry was performed to confirm the physical interaction between the predicted CBD of *Bd*QUAC1 and CaM.

An 18 amino acid long *Bd*QUAC1 CBD peptide (synthesized by Genscript) was used for the experiment. Binding between the peptide and CaM was demonstrated by the release of heat when solution of the peptide was titrated into the cell containing a solution of CaM (Figure 4.10A). Fit of the binding enthalpy (calculated and generated by NanoAnalyze) of *Bd*QUAC1 CBD and CaM presented a two-stage binding model, with two different dissociation constants Kd1 and Kd2. Additionally, interactions between the CBD peptide and CaM were also tested in the absence of Ca^{2+} or the presence of CaM inhibitors W-5 and W-7. For Ca^{2+} free condition, the CBD peptide and CaM were dialyzed in buffer containing 1.5 mM EGTA to chelate all Ca^{2+} that might be present from the manufacturing process. Under this condition, some binding between CBD peptide and CaM was still detected (Figure 4.10B), but with the two Kd values much larger compared to the initial binding with Ca^{2+} (Table 4.1), indicating significantly lower affinity. There was no binding detected in the presence of CaM inhibitors W-5 or W-7 (Figure 4.10C and D). Altogether, these results confirm the *Bd*QUAC1 region amino acids 334-351 is a CBD of *Bd*QUAC1.

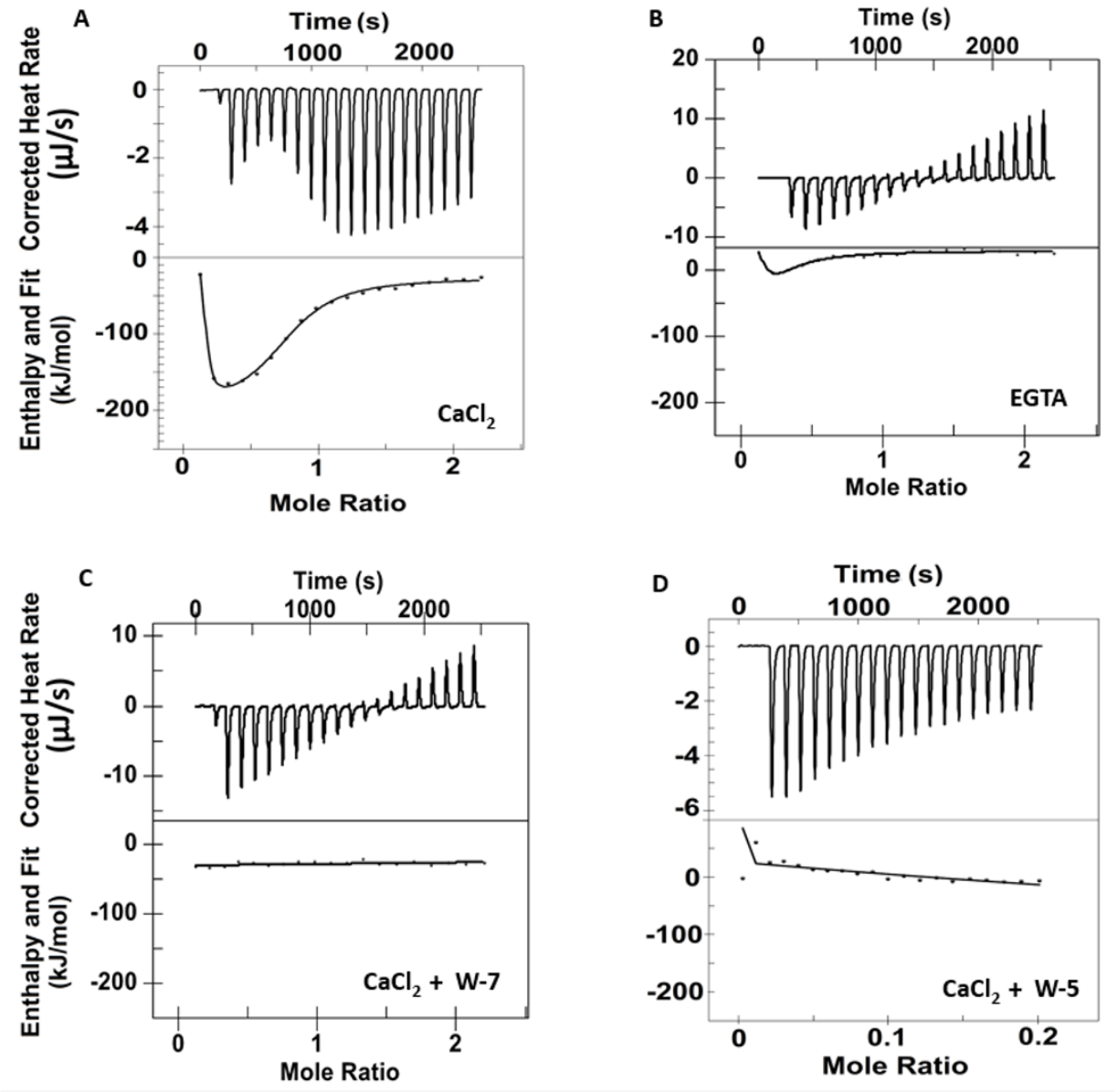

Figure 4. 10 ITC analyses of the binding of wildtype CaM-binding peptide to CaM.

A) in the presence of 5 mM Ca^{2+}. B) in the presence of 1.5 mM EGTA with no added Ca^{2+}. C) in the presence of 5 mM Ca^{2+} with 60 µM W-7. D) in the presence of 5 mM Ca^{2+} with 600 µM W-5. The amount of CaM used in all conditions is 60 µM. The 5 mM Ca^{2+} and no Ca^{2+} data were fit using the 'multiple sites' model and the 5 mM Ca^{2+} with W-7 and W-5 data was fit using the 'independent' model.

Peptide	Kd_1 (M)	ΔH1 (kJ/mol)	ΔS1 (J/mol.K)	Kd_2 (M)	ΔH2 (kJ/mol)	ΔS2 (J/mol.K)
Wild type peptide	$3.452E^{-8}$	105.4	$4.962E^{2}$	$3.925E^{-6}$	-174.0	$-4.8E^{2}$
Wildtype peptide, with 1.5 mM EGTA (no Ca^{2+})	$9.165E^{-7}$	69.16	$3.437E^{2}$	$1.003E^{-5}$	-199.9	$-5.636E^{2}$
Wildtype peptide, with 60 µM w-7	ND	ND	ND	ND	ND	ND
Wildtype peptide, with 600 µM w-5	ND	ND	ND	ND	ND	ND
Mutant 338D/342D peptide	$4.101E^{-8}$	-48.78	$-2.217E^{1}$	$6.366E^{-6}$	-199.2	$-5.685E^{2}$
Mutant 335D/338D peptide	$3.721E^{-7}$	-75.77	-131.1	ND	ND	ND
Mutant 335D/342D peptide	$5.5E^{-6}$	-470.8	-1478	ND	ND	ND
Mutant 335D/338D/342D peptide	ND	ND	ND	ND	ND	ND

Table 4. 1 Binding parameters of wildtype and mutant CaM-binding peptide

All measurements were made in the presence of 5 mM Ca^{2+} (with the exception of the 'no Ca^{2+}' condition) and 60 µM CaM.

4.3.3.2 Mutations in the CBD peptides affect binding affinity

To test the binding affinity of *Bd*QUAC1 mutants (described in the section above) to CaM, double and triple alanine mutant CBD peptides were synthesized for the ITC experiments. Unfortunately, the alanine substituted mutant peptides were too hydrophobic, causing the formation of aggregates at high concentrations (dynamic light scattering; data not shown), and therefore could not be used for the ITC experiment. As such, a new set of mutant peptides were synthesized with the polar acidic residue Asp substitutions instead of Ala for the ITC experiments.

There was no binding between the triple mutant peptide 335D/338D/342D and CaM (Figure 4.11). The two double mutants 335D/338D and 335D/342D showed decreased binding affinities for Kd1 and complete loss of the second stage Kd2 binding (Figure 4.11 and Table 4.1). The double mutant 338D/342D showed similar binding affinities compared to wildtype. These results are consistent with the electrophysiological data described above, confirming the involvement of the CaM-binding domain in *Bd*QUAC1 activities.

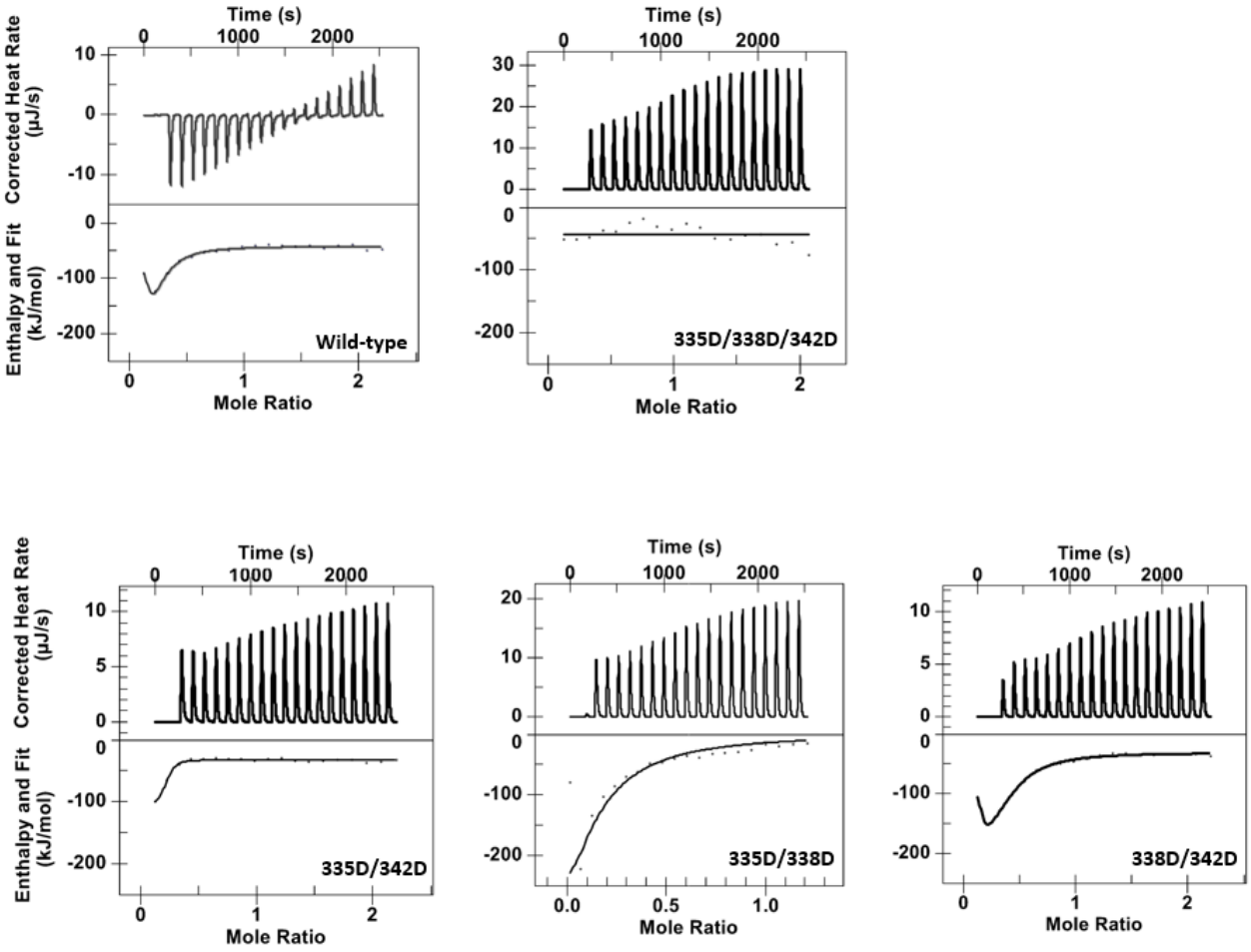

Figure 4. 11 Isothermal titration calorimetry of binding of mutant CaM-binding peptides to CaM.

The binding of all peptides was carried out in the presence of 5mM Ca^{2+}. Mutant 338/342 data were fit using the 'multiple sites' model yielding a two-state binding result. The others were fit using the 'independent' model and yielded either a single binding event (mutant335/338 and 335/342) or no binding (mutant335/338/342)

4.3.4. Binding of full-length wildtype and mutant *Bd*QUAC1 to CaM

Following the interactions between *Bd*QUAC1 CBD peptides and CaM detected by ITC, a CaM agarose affinity pull-down (CAP) experiment was performed to investigate whether these interactions also occur in the full-length *Bd*QUAC1. Beside wildtype *Bd*QUAC1, the full-length double mutant 335A/342A was also tested in this experiment. The mutant 335A/342A protein expressed well on HEK293 cell membranes (Figure 4.9A) but showed decreased activity in electrophysiological results (Figure 4.9B) and lower binding affinity in ITC (Table 1 and Figure 3.11), and therefore chosen for this experiment. Total protein extracts from HEK293 cells expressing either *Bd*QUAC1 or mutant 335A/342A were obtained by lysing the cells in buffer containing detergent. The lysates were applied directly to CaM resin, and following extensive washing to remove all unbound proteins. All CaM bound proteins were then eluted with buffer containing 20 mM EGTA. The eluate was analyzed by total protein stain and western blot. Western blot analysis showed a strong band at the expected molecular weight for wildtype *Bd*QUAC1 (Figure 4.12A). The intensity of the corresponding band was dramatically reduced for the double mutant 335A/342A sample and no band was detected in the negative control from HEK293 transfected with the empty vector pIRES-eGFP (Figure 4.12A). Quantification of the band intensity showed a ~ 75 % reduction (after subtraction of un-transfected background) in the amount of 335A/342A mutant eluted, compared to wildtype *Bd*QUAC1 (Figure 4.12B). This is consistent with the reduced binding affinity detect for this mutant by ITC.

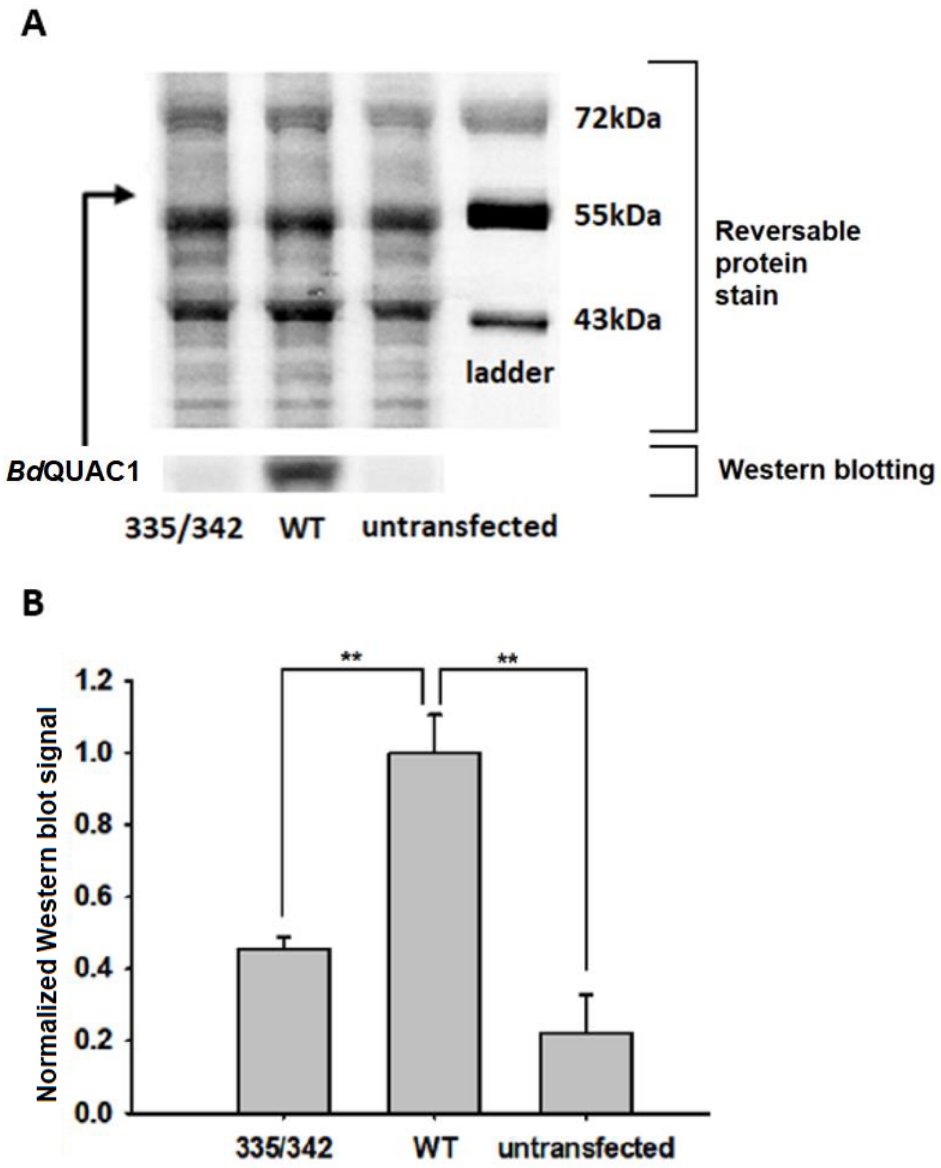

Figure 4. 12 Binding of full-length wildtype QUAC1 and mutant 335A/342A to CaM.

A) Representative Western Blot and reversible protein stain image of full-length wildtype QUAC1 and mutant 335A/342A eluted from CaM-affinity resin. B) Quantification of full-length *Bd*QUAC1 protein bound to CaM. Wildtype *Bd*QUAC1 and mutant 335/342 binding to CaM were analyzed by Western Blot using an anti-Myc-tag antibody, n = 4. Signals of wildtype and mutant QUAC1 from western blot were quantified against total proteins stain, and wild-type QUAC1 was normalized to 1. ** indicates $p \leq 0.01$.

4.4. QUAC1 affects rust infection by regulating stomatal opening

4.4.1. Relationship between QUAC1 and rust infection

Rusts require specific stomatal aperture width for infection. As mentioned in the above chapter, leaf rust was able to penetrate closed stomata while stem rust requires opened stomata for successful infection (Caldwell and Stone 1936, Hart 1929). At the same time, studies have suggested that rusts have the ability to control stomatal function via the toxins they release (Grimmer et al., 2012). Nonetheless, the mechanisms by which these toxins regulate stomata remain unknown. Therefore, the host plant components that are involved in plant stomatal function, such as QUAC1, could be crucial for rust infection. In the following experiments, the level of rust infection is examined in plants where the expression of QUAC1 gene is altered and stomata are not properly functioning.

4.4.2. Generation of QUAC1 knockdown plants in *Brachypodium distachyon* and qPCR confirmation

QUAC1 knockdown plants were generated in *Brachypodium distachyon* using the RNAi knockdown method. Initially, nine lines of knockdown plants were confirmed by qPCR at the T0 generation (Figure 4.13). Of these, three lines with the lowest QUAC1 gene expression KD2, KD5 and KD9 were chosen for seed collection and further experiments at T1 generation.

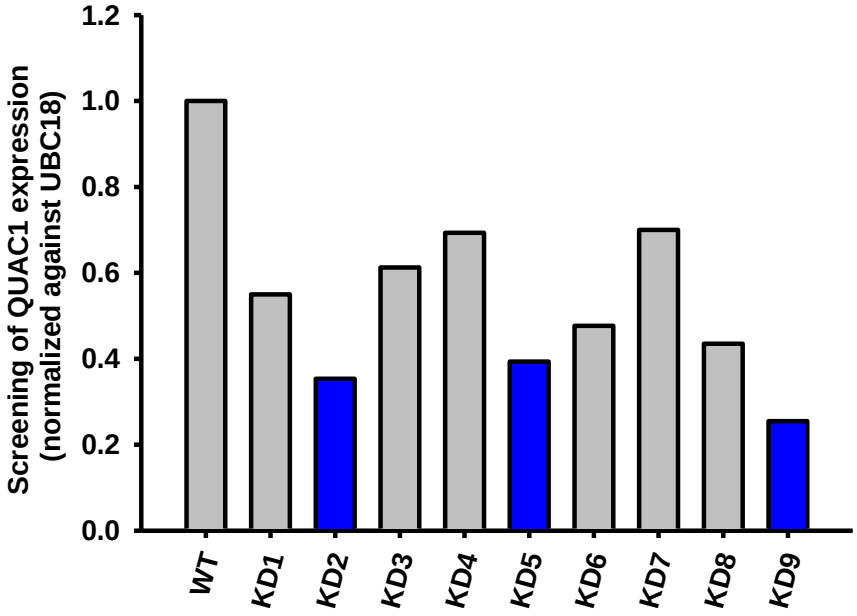

Figure 4. 13 PCR quantification of RNAi knockdown of QUAC1 in *B. distachyon* T0 generation plants.

Expression of QUAC1 in knockdown plants was normalized to wildtype as 1. Knockdown lines highlighted in blue had the lowest QUAC1 expression and were selected for further experiments at the T1 generation.

.

4.4.3. Stomatal measurement of transgenic *Brachypodium*

The expression of the *Bd*QUAC1 gene in knockdown plants was re-checked by qPCR at the T1 generation. Unexpectedly, *Bd*QUAC1 of KD5 and KD9 had rebounded back to expression levels either similar to or higher than wildtype. However, KD2 still showed a significant knockdown of QUAC1 as a young seedling (4-6 weeks old). Therefore, the KD2 line was used in further experiments. By the time KD2 plants matured (8-10 weeks old), the expression level of *Bd*QUAC1 had also rebounded to levels significantly higher than wildtype, creating a '*Bd*QUAC1 overexpressing' condition (Figure 4.14C). Measurement of stomata widths showed that KD2 plants had larger stomatal pores compared to wildtype at the younger stage (Figure 4.14B) and smaller pores at the mature stage (Figure 4.14D). Moreover, when treated with malate and A23187, stomata of the mature KD2 plants were much more responsive compared to wildtype (Figure 4.14D). These results further support the hypothesis that *Bd*QUAC1 channel plays an important role in stomatal closure and that activities of the channel are regulated by malate and Ca^{2+}.

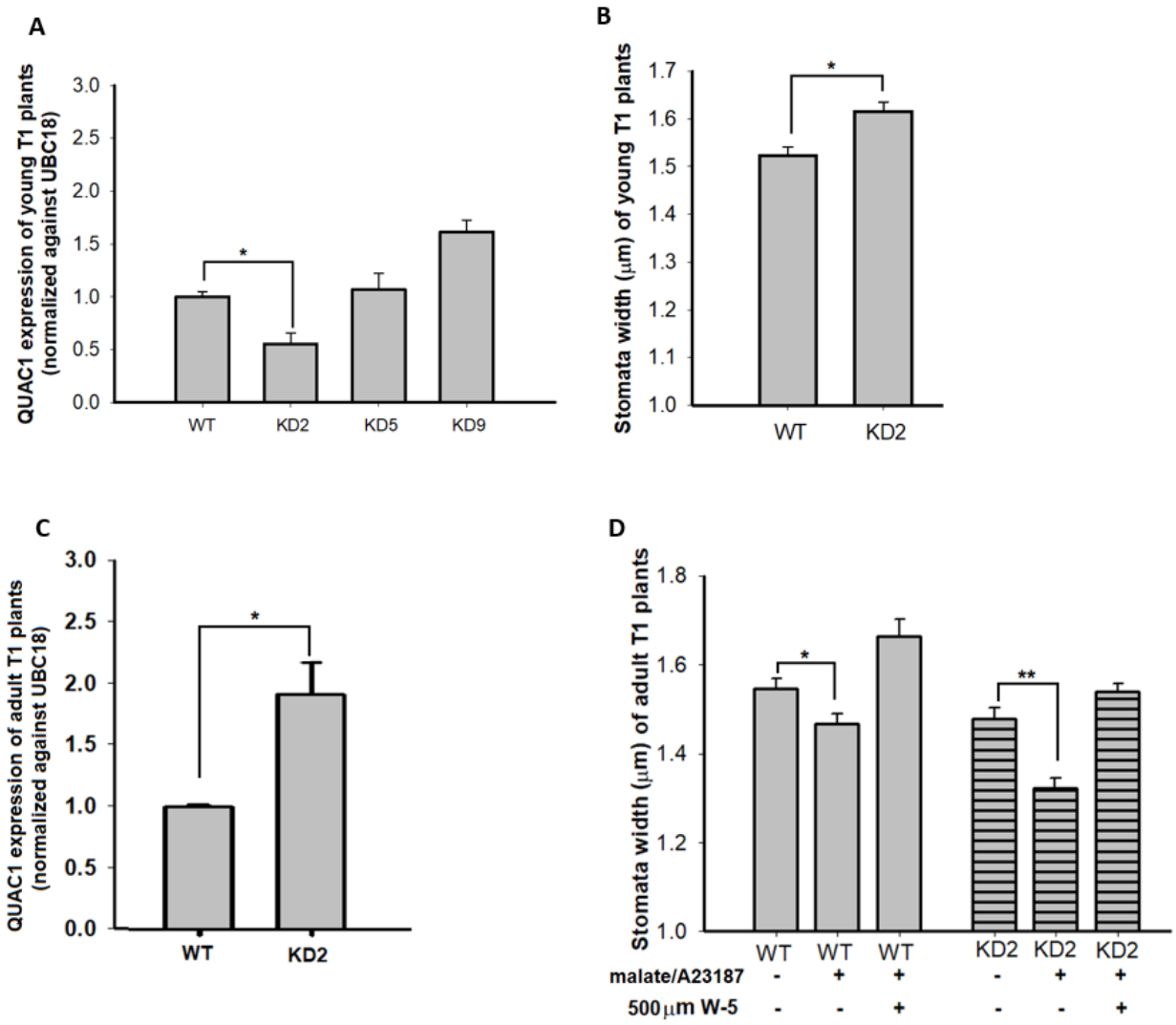

Figure 4. 14 Quantification of *Bd*QUAC1 expression in *Brachypodium* wildtype and the T1 generation KD2 plants.

A) qPCR quantification of QUAC1 expression of T1 generation seedlings (3-5 weeks), n = 3 for each line. B) Stomata width of the T1 generation KD2 seedlings (at 3-5 weeks), n = 100 stomata. C) qPCR quantification of QUAC1 expression of the T1 generation KD2 mature plants (at 8-10 weeks), n = 19. D) Stomata width of the T1 generation KD2 mature plants (at 8-10 weeks), n = 100 stomata for each treatment

4.4.4. *Bd*QUAC1 knockdown plants respond to stripe rust infection

To investigate whether overexpression of the *Bd*QUAC1 gene affects rust infection, mature 'overexpressing' KD2 and wildtype *Brachypodium* were inoculated with stripe rust. At three days after inoculation, leaves were treated with fluorophore-conjugated wheat germ agglutinin (WGA). WGA bound to the rust fungus and was used as a labeling probe for quantification of appressoria. Germ tubes with appressoria formation were counted under the microscope at three days after inoculation. The result shows that the number of germ tubes and appressoria developed on wildtype leaves is higher than on KD2 leaves (Figure 4.15A). At three weeks after inoculation, necrosis was observed on both wildtype and KD2 plants. However, visual inspection suggested that there was less infection on the KD2 plants than on wildtype (Figure 4.16). These results are consistent with what would be expected since stomata are predominantly more closed in mature KD2 plants, due to upregulation of *Bd*QUAC1, and stripe rust only infecting through open stomata.

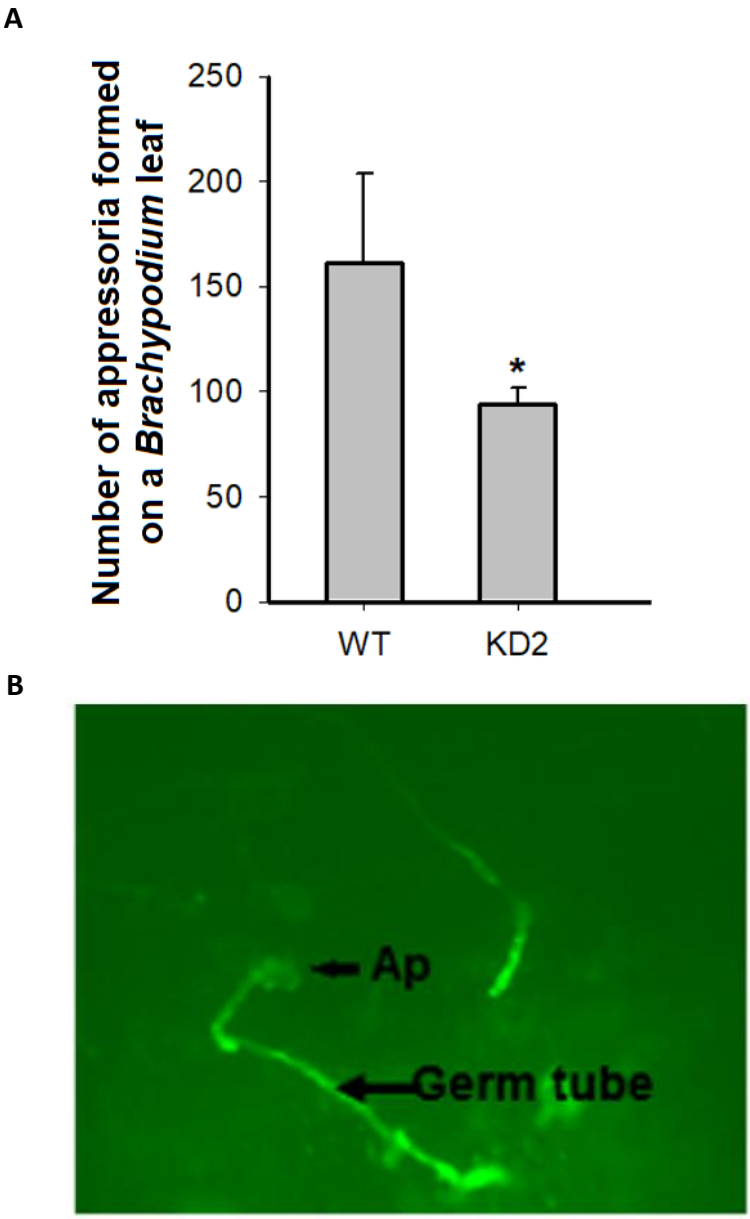

Figure 4. 15 Effect of QUAC1 upregulation on the formation of appressoria.

A) The number of germ tubes and appressoria observed on wildtype and KD2 leaves. Wildtype and KD2 leaves at approximately similar size were randomly selected for the experiments, n of 8 leaves for wildtype and KD2 in two separate experiments. * indicates $p < 0.05$. B) Representative images of germ tubes and appressoria under the fluorescence microscope at 100 x magnification.

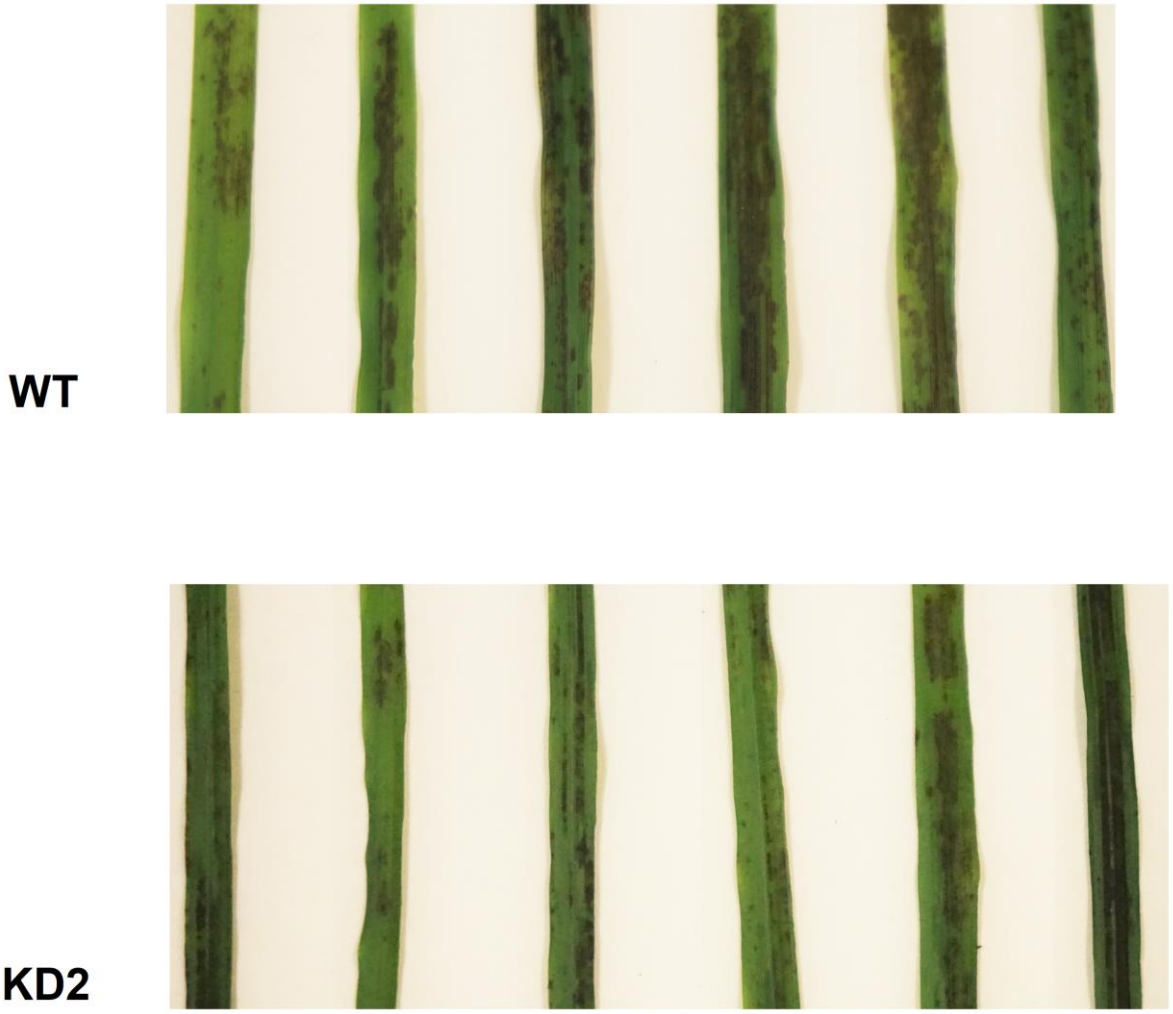

Figure 4. 16 Effect of QUAC1 upregulation on the ability of stripe rust to infect *Brachypodium distachyon*.

Whole *Brachypodium* plants were infected with stripe rust. Photos were taken at 3 weeks after infection.

4.5 The effect of ABA on *Bd*QUAC1 activation

An advantage of examinng the *Bd*QUAC1 in HEK293 system rather than in protoplasts is the absence of plant-specific substances that could potentially affect the results. Application of ABA has been shown to increase the activity of S-type channels in protoplasts (Sasaki, 2010). However, this could be due to other effects, such as increases in Ca^{2+} concentration caused by ABA, leading to S-type chanel activation indirectly. Here, the possibilty of any direct effect of ABA was tested on *Bd*QUAC1 expressed in HEK293 cells in patch clamp experiments. Currents of *Bd*QUAC1 were still observed with the addition of as much as 20 µM of ABA to the bath solution. However, there was no significant change to the channel activities with the presence of ABA (Figure 4. 17). This result shows that ABA does not *directly* interact with QUAC1, thus the modulation of QUAC1 by ABA is presumably through the Ca^{2+} -dependent and Ca^{2+} -independent pathways as mentioned earlier.

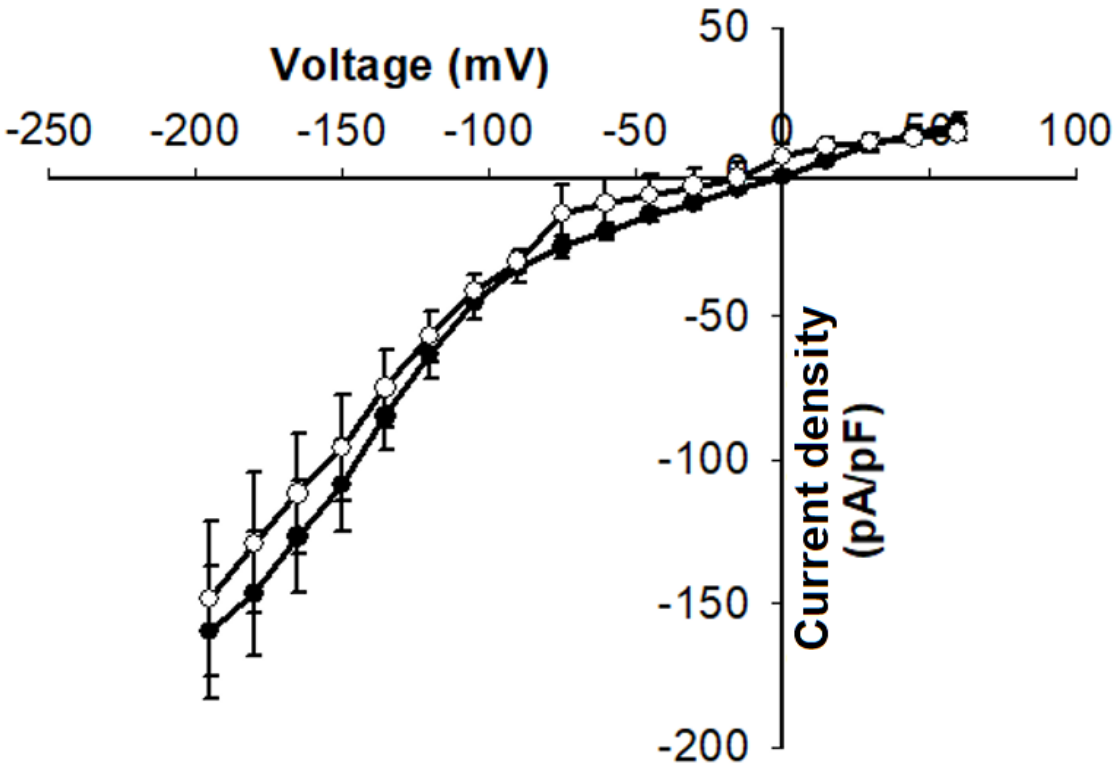

Figure 4. 17 The effect of ABA on *Bd*QUAC1 channel activity.

Currents of *Bd*QUAC1-HEK293 cells were recorded with 30 mM of malate in the external solution and 0.5 µM Ca^{2+} in the pipette solution. No ABA (black circles), 20 µM ABA (white circles) were added to the bath solution, with n = 6 cells.

5. GENERAL DISCUSSION AND CONCLUSION

5.1. Significance of the studies

Since sequence alignment showed only 56 % identity between *Arabidopsis* and *Brachypodium* QUAC1, this study first demonstrated that regulation of QUAC1 in monocot (*Brachypodium*) and its role in stomatal function were similar to what had been reported in previous studies for the dicot (*Arabidopsis*) QUAC1 (Meyer et al., 2010, Imes et al., 2013). As for the novel discovery aspect, the study showed, along with malate, a requirement for Ca^{2+} and CaM to activate the *Bd*QUAC1 channel. Furthermore, a CaM binding domain in *Bd*QUAC1 has been identified with evidence showing direct interactions between CaM and this *Bd*QUAC1 CBD. Sequence alignments showed the presence of this CBD sequence in other monocots. Additionally, the study also showed the effect that modified *Bd*QUAC1 expression has on stomatal function and stripe rust infection, thus supporting findings from other studies that pathogens require, and have the ability, to regulate stomata for successful infection (Grimmer et al., 2012).

5.2. Validation that *Bd*QUAC1 is an inward rectifying anion channel activated by malate.

Inward rectification is either the influx of cations or leaving of anions, and is indicated by negative currents. Prior to the identifying AtALMT12 as an R-type anion channel and renaming to AtQUAC1 (Meyer et al., 2010), AtALMT12 was reported, in a separate study, as an outward rectifying (positive currents) anion channel for chloride and nitrate (Figure 5, Sasaki et al., 2010). Besides renaming the channel, Meyer et al., (2010) showed that AtQUAC1 was also permeable to sulfate and malate. Activation of AtQUAC1 by malate showed both positive (anion uptake into cytosol) and negative (anion release) currents (Figure 5, Meyer et al., 2010). This suggests that

anions can be taken-up into the cytosol or released from the cell via malate-activated AtQUAC1. Indeed an earlier electrophysiological study (Colcombet et al., 2009) of R-type channels in *Arabidopsis* protoplasts showed both positive currents with chloride influx and negative current with sulfate efflux (Diatloff et al., 2009, Colombet et al., 2009). As for *Bd*QUAC1, the whole cell recordings (activated by malate) in this study showed negative current densities (Figure 4.2), indicating the release of anions. The positive currents observed at depolarized voltages were comparable to the negative control, GFP. With stomatal closure, it is the release of anions through anion channels (such as SLAC1 and QUAC1) that depolarizes the guard cell membrane and subsequently activates K^+ channels, causing an efflux of K^+ leading to the closing of stomata.

Meyer et al., 2010 reported the activation of AtQUAC1 in response to increasing malate concentrations in external solutions (Figure 5, Meyer et al., 2010). However, the authors did not provide a negative control; therefore the observed current could arguably be an effect malate had on the endogenous currents of oocytes rather than on AtQUAC1. In this study, testing of the activation of *Bd*QUAC1, along with the negative control GFP, at 30 mM external malate, validates the findings reported by Meyer (2010) and confirms its occurrence in a monocot QUAC1.

5.3. There is a cytosolic Ca^{2+} requirement for *Bd*QUAC1 activation

In previous studies, where AtQUAC1 was expressed in the *Xenopus* oocyte system, no specific requirement for Ca^{2+} was reported (Sasaki et al., 2010, Meyer et al., 2010). Here, *Bd*QUAC1 was expressed and studied in the HEK293 system. Unlike *Xenopus* oocytes, the HEK293 expression system allows the accurate control of intracellular solute concentrations via pipette solutions. Whole-cell recordings of HEK293 throughout the study were presented in Δ current densities as an indication of malate activation of the channel, calculated by subtracting the

current densities prior to malate addition from the current densities after (30 mM) malate addition. At 0 µM cytosolic Ca^{2+}, *Bd*QUAC1 was utterly unresponsive to malate activation, having a Δ current density near 0. However, *Bd*QUAC1 showed a dose-dependent response to cytosolic Ca^{2+} from 0, 0.05, 0.1, to 0.5 and 5 µM, in the presence of malate. This demonstrated the malate/ Ca^{2+} co-activation property of the channel. In the studies on AtQUAC1, malate-activation of the channel was also shown to be dose-dependent (Meyer et al., 2010). However, whether the cytosolic Ca^{2+} concentration affects the *Bd*QUAC1 channel's sensitivity to malate and remains unexplored. Nonetheless, it is certain that activation of *Bd*QUAC1 requires both cytosolic Ca^{2+} and external malate

Although working together, Ca^{2+} and malate seem to affect voltage-dependent properties differently. While increasing cytosolic Ca^{2+} concentrations had no effect on the *Bd*QUAC1 channel's voltage dependence of conductance, increasing malate concentrations shifted the AtQUAC1 channel conductance curve to the left, indicating a less depolarising voltage-dependence of the channel (Meyer et al., 2010). (However, this effect of increasing malate has not been tested on *Bd*QUAC1.) This suggests that though co-activating *Bd*QUAC1, the mechanisms by which the two modulators affect the channel are different. Moreover, Ca^{2+} interacts with the channel from the cytosolic side whereas malate interacts with the channel from the extracellular side, which would be consistent with different effects.

5.4. The mechanism and function associated with the Ca^{2+} requirement for *Bd*QUAC1 activation

Ca^{2+} -dependent mechanisms of *Bd*QUAC1 activation could possibly be mediated through kinases and CaM. Studies have reported that the AtQUAC1 channel as well as the TaALMT1

channel were controlled by kinases (Imes et al., 2013, Ligaba et al., 2009). Pre-incubation of TaALMT1 in the non-specific kinase inhibitor staurosporine significantly reduced the channel's currents (Ligaba et al., 2009). Unexpectedly, application of 60 nM staurosporine resulted in an increased current density rather than a loss of activity. This result is in contrast to what had been reported for TaALMT1. Thus, seemingly, the effect of the kinase inhibitor observed here is irrelevant to the Ca^{2+}-dependent properties of *Bd*QUAC1 channel, observed in earlier experiments. Therefore, the mechanism associated with kinase inhibition was not studied further.

The role of CaM in *Bd*QUAC1 activation was tested in the same manner using the CaM inhibitors W-5 and W-7. W-5 is a less effective antagonist for CaM and often even used as a negative (non-specific) control at lower concentrations (Hidaka et al., 1983). Upon application of either of the inhibitors (W-7 at lower and W-5 at higher concentrations), *Bd*QUAC1 showed a drastic reduction in Δ current density. Testing in a dose-dependent manner, *Bd*QUAC1 showed a dose-response to W-7 from 1 µM to 10 µM, validating the involvement of CaM in *Bd*QUAC1 activation.

For decades, Ca^{2+} and CaM have been known to play an important part in stomatal closure. Numerous CaM binding drugs, including W-7, have been tested by different studies to show the crucial role of CaM in response to ABA-induced stomatal closure in *Commelina* species (De Silva et al., 1985, Donovan et al., 1985). Additionally, stomata treated with CaM-binding drugs showed significant increases in stomatal aperture widths. However this effect occurred only at lower Ca^{2+} concentrations, as higher Ca^{2+} concentrations overwhelmed the effect of CaM inhibitors (Donovan et al., 1985). Toward relating this event of Ca^{2+}/CaM induced stomatal closure with *Bd*QUAC1, the stomata measurement assay was carried out on *Brachypodium* leaves with the use of malate, low concentration of Ca^{2+} (delivered by the Ca^{2+} ionophore A23187), and W-7. A23187 is a Ca^{2+}

ionophore which is known to allow the transport of Ca^{2+} across the guard cell membrane, and has been shown to be effective in previous stomatal studies (De Silva et al., 1985). Notably it introduces Ca^{2+} into the cytosol without invoking the traditional ABA-induced stomatal regulation mechanism. Here, malate/Ca^{2+} was found to induce stomatal closure in *Brachypodium*, and more importantly, the presence of W-7 reversed this event in a dose-response manner. These effects of malate/Ca^{2+}/CaM on stomata are consistent with the effects observed on electrophysiological analysis of *Bd*QUAC1. Stomata of mature KD2 plants, overexpressing QUAC1, under all conditions, showed smaller stomatal aperture widths. In addition, when treated with malate/A23187, while wildtype showed a 5% decrease in stomatal widths, KD2 showed an 11% decrease in stomatal width, highlighting a much stronger response with upregulated *Bd*QUAC1. With the transgenic plant data, the role of *Bd*QUAC1 in stomatal closure is validated, consistent with general functionality reported for AtQUAC1 (Meyer et al., 2010, Sasaki et al., 2010).

5.5. Validation of the CaM-binding domain of *Bd*QUAC1

Having computational predictions generate a putative CBD for *Bd*QUAC1, the three basic residues (a.a 335, 338, 342) of the domain were changed to Ala in the combination of double or triple mutations for electrophysiological studies. A decrease in Δ current densities and change in kinetics were observed in mutants containing the residue K335A (mutants K335A/K338A, K335A/R342A, and K335A/K338A/R342A). These two double mutants showed a small shift in the activation voltage of the normalized conductance curve, indicating less hyperpolarizion is required for the channel activation. In addition, the deactivation process of K335A containing mutants was slowed significantly compared to wildtype. These two kinetic changes suggest a link between the CBD and the voltage-dependent property of the channel. However, experiments with

different concentration of cytosolic Ca^{2+} or W-7 did not result in a significant kinetic change. Therefore, it is likely the structural changes in the mutants somehow changed the structure of the channel, slowing its kinetics and affecting the CaM interaction. These changes in kinetics and effects on CaM interaction would seem to occur somewhat independently. Nonetheless, the decrease in Δ current densities in these mutants again indicates *Bd*QUAC1 activation is CaM-dependent.

Direct binding between *Bd*QUAC1 CBD peptide and CaM was confirmed by ITC and the interaction between full-length *Bd*QUAC1 and CaM was confirmed again by CAP. In the ITC analysis, wildtype *Bd*QUAC1 CBD - CaM interaction yielded a two-state binding model, which is commonly reported in other functional CBD-CaM interactions (Reichow et al., 2013). Under the two-state binding model, two separate CBD peptides bind to one single CaM, one after the other with a small conformational change. Interestingly, in the absence of Ca^{2+}, binding of the wildtype CBD to CaM was still observed but with low binding affinity. It could be the presence of Ca^{2+} - independent CaM binding, which had been observed in other CaM binding proteins (Yuan et al., 1999, Shen et al., 2005). However, this could also be due to residual Ca^{2+} in the system which was not eliminated entirely.

Investigation of mutated CBD peptides by ITC yielded results consistent with the electrophysiological data. The Ala substituted mutant peptides was too hydrophobic and formed large particle complexes (detected by dynamic light scattering), the chosen residues (a.a 335, 338, 342) were substituted with Asp, a negatively charged amino acid. CaM interacting with CBD peptides carrying the mutated amino acid K335D fit only a one-state binding model with low binding affinities, and no interactions were observed with the K335D/K338D/R342D peptide. The loss of a binding state in the mentioned peptides could be due to the K335D mutation which results

in the loss of a conformational change that allows binding of the second peptide to CaM. Consistent with the patch clamp result, the double mutant K338D/R342D was indistinguishable from WT control.

The CAP results again showed that the full-length wildtype *Bd*QUAC1 was effectively pulled-down by CaM, demonstrating their interaction. In contrast, pull-down of the full-length K335A/K338A mutant was drastically reduced. The result obtained from pull-down of the full-length K335A/K338A explains the low whole cell current density observed in patch clamp. Substitution at R335 with either Ala or Asp reduces binding to CaM and thus decreases activation of whole cell currents of *Bd*QUAC1. The ITC and CAP, together with the patch clamp data validate the hypothesis that *Bd*QUAC1 contain a CaM-binding domain, and interaction with CaM directly modify the channel's activity. Though closure of stomata does not rely solely on QUAC1, nonetheless these findings support the physiological response of stomata to CaM.

5.6. The role of *Bd*QUAC1 in pathogen infections

The infection of stripe rust was examined on mature wildtype and KD2 plants, the latter having more closed stomata due to overexpression of *Bd*QUAC1. By observation, there were more infection symptoms on wildtype leaves compared to KD2 leaves. Unfortunately, there is no reliable method of quantifying the symptoms shown on *Brachypodium*, thus interpretation of the data is based solely on the numbers of germ tubes and appressoria formation. As expected, wildtype leaves inoculated with stripe rust had significantly higher appressoria counts compared to KD2, which is consistent with the degree of infection symptoms that appear on the leaf surface. Although not indicated in figure 4.14D, the average stomatal widths of untreated wildtype were 1.55 µM and of untreated KD2 was 1.48 µM. Whether this difference of 0.07 µM has a significant

impact on stripe rust is unclear, however these results imply *Bd*QUAC1 perhaps also plays a role in stripe rust infection.

Of the three types of wheat rust, stem rust has been shown to penetrate only through open stomata, and leaf rust has the ability to penetrate through both opened and closed stomata. However, there have not yet been reports indicating whether stripe rust could penetrate through open or closed stomata. Findings here show stripe rust is likely to prefer penetration through open stomata.

5.7. Limitation of studies

Use of the mammalian system. The HEK293 system was used to express *Bd*QUAC1 for the patch clamp experiments. Mammalian expression systems such as HEK293 cells and *Xenopus* oocytes have previously been used for the study of plant ion channels. Evidently, the study in which the *At*QUAC1 was identified, the protein was expressed and studied in *Xenopus* oocytes (Meyer et al., 2010). Examples of studies in which plant ion channels were cloned and expressed in HEK293 cells include Ooi et al., 2016, Ooi et al., 2017. Besides the use of HEK293 cells, bovine CaM was used for the ITC experiments. Sequence alignments yielded 90% identity between the *Bos Taurus* CaM (NP_001159980.2) and *Brachypodium* CaM (XP_014755014.1). However, bovine CaM have also been used previously in the detection of plant CaM-binding proteins (Nakamura et al., 2006, Yang et al., 2010)

Limitation of the HEK293 expression system. Since activities of the channel were observed starting at -100 mV, the clamped voltage in this study was quite low. Since the pulse protocol included such low voltage, the recording time for each pulse had to be shortened to avoid disruption of the membrane and leakage of currents. For such low voltage, Xenopus oocytes would

be a better choice due to its bigger size and stability. However, the Xenopus doesn't allow the control of intracellular solutes.

Unequal expression of wildtype and mutant *Bd*QUAC1 in HEK293 cells. Mutants of *Bd*QUAC1 were not expressed as well as wildtype on HEK293 membrane. This was compensated by normalizing currents against the amount of protein expressed. However, the interpreted results would become incorrect without checking the amount of protein expression.

The small size of *Brachypodium* leaves. Although QUAC1 knockdown transgenic plants were generated, a number of standard phenotyping experiments were not achievable due to the small sizes of *Brachypodium* leaves, such as comparing transpiration, measuring the rate of water loss between wildtype and transgenic plants, and isolating guard cell protoplast for patch clamp.

5.8. Conclusion and future direction

QUAC1, to date, is the only identified R-type anion channel in plant guard cells. Overall, this study has explored the regulation of QUAC1 activation in monocot using the *Brachypodium* model. The activation of *Bd*QUAC1 is co-regulated by malate, Ca^{2+} and CaM (Figure 5.1). A CaM-binding domain (residues 334 to 351) has been identified within *Bd*QUAC1 and shown to interact with CaM physically. As an R-type channel, *Bd*QUAC1 is expected to be required for stomatal closure. Consistent with this, overexpression of the *Bd*QUAC1 gene leads to stomatal closure and less stripe rust infection.

Alignment of the *Bd*QUAC1 sequence with the QUAC1 sequence of other monocot species showed a conserved CBD domain (Figure 4.1). However, the same region in dicot QUAC1 sequences did not have the same common properties of a CBD. Therefore, the sensitivity to Ca^{2+} and CaM of QUAC1 from other monocot and dicot species remains to be tested. Additionally, the

association between QUAC1 and the mechanism by which pathogens might regulate stomata are yet to be explored.

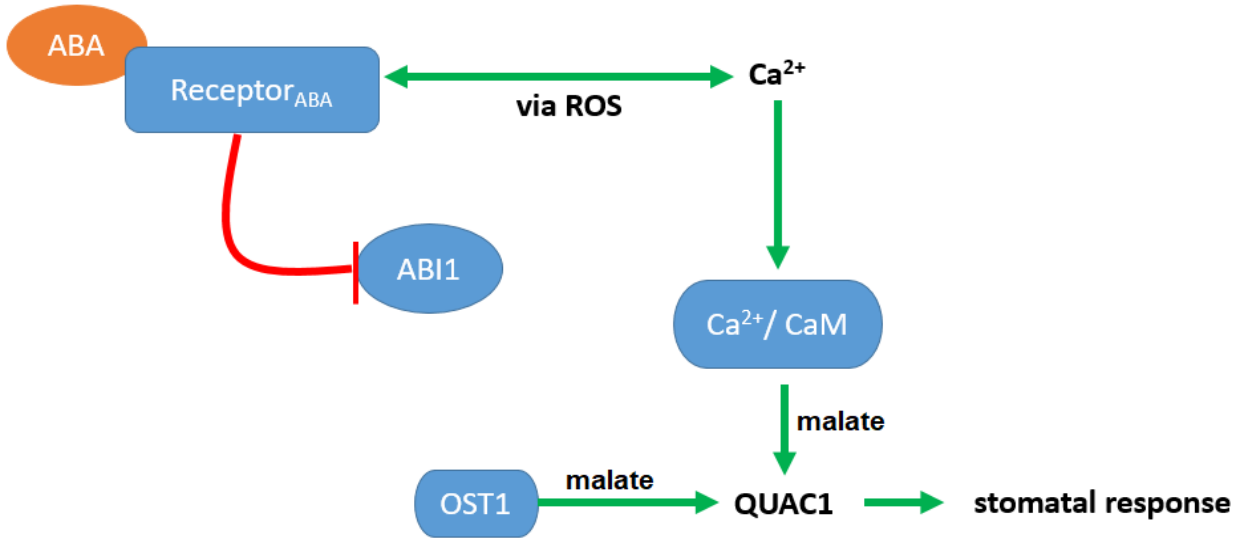

Figure 5. 1 Regulation of QUAC1 through ABA signaling pathways.

Through the Ca^{2+} -independent pathway, OST1, in the presence of malate, interacts with QUAC1 and stimulates the activation of the channel. Through the Ca^{2+} -dependent pathway, ABA causes an elevation of calcium concentration. The Ca^{2+}/CaM complex with malate activates QUAC1, leading to stomatal closure.

REFERENCES

Ache, P., Becker, D., Ivashikina, N., Dietrich, P., Roelfsema, M. R. G., & Hedrich, R. (2000). GORK, a delayed outward rectifier expressed in guard cells of Arabidopsis thaliana, is a K^+ -selective, K^+ -sensing ion channel. FEBS Letters, 486, 3–8.

Aktar-Uz-Zaman, M., Tuhina-khatun, M., Hanafi, M. M., & Sahebi, M. (2017). Genetic analysis of rust resistance genes in global wheat cultivars : an overview. Biotechnology & Biotechnological Equipment, 31(3), 431–445.

Al-rasheid, K. A. S., Marten, I., Geiger, D., Imes, D., Mumm, P., & Jennifer, B. (2013). Open stomata 1 (OST1) kinase controls R – type anion channel QUAC1 in Arabidopsis guard cells. The Plant Cell, 74, 372–382.

Alexopoulos, C. J., Mims, C. W. & Blackwell, M. (1996). Introductory Mycology. John Wiley & Sons, New York, NY, 868.

Almasalmeh, A., Krenc, D., Wu, B., and Beitz, E. (2014). Structural determinants of the hydrogen peroxide permeability of aquaporins. FEBS letters, 281, 647–656.

Almeida, D. M., Margarida Oliveira, M., & Saibo, N. J. M. (2017). Regulation of Na^+ and K^+ homeostasis in plants: Towards improved salt stress tolerance in crop plants. Genetics and Molecular Biology, 40(1), 326–345.

Alves, S. C., Worland, B., Thole, V., Snape, J. W., Bevan, M. W., Vain, P. (2009). A protocol for Agrobacterium-mediated transformation of Brachypodium distachyon community standard line Bd21. Nature Protocol, 4(5), 638 – 649.

Angeli, A. De, Baetz, U., Francisco, R., & Regalado, A. (2013). The vacuolar channel VvALMT9 mediates malate and tartrate accumulation in berries of Vitis vinifera. Planta, 238(2), 283–291.

Angeli, A. De, Monachello, D., Ephritikhine, G., Frachisse, J. M., Thomine, S., & Gambale, F. (2006). The nitrate / proton antiporter AtCLCa mediates nitrate accumulation in plant vacuoles. Nature, 442(August), 939–942.

Angeli, A. De, Zhang, J., Meyer, S., & Martinoia, E. (2013). AtALMT9 is a malate-activated vacuolar chloride channel required for stomatal opening in Arabidopsis. Nature Communications, 4, 1804–1810.

Antoni, R., Gonzalez-guzman, M., Rodriguez, L., Peirats-llobet, M., Pizzio, G. A., Fernandez, M. A., … Rodriguez, P. L. (2013). PYRABACTIN RESISTANCE1-LIKE8 plays an important role for the regulation of abscisic acid signaling in root. Plant and Cell Physiology, 161(February), 931–941.

Arimura, G., Maffei M. E. (2010). Calcium and secondary CPK signaling in plants in response to herbivore attack. Biochemical and Biophysical Research Communications, 400 (4), 455 – 460.

Assmann, S. M., Simoncini, L., & Schroeder, J. I. (1985). Blue light activates electrogenic ion pumping in guard cell protoplasts of Vicia faba. Nature, 318, 285–287.

Assmann, S. M., & Wang, X. Q. (2001). From milliseconds to millions of years: guard cells and environmental responses. Current Opinion in Plant Biology, 4, 421–428.

Auerbach, A. (2013). The energy and work of a ligand-gated ion channel. Journal of Molecular Biology, 425(9), 1461–1475.

Bai, Y., Dougherty, L., & Li, M. (2012). A natural mutation-led truncation in one of the two aluminum-activated malate transporter-like genes at the Ma locus is associated with low fruit acidity in apple. Molecular Genet Genomics, 287, 663–678.

Barker, B. S., Young, G. T., Soubrane, C. H., Stephens, G. J., Stevens, E. B., & Patel, M. K. (2017). Chapter 2 - Ion Channels. Conn's Translational Neuroscience. Elsevier Inc.

Barragan, V., Leidi, E. O., Andres, Z., Rubio, L., De Luca, A., Fernandez, J. A., … Pardo, J. M. (2012). Ion exchangers NHX1 and NHX2 mediate active potassium uptake into vacuoles to regulate cell turgor and stomatal function in Arabidopsis. The Plant Cell, 24(3), 1127–1142.

Becker, D., Geiger, D., Dunkel, M., Roller, A., Bertl, A., Latz, A., … Hedrich, R. (2004). AtTPK4, an Arabidopsis tandem-pore K^+ channel, poised to control the pollen membrane voltage in a pH- and Ca^{2+} -dependent manner. Proceedings of the National Academy of Sciences, 101(44), 15621–15626.

Bienert, G. P., Møller A. L., Kristiansen, K. A., Schulz, A., Møller, I. M., Schjoerring, J. K.,et al. (2007). Specific aquaporins facilitate the diffusion of hydrogen peroxide across membranes. Journal of Biochemistry, 282, 1183–1192.

Blatt, M. R., Thiel, G., & Trentham, R. D. (1990). Reversible inactivation of K+ channels of Vicia stomatal guard cells following the photolysis of caged inositol 1,4,5-triphosphate. Nature, 346, 766–769.

Bolton, M. D., Kolmer, J. A., & Garvin, D. F. (2008). Wheat leaf rust caused by Puccinia triticina. Molecular Plant Pathology, 9, 563–575.

Bowling, D. J. F., Spanswick, R. M., & MACKLON, A. E. (1966). Active and passive transport of the major nutrient ions across the root of Ricinus cummunis. Journal of Experimental Botany, 17(2), 410–416.

Brandt, B., Brodsky, D. E., Xue, S., Negi, J., Iba, K., Kangasjarvi, J., … Schroeder, J. I. (2012). Reconstitution of abscisic acid activation of SLAC1 anion channel by CPK6 and OST1 kinases and branched ABI1 PP2C phosphatase action. Proceedings of the National Academy of Sciences, 109(26), 10593–10598.

Brkljacic, J., Grotewold, E., Scholl, R., Mockler, T., Garvin, D. F., … & Vogel., J. P. (2011). Brachypodium as a Model for the Grasses: Today and the Future. Plant Physiology, 157(1), 3 – 13.

Brown, K. M. (1997). Ethylene and abscission. Physiologia Plantarum, 100, 567–576.

Brueggeman, R., Druka, A., Nirmala, J., Cavileer, T., Drader, T., Rostoks, N., … Kleinhofs, A. (2008). The stem rust resistance gene Rpg5 encodes a protein with nucleotide-binding-site, leucine-rich, and protein kinase domains. Proceedings of the National Academy of Sciences, 105(39), 14970–14975.

Caldwell, R. M. & Stone, G. M. (1936). Relation of stomatal function of wheat to invasion and infection by leaf rust (Puccinia triticina). Journal of Agricultural Research, 52, 917-932.

Calvin, M. (1976). Photosynthesis as a resource for energy and materials. Photochemistry and Photobiology, 23(6), 425–444.

Carafoli, E. (1992). The Ca^{2+} pump of the plasma membrane. The Journal of Biological Chemistry, 267(4), 2115–2118.

Carafoli, E., & Brini, M. (2000). Calcium pumps: structural basis for and mechanism of calcium transmembrane transport. Current Opinion in Chemical Biology, 4, 152–161.

Catterall, W. A. (1995). Structure and function of voltage-gated ion channels. Annual Review of Biochemistry, 64, 493–531.

Chattopadhyaya, R., Meador, W. E., Means, A. R., & Florante, A. Q. (1992). Structure refined at l-7 Å resolution. Journal of Molecular Biology, 228, 1177–1192.

Chen, G., Hu, Q., Luo, L., Yang, T., Zhang, S., Hu, Y., … Xu, G. (2015). Rice potassium transporter OsHAK1 is essential for maintaining potassium-mediated growth and functions in salt tolerance over low and high potassium concentration ranges. Plant, Cell & Environment, 38, 2747–2765.

Cho, D., Villiers, F., Kroniewicz, L., Lee, S., Seo, Y. J., Hirschi, K. D., … Kwak, J. M. (2012). Vacuolar CAX1 and CAX3 influence auxin transport in guard cells via regulation of apoplastic pH. Plant Physiology, 160(3), 1293–1302.

Cohen, P., & Cohen, P. T. W. (1989). Protein phosphatases come of age. The Journal of Biological Chemistry, 264(36), 21435–21438.

Conn S.J., Gilliham M., Athman A., Schreiber A.W., Baumann U., Moller I., & Tyerman S.D., Leigh R.A. (2011). Cell-specific vacuolar calcium storage mediated by CAX1 regulates apoplastic calcium concentration, gas exchange, and plant productivity in Arabidopsis. The Plant Cell, 23, 240–257.

Cox, J. A., Comte, M., Fittonsll, J. E., & Degradoll, W. F. (1985). The interaction of calmodulin with amphiphilic peptides. The Journal of Biiological Chemistry, 260(4), 2527–2534.

Cubero-Font, P., Maierhofer, T., Jaslan, J., Rosales, M. A., Espartero, J., Díaz-Rueda, P., Geiger, D. (2016). Silent S-type anion channel subunit SLAH1 gates SLAH3 open for chloride root-to-shoot translocation. Current Biology, 26(16), 2213–2220.

Czempinski, K., Frachisse, J., Maurel, C., Barbier-brygoo, H., & Mueller-roeber, B. (2002). Vacuolar membrane localization of the Arabidopsis 'two-pore' K + channel KCO1. The Plant Journal, 29(6), 809–820.

Darwin, F. (1989). Observations on stomata. Philossophical Transactions of the Royal Society of London. Series B, Biological sciences, 190, 531-621.

Dash, S., Niemaczura, W., & Harrington, H. M. (1997). Characterization of the basic amphiphilic α-helix calmodulin-binding domain of a 61.5 kDa tobacco calmodulin-binding protein. Biochemistry, 2960(96), 2025–2029.

De Silva, D. L. R., Cox, R. C., Hetherington, A. M., & Mansfield, T. A. (1985). Suggested involvement of calcium and calmodulin in the responses of stomata to abscisic acid. New Phytologist, 10, 555–563.

De Silva, D. L. R., Hetherington, A. M., & Mansfield, T. A. (1985). Synergism between calcium ions and abscisic acid in preventing stomatal opening. New Phytologist, 100, 473–483.

Deger, A. G., Nuhkat, M., Kedzierska, J., Kollist, H., Brosch, M., Unyayar, S., … Roelfsema, M. R. G. (2015). Guard cell SLAC1-type anion channels mediate flagellin-induced stomatal closure. New Phytologist, 208, 162–173.

Delhaize, E., Gruber, B. D., & Ryan, P. R. (2007). The roles of organic anion permeases in aluminium resistance and mineral nutrition. FE, 581, 2255–2262.

Demo, S. D., & Yellen, G. (1991). The inactivation gate of the shaker K+ channel behaves like an open-channel blocker. Neuron, 7, 743–753.

Dietrich, P., Sanders, D., & Hedrich, R. (2001). The role of ion channels in light-dependent stomatal opening. Journal of Experimental Botany, 52(363), 1959–1967.

Donovan, N., Martin, S., & Donkin, M. E. (1985). Calmodulin binding drugs Trifluoperazine and compound 48/80 modify stomatal responses of Commelina communis L. Journal of Plant Physiology, 118(2), 177-187.

Draper, J., Mur, L.A.J., Jenkins, G., Ghosh-Biswas, G.C., … & Routledge, A.P.M. (2001). Brachypodium distachyon. A new model system for functional genomics in grasses. Plant Physiology, 127, 1539–1555

Dreyer, I., Gomez-porras, J. L., Riaño-pachón, D. M., & Hedrich, R. (2012). Molecular evolution of slow and quick anion channels (SLACs and QUACs / ALMTs). Frontiers in Plant Science, 3, 1–12.

Dunkel, M., Latz, A., Schumacher, K., Müller, T., Becker, D., & Hedrich, R. (2008). Targeting of vacuolar membrane localized members of the TPK channel family. Molecular Plant, 1(6), 938–949.

Eisenach, C., Baetz, U., Huck, N. V., Zhang, J., De Angeli, A., Beckers, G., & Martinoia, E. (2017). ABA-induced stomatal closure involves ALMT4, a phosphorylation-dependent vacuolar anion channel of Arabidopsis. The Plant Cell, 29, 2552-2569.

Elumalai, R. P., Nagpal, P., & Reed, J. W. (2002). A mutation in the Arabidopsis KT2/KUP2 potassium transporter gene affects shoot cell expansion. The Plant Cell, 14, 119–131.

Epstein, E. (1951). Passive permeation and active transport of ions in plants roots. Plant Physiology, 6(37), 417–424.

Epstein, E. (1956). Mineral nutrition of plants: mechanisms of uptake and transport. Annual Review of Plant Physiology, 7(1), 1–24.

Feher, J. (2012). Active Transport: Pumps and Exchangers in Quantitative Human Physiology, 134-140.

Fischer, R. A. (1973). The relationship of stomatal aperture and guard-cell turgor pressure in Vicia faba. Journal of Experimental Botany, 24(2), 387–399.

Fu, H., & Luan, S. (1998). AtKUP1 : A dual-affinity K^+ transporter from Arabidopsis. The Plant Cell, 10, 63–73.

Furuichi, T., Sasaki, T., Tsuchiya, Y., Ryan, P. R., Delhaize, E., & Yamamoto, Y. (2010). An extracellular hydrophilic carboxy-terminal domain regulates the activity of TaALMT1, the aluminum-activated malate transport protein of wheat. The Plant Journal, 1, 47–55.

Gao, Y., Zeng, Q., Guo, J., Cheng, J., Ellis, B. E., Chen, J., & Laboratories, M. S. (2007). Genetic characterization reveals no role for the reported ABA receptor, GCR2, in ABA control of seed germination and early seedling development in Arabidopsis. The Plant Journal, 52, 1001–1013.

Garnica, D. P., Upadhyaya, N. M., Dodds, P. N., & Rathjen, J. P. (2013). Strategies for wheat stripe rust pathogenicity identified by transcriptome sequencing. PloS ONE, 8(6), 1–17.

Gaymard, F., Pilot, G., Bouchez, D., Bruneau, D., Boucherez, J., Thibaud, J., … Sentenac, H. (1998). Identification and disruption of a plant shaker-like outward channel involved in K^+ release into the xylem sap. Cell, 94, 647–655.

Geiger, D., Scherzer, S., Mumm, P., Marten, I., Ache, P., Matschi, S., Al-rasheid, K. A. S. (2010). Guard cell anion channel SLAC1 is regulated by CDPK protein kinases with distinct Ca^{2+} affinities. Proceedings of the National Academy of Sciences, 107(17), 8023–8028.

Geiger, D., Scherzer, S., Mumm, P., Stange, A., Marten, I., Bauer, H., … Hedrich, R. (2009). Activity of guard cell anion channel SLAC1 is controlled by drought-stress signaling kinase-phosphatase pair. Proceedings of the National Academy of Sciences, 106(50), 21425–21430.

Gelli, A., & Blumwald, E. (1997). Hyperpolarization-activated Ca^{2+} -permeable Channels in the Plasma Membrane of Tomato Cells. The Journal of Membrane Biology, 155, 35–45.

Gierth, M., & Ma, P. (2007). Potassium transporters in plants – Involvement in K^+ acquisition, redistribution and homeostasis. FEBS Letters, 581, 2348–2356.

Gierth, M., & Maser, P. (2007). Potassium transporters in plants – Involvement in K^+ acquisition, redistribution and homeostasis. FEBS Letters, 581, 2348–2356.

Gilroy, S., Fricker, M. D., Read, N. D., & Trewavas, A. J. (1991). Role of calcium in signal transduction of Commelina guard cells. The Plant Cell, 3, 333–344.

Goldstein, S. A. N., Bockenhauer, D., Kelly, I. O., & Zilberberg, N. (2001). Potassium leak channels and the KCNK family of two-p-domain subunits. Nature Reviews, 2, 175-184.

Gosti, F., Beaudoin, N., Serizet, C., Webb, A. A. R., Vartanian, N., & Giraudat, J. (1999). ABI1 protein phosphatase 2C is a negative regulator of abscisic acid signaling. The Plant Cell, 11(10), 1897–1910.

Grambow, H. J., & Riedel, S. (1977). The effect of morphogenically active factors from host and nonhost plants on the in vitro differentiation of infection structures of Puccinia graminis f. sp. tritici. Physiological Plant Pathology, 11(2), 213–224.

Grimmer, M. K., Foulkes, M. J., Paveley, N. D., & Chiappetta, A. (2012). Foliar pathogenesis and plant water relations: a review. Journal of Agricultural Research, 63(12), 4321–4331.

Gullingsrud, J., & Schulten, K. (2004). Lipid bilayer pressure profiles and mechanosensitive channel gating. Biophysical Journal, 86(6), 3496–3509.

Guo, F., Young, J., & Crawford, N. M. (2003). The nitrate transporter AtNRT1.1 (CHL1) functions in stomatal opening and contributes to drought susceptibility in Arabidopsis. The Plant Cell, 15, 107–117.

Guo, J., Zeng, Q., Emami, M., Ellis, B. E., & Chen, J. (2008). The GCR2 gene family is not required for aba control of seed germination and early seedling development in Arabidopsis. PloS ONE, 3(8), 1–7.

Hamilton, D. W. A., Hills, A., Kohler, B., & Blatt, M. R. (2000). Ca^{2+} channels at the plasma membrane of stomatal guard cells are activated by hyperpolarization and abscisic acid. Proceedings of the National Academy of Sciences, 97(9), 4967-4972.

Harder, D. E. (1986). Cytochemical studies on Puccinia graminis f. sp. tritici in a compatible wheat host. II. Haustorium mother cell walls at the host cell penetration site, haustorial walls, and the extrahaustorial matrix. Canadian Journal of Botany, 64, 2561–2575.

Harder, D. E., Chong, J., Rohringer, R., & Kim, W. K. (1986). Structure and cytochemistry of the walls of urediospores, germ tubes , and appressoria of Puccinia graminis triticil. Canadian Journal of Botany, 64, 476–485.

Harmon, A. C., Harmon, A. C., Gribskov, M., Gubrium, E., & Harper, J. F. (2001). The CDPK superfamily of protein kinases. New Phytologist, 151, 175–183.

Haro, R., Sainz, L., Rubio, F., & Rodrı, A. (1999). Cloning of two genes encoding potassium transporters in Neurospora crassa and expression of the corresponding cDNAs in Saccharomyces cerevisiae. Molecular Microbiology, 31(2), 511–520.

Hart, H. (1929). Relation of stomatal behavior to stem-rust resistance in wheat. Journal of Agricultural Research, 39(12), 929–948.

Hetherington, A. M., & Woodward, F. I. (2003). The role of stomata in sensing and driving environmental change. Nature, 424, 6951–6951.

Hilu, K. W., & Randall, J. L. (1984). Convenient method for studying grass leaf epidermis. Taxon, 33(3), 413 – 415.

Hirschi, K. D., Zhent, R., Cunningham, K. W., Reat, P. A., & Fink, G. R. (1996). CAX1, an H^{+}/Ca^{2+} antiporter from Arabidopsis. Proceedings of the National Academy of Sciences, 93, 8782–8786.

Hoekenga, O. A., Maron, L. G., Shaff, J., Kobayashi, Y., Pin, M. A., Ryan, P. R., … Kochian, L. V. (2006). AtALMT1, which encodes a malate transporter, is identified as one of several genes critical for aluminum tolerance in Arabidopsis. Proceedings of the National Academy of Sciences, 103(25), 9738–9743.

Hosy, E., Vavasseur, A., Mouline, K., Dreyer, I., Pore, F., Boucherez, J., … Bouchez, D. (2003). The Arabidopsis outward K+ channel GORK is involved in regulation of stomatal movements and plant transpiration. Proceedings of the National Academy of Sciences, 100(6), 3197–3202.

Huang, C., Flucher, B. E., Schmidt, M. M., Stroud, S. K., & Schmidt, J. (1994). Depolarization-transcription signals in skeletal muscle use calcium flux through L channels, but bypass the sarcoplasmic reticulum. Neuron, 13, 167–177.

Huang, Y., Sun, M. M., Ye, Q., Wu, X. Q., Wu, W. H., & Chen, Y. F. (2017). Abscisic acid modulates seed germination via ABA INSENSITIVE5-mediated PHOSPHATE1. Plant Physiology, 175, 161-1668.

Ingebritsen, T. S., & Cohen, P. (1963). Protein phosphatases : properties and role in cellular regulation. Science, 221, 331–338.

Islam, M. M., Munemasa, S., & Hossain, M. A. (2010). Roles of AtTPC1, vacuolar two pore channel 1, in Arabidopsis Stomatal Closure. Plant and Cell Physiology, 51(2), 302–311.

Iwano, M., Igarashi, M., Tarutani, Y., Kaothien-nakayama, P., Nakayama, H., Moriyama, H., … Takayama, S. (2014). A pollen coat–inducible autoinhibited Ca^{2+} -ATPase expressed in stigmatic papilla cells is required for compatible pollination in the Brassicaceae. The Plant Cell, 26, 636–649.

Jentsch, T. J. (2008). CLC chloride channels and transporters: from genes to protein structure, pathology and physiology. Critical Reviews in Biochemistry and Molecular Biology, 43, 9–36.

Jia, Q., Zheng, C., Sun, S., Amjad, H., Liang, K., & Lin, W. (2018). The role of plant cation/proton antiporter gene family in salt tolerance. Biologia Plantarum, 62(4), 617–629.

Jossier, M., Dalmas, F., Thiec, D. Le, Vavasseur, A., Filleur, S., Leonhardt, N., & Universite, N. (2010). The Arabidopsis vacuolar anion transporter, AtCLCc, is involved in the regulation of stomatal movements and contributes to salt tolerance. The Plant Journal, 64, 563–576.

Kaleka, K. S., Petersen, A. N., Florence, M. A., & Gerges, N. Z. (2012). Pull-down of calmodulin-binding proteins. Journal of Visualized Experiments, (59), 3502.

Kang, J., Hwang, J.-U., Lee, M., Kim, Y.-Y., Assmann, S. M., Martinoia, E., & Lee, Y. (2010). PDR-type ABC transporter mediates cellular uptake of the phytohormone abscisic acid. Proceedings of the National Academy of Sciences, 107(5), 2355–2360.

Kato, Y., Sakaguchi, M., Mori, Y., Saito, K., Nakamura, T., Bakker, E. P., … Uozumi, N. (2001). Evidence in support of a four transmembrane- pore-transmembrane topology model for the Arabidopsis thaliana Na+ /K+ translocating AtHKT1 protein , a member of the superfamily of K+ transporters. Proceedings of the National Academy of Sciences, 99(11), 6488–6493.

Keller, B. U., Hedrich, R., & Raschke, K. (1989). Voltage-dependent anion channels in the plasma membrane of guard cells. Nature, 341, 450–453.

Kharenko, O. A., Polichuk, D., Nelson, K. M., Abrams, S. R., & Loewen, M. C. (2013). Identification and characterization of interactions between abscisic acid and human heat shock protein 70 family members. Journal of Biochemistry, 154(4), 383–391.

Kim, E. J., Kwak, J. M., Uozumi, N., & Schroeder, J. I. (1998). AtKUP1 : An Arabidopsis gene encoding high-affinity potassium transport activity. The Plant Cell, 10, 51–62.

Kinoshita, T., Nishimura, M., & Shimazaki, K. (1995). Cytosolic Concentration of Ca^{2+} regulates the plasma membrane H^{+} -ATPase in guard cells of fava bean. The Plant Cell, 7(8), 1333–1342.

Kinoshita, T., & Shimazaki, K. (1999). Blue light activates the plasma membrane H^+ -ATPase by phosphorylation of the C-terminus in stomatal guard cells. The EMBO Journal, 18(20), 5548–5558.

Kohler, B., Hills, A., & Blatt, M. R. (2003). Control of guard cell ion channels by hydrogen peroxide and abscisic acid indicates their action through alternate signaling pathways. Plant and Cell Physiology, 131(February), 385–388.

Koiwai, H., Nakaminami, K., Seo, M., & Mitsuhashi, W. (2004). Tissue-specific localization of an abscisic acid biosynthetic enzyme, AAO3, in Arabidopsis. Plant Physiology, 134, 1697–1707.

Kotur, Z., Mackenzie, N., Ramesh, S., Tyerman, S. D., Kaiser, B. N., & Glass, A. D. M. (2012). Nitrate transport capacity of the Arabidopsis thaliana NRT2 family members and their interactions with AtNAR2.1. New Phytologist, 194, 724–731.

Kovermann, P., Meyer, S., Ho, S., Picco, C., Scholz-starke, J., Ravera, S., … Martinoia, E. (2007). The Arabidopsis vacuolar malate channel is a member of the ALMT family. The Plant Journal, 52, 1169–1180.

Krattinger, S. G., Lagudah, E. S., Spielmeyer, W., Singh, R. P., Huerta-espino, J., Mcfadden, H., … Keller, B. (2009). A putative ABC transporter confers durable resistance to multiple fungal pathogens in wheat. Science, 323, 1360–1363.

Krattinger, S. G., Lagudah, E. S., Wicker, T., Risk, J. M., Ashton, A. R., & Selter, L. L. (2011). Lr34 multi-pathogen resistance ABC transporter : molecular analysis of homoeologous and orthologous genes in hexaploid wheat and other grass species. The Plant Journal, 65, 392–403.

Krogh, A., Larsson, B., von Heijne, G., Sonnhammer, E. L. (2001). Predicting transmembrane protein topology with a hidden Markov model: application to complete genomes. Journal of Molecular Biology, 305(3), 567 – 580.

Kuromori, T., & Shinozaki, K. (2010). ABA transport factors found in Arabidopsis ABC transporters. Plant Signaling & Behavior, 5(9), 1124–1126.

Kuromori, T., Sugimoto, E., & Shinozaki, K. (2014). Intertissue signal transfer of abscisic acid from vascular cells to guard cells. Plant Physiology, 164(4), 1587–1592.

Kwak, J. M., Mori, I. C., Pei, Z., Leonhardt, N., Torres, M. A., Dangl, J. L., … Schroeder, J. I. (2003). NADPH oxidase AtrbohD and AtrbohF genes function in ROS-dependent ABA signaling in Arabidopsis. The EMBO Journal, 22(11), 2623–2633.

LaPorte, D. C., Wierman, B. M., & Storm, D. R. (1980). Calcium-induced exposure of a hydrophobic surface on calmodulin. Biochemistry, 19, 3814–3819.

Larkin M. A., Blackshields G., Brown N. P., Chenna R., McGettigan P. A., McWilliam H., … & Higgins D. G. (2007). ClustalW and ClustalX version 2. Bioinformatics, 23(21), 2947-2948.

Lee, S. M., Hanh, M., Hoang, T., Han, H. J., Kim, H. S., Lee, K., … Chung, W. S. (2009). Pathogen inducible voltage-dependent anion channel (AtVDAC) isoforms are localized to mitochondria membrane in Arabidopsis. Molecules and Cells, 27, 321–327.

Leung, J., Bouvier-Durand, M., Morris, P. C., Guerrier, D., Chefdor, F., & Giraudat, J. (1994). Arabidopsis ABA response gene ABI1: Features of a calcium-modulated protein phosphatase. Science, 264(5164), 1448–1452.

Leung, J., Merlot, S., & Giraudat, J. (1997). ABIf genes encode homologous protein phosphatases 2C lnvolved in abscisic acid signal transduction. The Plant Cell, 9, 759–771.

Li, J., Wang, X., Watson, M. B., & Assmann, S. M. (2000). Regulation of abscisic acid – induced stomatal closure and anion channels by guard cell AAPK kinase. Science, 287, 300–304.

Liang, C., Pineros, M., Tian, J., Yao, Z., Sun, L., Liu, J., … Liao, H. (2013). Low pH, aluminum, and phosphorus coordinately regulate malate exudation through GmALMT1 to improve soybean adaptation to acid soils. Plant Physiology, 161(3), 1347–1361.

Ligaba, A., Katsuhara, M., Ryan, P. R., Shibasaka, M., & Matsumoto, H. (2006). The BnALMT1 and BnALMT2 genes from rape encode aluminum-activated malate transporters that enhance the aluminum resistance of plant cells. Plant Physiology, 142(3), 1294–1303.

Ligaba, A., Maron, L., Shaff, J. O. N., Kochian, L., & Piñeros, M. (2012). Maize ZmALMT2 is a root anion transporter that mediates constitutive root malate efflux. Plant, Cell & Environment, 35, 1185–1200.

Lisal, J., & Maduke, M. (2009). Proton-coupled gating in chloride channels. Philosophical Transactions of the Royal Society, 364, 181–187.

Liu, J., & Zhou, M. (2018). The ALMT gene family performs multiple functions in plants. Agronomy, 20, 1–18.

Liu, W., Frick, M., Huel, R., Nykiforuk, C. L., Wang, X., Gaudet, D. A., … Laroche, A. (2014). The stripe rust resistance gene Yr10 encodes an evolutionary-conserved and unique CC-NBS-LRR sequence in wheat. Molecular Plant, 7(12), 1740–1755

Liu, X., Yue, Y., Li, B., Nie, Y., Wu, W.-H., & Ma, L. (2007). A G protein-coupled receptor is a plasma membrane receptor for the plant hormone abscisic acid. Science, 318(5852), 17–19.

Luan, S. (2009). The CBL-CIPK network in plant calcium signaling. Trends in Plant Science, 14(1), 37–42.

Lucca, N., & Leo, G. (2012). Arabidopsis ACA7, encoding a putative auto-regulated Ca^{2+} - ATPase, is required for normal pollen development. Plant Cell Reports, 31, 651–659.

Ma, Y., Szostkiewicz, I., Korte, A., Moes, D., Yang, Y., Christmann, A., & Grill, E. (2009). Regulators of PP2C phosphatase activity function as abscisic acid sensors. Science, 324, 1064–1069.

Maierhofer, T., Lind, C., Huttl, S., Scherzer, S., Papenfuss, M., Simon, J., … Geiger, D. (2014). A single-pore residue renders the Arabidopsis root anion channel SLAH2 highly nitrate selective. The Plant Cell, 26(6), 2554–2567.

Mains, E. B. (1926). Studies in rust resistance. Journal of Heredity, 17(9), 313–325.

Mann, D. G. J., LaFayette, P. R., Abercrombie, L. L., King, Z. R., Mazarei, M., Halter, M. C., … & Stewart Jr, C. N. (2012). Gateway-compatible vectors for high-throughput gene functional analysis in switchgrass (Panicum virgatum L.) and other monocot species. Plant Biotechnology Journal, 10, 226 – 236.

Mao, J., Manik, S. M. N., Shi, S., Chao, J., Jin, Y., Wang, Q., & Liu, H. (2016). Mechanisms and physiological roles of the CBL-CIPK networking system in Arabidopsis thaliana. Genes, 62(7), 1–15.

Marten, H., Hedrich, R., & Roelfsema, M. R. G. (2007). Blue light inhibits guard cell plasma membrane anion channels in a phototropin-dependent manner. The Plant Journal, 50, 29–39.

Maser, P., Hosoo, Y., Goshima, S., Horie, T., Eckelman, B., Yamada, K., … Uozumi, N. (2002). Glycine residues in potassium channel-like selectivity filters determine potassium selectivity in four-loop- per-subunit HKT transporters from plants. Proceedings of the National Academy of Sciences, 99(9), 6428–6433.

McWilliam, H., Li, W., Uludag M., Squizzato, S., Park Y. M., Buso, N., … & Lopez, R. (2013). Analysis tool web services from the EMBL-EBI. Nucleic Acid Research, 41, W597 – 600.

Meidner, H., & Edwards, M. (1975). Direct measurements of turgor pressure potentials of guard cells, I. Journal of Experimental Botany, 26(3), 319–330.

Merilo, E., Jalakas, P., Kollist, H., & Brosché, M. (2015). The Role of ABA recycling and transporter proteins in rapid stomatal responses to reduced air humidity, elevated CO_2, and exogenous ABA. Molecular Plant, 8(4), 657–659.

Meyer, K., Leube, M. P., & Grill, E. (1994). A protein phosphatase 2C involved in ABA signal transduction in Arabidopsis thaliana. Science, 264(5164), 1452–1455.

Meyer, S., Mumm, P., Imes, D., Endler, A., Weder, B., Al-rasheid, K. A. S., … Hedrich, R. (2010). At ALMT12 represents an R-type anion channel required for stomatal movement in Arabidopsis guard cells. The Plant Journal, 63, 1054–1062.

Meyer, S., Scholz-starke, J., Angeli, A. De, Kovermann, P., Burla, B., Gambale, F., & Martinoia, E. (2011). Malate transport by the vacuolar AtALMT6 channel in guard cells is subject to multiple regulation. The Plant Journal, 67, 247–257.

Mikołajczyk, M., Awotunde, O. S., Muszyńska, G., Klessig, D. F., & Dobrowolska, G. (2000). Osmotic stress induces rapid activation of a salicylic acid-induced protein kinase and a homolog of protein kinase ASK1 in tobacco cells. The Plant Cell, 12(1), 165–178.

Moldenhauer, J., Moerschbacher, B. M., & Westhuizen, A. J. Van Der. (2006). Histological investigation of stripe rust (Puccinia striiformis f. sp . tritici) development in resistant and susceptible wheat cultivars. Plant Physiology, 55, 469–474.

Morgan, P. W., & Durham, J. I. (1973). Leaf age and ethylene-induced abscission. Plant Physiology, 52, 667–670.

Mori, I. C., Murata, Y., Yang, Y., Munemasa, S., Wang, Y., Andreoli, S., … Schroeder, J. I. (2006). CDPKs CPK6 and CPK3 function in ABA regulation of guard cell S-type anion- and Ca 2+ -permeable channels and stomatal closure. PLOS Biology, 4(10), 1749–1762.

Mur, L. A. J., Simpson, C., Gay, A., Smith, J. A., Paveley, N., Sanchez-Martin, J., & Prats, E. (2013). Stomatal lock-up following pathogenic challenge : source or symptom of costs of resistance in crops ? Plant Physiology, 62, 72–82.

Mustilli, A., Merlot, S., Vavasseur, A., Fenzi, F., & Giraudat, J. (2002). Arabidopsis OST1 protein kinase mediates the regulation of stomatal aperture by abscisic acid and acts upstream of reactive oxygen species production. The Plant Cell, 14, 3089–3099.

Nakamura, S., Hayashi, H., & Chino, M. (2006). Detection of calmodulin and calmodulin binding proteins in pure sap of rice plants. Soil Science and Plant Nutrition, 52, 195 – 202.

Nakashima, K., & Yamaguchi-shinozaki, K. (2013). ABA signaling in stress-response and seed development. Plant Cell Reports, 32, 959–970.

Nejidat, A. (1987). Effect of Ophiobolin A on stomatal movement: role of calmodulin. Plant and Cell Physiology, 28(3), 455–460.

Nicholas, K. B., & Nicholas, H. B., Deerfield, D. W., Nicholas, H. B. J., Nicholas, K., Nicholas, H. J., … & Gauch, H. (1997). GeneDoc: a tool for editing and annotating multiple sequence alignments. Embnet.news.

Nishimura, N., Sarkeshik, A., Nito, K., Park, S., Wang, A., Carvalho, P. C., … Schroeder, J. I. (2010). PYR/PYL/RCAR family members are major in-vivo ABI1 protein phosphatase 2C-interacting proteins in Arabidopsis. The Plant Journal, 61, 290–299.

O'Neil, K. T., & DeGrado, W. F. (1990). How calmodulin binds its targets: sequence independent recognition of amphiphilic α-helices. Trends in Biochemical Sciences, 15(2), 59–64.

Ooi, A., Lemtiri-Chlieh, F., Wong, A., & Gehring, C. (2017). Direct modulation of the guard cell outward-rectifying potassium channel (GORK) by abscisic acid. Molecular plant, 10 (11), 1469 – 1472.

Ooi, A. Wong, A., Esau, L., Lemtiri-Chlieh, F., & Gehring, C. (2016). A guide to transient expression of membrane proteins in HEK-293 cells for functional characterization. Frontiers in Physiology, 7, 300

Open, P. M. H., Inoue, S., & Kinoshita, T. (2017). Blue light regulation of stomatal opening and the plasma membrane H^+ -ATPase. Plant Physiology, 174, 531–538.

Osakabe, Y., Arinaga, N., Umezawa, T., Katsura, S., Nagamachi, K., Tanaka, H., … Yamaguchi-shinozaki, K. (2013). Osmotic stress responses and plant growth controlled by potassium transporters in Arabidopsis. The Plant Cell, 25, 609–624.

Padmanaban, S., Chanroj, S., Kwak, J. M., Li, X., Ward, J. M., & Sze, H. (2007). Participation of endomembrane cation/H^+ exchanger AtCHX20 in osmoregulation of guard cells. Plant Physiology, 144(3), 82–93.

Pandey, S., Nelson, D. C., & Assmann, S. M. (2009). Two novel GPCR-type G proteins are abscisic acid receptors in Arabidopsis. Cell, 136(1), 136–148.

Park, S. S.-Y., Fung, P., Nishimura, N., Jensen, D. R., Fujii, H., Zhao, Y., … Cutler, S. R. (2009). Abscisic acid inhibits type 2C protein phosphatases via the PYR/PYL Family of START proteins. Science, 324, 1068–1069.

Pavlovic-Djuranovic, S., Kun, J.F.J., Schultz, J.E. & Beitz, E. (2006). Dihydroxyacetone and methylglyoxal as permeants of the Plasmodium aquaglyceroporin inhibit parasite proliferation. Biochimica et Biophysica Acta, 1758, 1012 – 1017.

Pei, Z., Murata, Y., Benning, G., Thomine, S., Klusener, B., Allen, G. J., & Grill, E. (2000). Calcium channels activated by hydrogen peroxide mediate abscisic acid signalling in guard cells. Nature, 190(1999), 731–734.

Peiter, E., Maathuis, F. J. M., Mills, L. N., & Knight, H. (2005). The vacuolar Ca^{2+} -activated channel TPC1 regulates germination and stomatal movement. Nature, 434, 404–408.

Perozo, E., Kloda, A., Cortes, D. M., & Martinac, B. (2002). Physical principles underlying the transduction of bilayer deformation forces during mechanosensitive channel gating. Nature Structural Biology, 9(9), 696–703.

Pineros, M. A., Cancado, G. M. A., & Kochian, L. V. (2008). Novel properties of the wheat aluminum tolerance organic acid transporter (TaALMT1) revealed by electrophysiological characterization in Xenopus oocytes: functional and structural implications. Plant Physiology, 147(4), 2131–2146.

Qiu, J., Sam, W., Mark, A., Stuart, J., Qiu, J., Henderson, S. W., … Gilliham, M. (2016). SLAH1, a homologue of the slow type anion channel SLAC1, modulates shoot Cl −

accumulation and salt tolerance in Arabidopsis thaliana. Journal of Experimental Botany, 47(15), 4495–4505.

Quesada, A., & Fern, E. (1994). Expression of nitrate assimilation related genes in Chlamydomonas reinhardtii. Plant Molecular Biology, 24, 185–194.

Quintero, F. J., & Blatt, M. R. (1997). A new family of K^+ transporters from Arabidopsis that are conserved across phyla. FEBS Letters, 415(2), 206–211.

Reichow, S. L., Clemens D. M., Freites, J. A., Nemeth-Cahalan, K. L., … & Gonen, T. (2013) Allosteric mechanism of water-channel gating by Ca^{2+}-calmodulin. Nature structural and molecular biology, 20(9), 1085-1092.

Ren, D. (2011). Sodium leak channels in neuronal excitability and rhythmic behaviors. Neuron, 72(6), 899–911.

Rodriguez, P. L., Leube, M. P., & Grill, E. (1998). Molecular cloning in Arabidopsis thaliana of a new protein phosphatase 2C (PP2C) with homology to ABI1 and ABI2. Plant Molecular Biology, 38, 879–883.

Rubio, F., Santa-marı, G. E., & Rodrı, A. (2000). Cloning of Arabidopsis and barley cDNAs encoding HAK potassium transporters in root and shoot cells. Physiologia Plantarum, 109, 34–43.

Sack, F. D. (1987). The development and structure of stomata, in Stomatal Function (eds E. Zeiger , G.D. Farquhar, I.R. Cowan IR), Stanford University Press, Standford, CA, 59–89

Saez, A., Apostolova, N., Gonzalez-guzman, M., Gonzalez-garcia, M. P., Nicolas, C., Lorenzo, O., & Rodriguez, P. L. (2004). Gain-of-function and loss-of-function phenotypes of the protein phosphatase 2C HAB1 reveal its role as a negative regulator of abscisic acid signalling. The Plant Journal, 37, 354–369.

Sah, S. K., Reddy, K. R., & Li, J. (2016). abscisic acid and abiotic stress tolerance in crop plants. Frontiers in Plant Science, 7, 1–26.

Santa-Marıa, G. E., Rubio, F., Dubcovsky, J., & Rodriguez-Navarro, A. (1997). The HAKl gene of barley is a member of a large gene family and encodes a high-affinity potassium transporter. The Plant Cell, 9, 2281–2289.

Sasaki, T., Mori, I. C., Furuichi, T., Munemasa, S., Toyooka, K., Matsuoka, K., … Yamamoto, Y. (2010). Closing plant stomata requires a homolog of an aluminum-activated malate transporter. Plant and Cell Physiology, 51(3), 354–365.

Sasaki, T., Yamamoto, Y., Ezaki, B., Katsuhara, M., Ahn, S. J., Ryan, P. R., … Matsumoto, H. (2004). A wheat gene encoding an aluminum-activated malate transporter. The Plant Journal, 37, 645–653.

Sauguet, L., Shahsavar, A., Poitevin, F., Huon, C., Menny, A., & Nemecz, À. (2014). Crystal structures of a pentameric ligand-gated ion channel provide a mechanism for activation. Proceedings of the National Academy of Sciences, 111(3), 966–971.

Scheidegger, Y., Saurer, M., Bahn, M., & Siegwolf, R. (2000). Linking stable oxygen and carbon isotopes with stomatal conductance and photosynthetic capacity: A conceptual model. Oecologia, 125(3), 350–357.

Scherzer, S., Maierhofer, T., Al-Rasheid, K. A. S., Geiger, D., & Hedrich, R. (2012). Multiple calcium-dependent kinases modulate ABA-activated guard cell anion channels. Molecular Plant, 5(6), 1409–1412.

Schiøtt, M., Romanowsky, S. M., Bækgaard, L., Jakobsen, M. K., Palmgren, M. G., & Harper, J. F. (2004). A plant plasma membrane Ca2+ pump is required for normal pollen tube growth and fertilization. Proceedings of the National Academy of Sciences, 101(25), 9502–9507.

Scholthof, K. G., Irigoyen, S., Catalan, P., Mandadi, K. K. (2018). *Brachypodium*: A monocot grass model genus for plant biology. The Plant Cell, 30(8), 1673 – 1694.

Schonknecht, G., Y, P. S., Steinmeyer, R., Bru, L., Ache, P., Dutta, R., … Y, K. P. (2002). KCO1 is a component of the slow-vacuolar (SV) ion channel. FEBS Letters, 511, 28–32.

Schroeder, J., & Hagiwar, S. (1989). Cytosolic calcium regulates ion channels in the plasma membrane of Vicia faba guard cells. Nature, 338, 427–430.

Schroeder, J. I., & Hagiwara, S. (1990). Repetitive increases in cytosolic Ca^{2+} of guard cells by abscisic acid activation of nonselective Ca^{2+} permeable channels. Proceedings of the National Academy of Sciences, 87, 9305–9309.

Schroeder, J. I., Raschket, K., & Neher, E. (1987). Voltage dependence of K + channels in guard-cell protoplasts. Proceedings of the National Academy of Sciences, 84, 4108–4112.

Schroeder, J., & Keller, B. U. (1992). Two types of anion channel currents in guard cells with distinct voltage regulation. Proceedings of the National Academy of Sciences, 89, 5025–5029.

Schumacher, M., & Adelman, J. P. (2002). An open and shut case. Nature, 417, 501–502.

Schwartz, A., Ilan, N., & Grantz, D. A. (1988). Calcium effects on stomatal movement in Commelina communis L . Plant Physiology, 87, 583–587.

Shen, Y., Wang, X., Wu, F., Du, S., Cao, Z., Shang, Y., … Zhang, D. (2006). The Mg-chelatase H subunit is an abscisic acid receptor. Nature, 443(October), 823–826.

Shimazaki, K., Doi, M., Assmann, S. M., & Kinoshita, T. (2007). Light regulation of stomatal movement. Annual Review of Plant Biology, 58, 219–247.

Shimazaki, K., Iino, M., & Zeiger, E. (1986). Blue light-dependent proton extrusion by guard-cell protoplasts of Vicia faba. Nature, 319, 324–326.

Sigworth, F. J. (2003). Life's transistors. Nature, 423, 3–4.

Siivari, K., Zhang, M., Palmer, A. G., & Hans, J. (1995). NMR studies of the methionine methyl groups in calmodulin. FEBS Letters, 366, 104–108.

Singh, A., Giri, J., Kapoor, S., Tyagi, A. K., & Pandey, G. K. (2010). Protein phosphatase complement in rice: genome-wide identification and transcriptional analysis under abiotic stress conditions and reproductive development. BioMed Central Genomics, 435, 1–18.

Sirichandra, C., Gu, D., Hu, H., Davanture, M., Lee, S., Djaoui, M., … Kwak, J. M. (2009). Phosphorylation of the Arabidopsis AtrbohF NADPH oxidase by OST1 protein kinase. FEBS Letters, 583(18), 2982–2986.

Soon, F., Ng, L., Zhou, X. E., West, G. M., Xu, Y., Chalmers, M. J., … Yang, H. (2012). Molecular Mimicry Regulates ABA Signaling by SnRK2 Kinases and PP2C Phosphatases. Science, 335, 85–89.

Staples, R. C. (2001). Nutrients for a rust fungus: the role of haustoria. Trends in Plant Science, 6(11), 496–498.

Stillwell, W. (2016). Chapter 19. An introduction to Biological Membranes: Composition, structure, and function. Elsevier Inc.

Thuleau, P., Ward, J. M., Ranjeva, R., & Schroeder, J. I. (1994). Voltage-dependent calcium-permeable channels in the plasma membrane of a higher plant cell. The EMBO Journal, 13(13), 2970–2975.

Tian, Y., Kongsuphol, P., Hug, M., Ousingsawat, J., Witzgall, R., Schreiber, R., & Kunzelmann, K. (2010). Calmodulin-dependent activation of the epithelical calcium-dependent chloride channel TMEM16A. FASEB Journal, 25(3), 1058 – 1068.

Tong, Y., Zhou, J.-J., Li, Z., & Miller, J. (2005). A two-component high-affinity nitrate uptake system in barley. The Plant Journal, 41, 442–450.

Tseng, T., Whippo, C., Hangarter, R. P., & Briggs, W. R. (2012). The role of a 14-3-3 protein in stomatal opening mediated by PHOT2 in Arabidopsis. The Plant Cell, 1–14.

Tuteja, N. (2007). Abscisic acid and abiotic stress signaling. Plant Signaling & Behavior, 2(3), 135–138.

Vahisalu, T., Kollist, H., Wang, Y., Nishimura, N., Chan, W., Valerio, G., … Brosche, M. (2008). SLAC1 is required for plant guard cell S-type anion channel function in stomatal signalling. Nature, 452, 487-493.

Valmonte, G. R., Arthur, K., Higgins, C. M., MacDiarmid R. M (2014). Calcium-Dependent Protein Kinases in Plants: Evolution, Expression and Function. Plant and Cell Physiology, 55(3), 551-569.

Very, A.-A., & Davies, J. M. (2000). Hyperpolarization-activated calcium channels at the tip of Arabidopsis root hairs. Proceedings of the National Academy of Sciences, 97(17), 9801–9806.

Vishwakarma, K., Upadhyay, N., Kumar, N., & Yadav, G. (2017). Abscisic Acid Signaling and Abiotic Stress Tolerance in Plants: A Review on Current Knowledge and Future Prospects. Frontiers in Plant Science, 8, 1–12.

Vlad, F., Rubio, S., Rodrigues, A., Sirichandra, C., Belin, C., Robert, N., … Merlot, S. (2009). Protein phosphatases 2C regulate the activation of the Snf1-related kinase OST1 by abscisic acid in Arabidopsis. The Plant Cell, 21, 3170–3184.

Voegele, R. T., Voegele, R. T., & Mendgen, K. (2003). Rust haustoria: nutrient uptake and beyond. New Phytologist, 159, 93–100.

Voelker, C., Schmidt, D., Mueller-roeber, B., Czempinski, K., & Mu, A. (2006). Members of the Arabidopsis AtTPK/KCO family form homomeric vacuolar channels in planta. The Plant Journal, 48, 296–306.

Wang, Y., Noguchi, K., Ono, N., Inoue, S., Terashima, I., & Kinoshita, T. (2014). Overexpression of plasma membrane H^+ -ATPase in guard cells promotes light-induced stomatal opening and enhances plant growth. Proceedings of the National Academy of Sciences, 111(1), 533–538.

Ward, J. M., Pascal, M., & Schroeder, J. I. (2009). Plant Ion Channels : Gene Families, Physiology , and Functional Genomics Analyses. Annual Review of Physiology, 71, 59–82.

West, J. W., Patton, D. E., Scheuer, T., Wang, Y., Goldin, A. L., & Catterall, W. A. (1992). A cluster of hydrophobic amino acid residues required for fast Na^+ -channel inactivation. Proceedings of the National Academy of Sciences, 89(22), 10910–10914.

Wu, F.-Q., Xin, Q., Cao, Z., Liu, Z.-Q., Du, S.-Y., Mei, C., … Zhang, D.-P. (2009). The magnesium-chelatase H subunit binds abscisic acid and functions in abscisic acid signaling: New evidence in Arabidopsis. Plant Physiology, 150(4), 1940–1954.

Xiao, Z., Miao, Y. C., An, G. Y., Zhou, Y., ShangGuan, Z. P., Gao, F. J., & Song, C. P. (2001). K^+ channels inhibited by hydrogen peroxide mediate abscisic acid signaling in Vicia guard cells. Cell Research, 11(3), 195–202.

Yamauchi, S., Takemiya, A., Sakamoto, T., Kurata, T., & Tsutsumi, T. (2016). The plasma membrane H^+ -ATPase AHA1 plays a major role in stomatal opening in response to blue light. Plant Physiology, 171, 2731–2743.

Yang, T., & Colecraft, H. M. (2015). Calmodulin regulation of TMEM16A and 16B Ca^{2+} -activated chloride channels. Channels, 10(1), 38 – 44.

Yang, T., Chaudhuri, S., Yang, L., Du, L., & Poovaiah, B. W. (2010). The Journal of Biological Chemistry, 285, 7119 – 7126.

Yirgou, D., & Caldwell, R. M. (1963). Stomatal penetration of wheat seedlings by stem and leaf rust: effect of light and carbon dioxide. Science, 141(1958), 272–273.

Yong, Z., Kotur, Z., & Glass, A. D. M. (2010). Characterization of an intact two-component high-affinity nitrate transporter from Arabidopsis roots. The Plant Journal, 63, 739–748.

Yoshida, R., Hobo, T., Ichimura, K., Mizoguchi, T., Takahashi, F., Aronso, J., … Shinozaki, K. (2002). ABA-activated SnRK2 protein kinase is required for dehydration stress signaling in Arabidopsis. Plant Cell Physiol, 43(12), 1473–1483.

Yoshida, R., Umezawa, T., Mizoguchi, T., Takahashi, S., Takahashi, F., & Shinozaki, K. (2006). The regulatory domain of SRK2E/OST1/SnRK2.6 interacts with ABI1 and integrates abscisic acid (ABA) and osmotic stress signals controlling stomatal closure in Arabidopsis. The Journal of Biological Chemistry, 281(8), 5310–5318.

Yoshida, T., Nishimura, N., Kitahata, N., Kuromori, T., Ito, T., Asami, T., … Hirayama, T. (2005). ABA-hypersensitive germination3 encodes a protein phosphatase 2C (AtPP2CA) that strongly regulates abscisic acid signaling during germination among Arabidopsis protein phosphatase 2Cs. Plant Physiology, 140, 115–126.

Young, J. J., Mehta, S., Israelsson, M., Godoski, J., Grill, E., & Schroeder, J. I. (2006). CO_2 signaling in guard cells : Calcium sensitivity response modulation, a Ca^{2+}-independent phase, and CO_2 insensitivity of the gca2 mutant. Proceedings of the National Academy of Sciences, 103(19), 7506–7511.

Zeiger, E. (1983). The biology of stomatal guard cells. Annual Review of Plant Physiology, 34, 441–475.

Zhang, A., Ren, H., Tan, Y., Qi, G., Yao, F., Wu, G., & Yang, L. (2016). S-Type anion channels SLAC1 and SLAH3 function as essential negative regulators of inward K^+ channels and stomatal opening in Arabidopsis. The Plant Cell, 28, 949–965.

Zhang, D.-P., Wu, Z., Li, X., & Zhao, Z. (2002). Purification and identification of a 42-kilodalton abscisic acid-specific-binding protein from epidermis of broad bean leaves. Plant Physiology, 128, 714–725.

Zhao, Y., Chow, T. F., Puckrin, R. S., Alfred, S. E., Korir, A. K., Larive, C. K., & Cutler, S. R. (2007). Chemical genetic interrogation of natural variation uncovers a molecule that is glycoactivated. Nature Chemical Biology, 3(11), 716–721.

Zhou, J., Ferna, EmilioGalva, A., & Y, A. J. M. (2000). A high affnity nitrate transport system from Chlamydomonas requires two gene products. FEBS Letters, 466, 225–227.

Zhou, X. E., Soon, F., Ng, L., Kovach, A., Suino-, K. M., Li, J., … Kelly, M. (2012). Catalytic mechanism and kinase interactions of ABA-signaling PP2C phosphatases. Plant Signaling & Behavior, 7(5), 581–588.

Ziem-Hanck, U., & Heber, U. (1980). Oxygen Requirement of Photosynthetic CO_2 Assimilation. Biochimica et Biophysica Acta, 591, 266–274.

Zifarelli, G., & Pusch, M. (2010). CLC transport proteins in plants. FEBS Letters, 584(10), 2122–2127.